How to Stay in Shape –

The Role of the Cell-Spanning Actomyosin Ring in Colonies of Human Induced Pluripotent Stem Cells

Aufrechterhaltung der Koloniestruktur – Die Rolle des zellübergreifenden Aktomyosinrings in humanen induzierten pluripotenten Stammzellen

Zur Erlangung des akademischen Grades einer

DOKTORIN DER NATURWISSENSCHAFTEN

(Dr. rer. nat.)

von der KIT-Fakultät für Chemie und Biowissenschaften

des Karlsruher Instituts für Technologie (KIT)

genehmigte

DISSERTATION

von

M.Sc. Elisa Genthner

1. Referent/Referentin: Prof. Dr. Martin Bastmeyer
2. Referent/Referentin: Prof. Dr. Sylvia Erhardt

Tag der mündlichen Prüfung: 12.12.2024

Eidesstattliche Erklärung

Der experimentelle Teil der vorliegenden Arbeit wurde in der Zeit von Januar 2021 bis September 2024 am Zoologischen Institut in der Abteilung für Zell- und Neurobiologie des Karlsruher Instituts für Technologie (KIT) durchgeführt.

Ich versichere hiermit, dass ich diese Arbeit selbständig verfasst und keine anderen, als die angegebenen Quellen und Hinweise verwendet habe. Wörtlich oder inhaltlich übernommene Stellen sind als solche gekennzeichnet und die Satzung des Karlsruher Instituts für Technologie (KIT) zur Sicherung guter wissenschaftlicher Praxis habe ich in der gültigen Fassung beachtet. Diese Arbeit wurde in keiner Form einer anderen Prüfungsbehörde vorgelegt. Ich versichere außerdem, dass die beigelegte elektronische Version der Arbeit mit der schriftlichen übereinstimmt.

Datum, Ort Unterschrift

Abstract

Over the last years, the mechanical influence on pluripotency regulation has become increasingly evident. Human induced pluripotent stem cells (hiPSCs) are a valuable and accessible tool to study the relationship between cytomechanics and pluripotency regulation *in vitro*. When cultivated under standard conditions, hiPSC colonies display two distinct actin structures: the previously published actin fence and the here described cell-spanning actomyosin ring. Given the importance of cell-cell interaction during pluripotency dynamics *in vivo*, this work aimed to elucidate the role of the cell-spanning actomyosin ring in hiPSC colonies.

HiPSCs self-organize a continuous cell-spanning actomyosin ring, associated with non-muscle myosin IIB (NMIIB), at the apical side of the colony. This cell-spanning ring divides the colony into inner and outer cell populations, where the inner population displays a prominent actomyosin network and enrichment in the apical markers podocalyxin and ezrin. Three key findings underline the significance of the cell-spanning actomyosin ring in hiPSC colony architecture: (1) its establishment is independent of substrate and hiPSCs cell line, (2) it forms on soft substrates comparable to *in vivo* physical conditions, and (3) it re-establishes after perturbation. Taken together, these findings suggest that the cell-spanning actomyosin ring is essential for colony morphology. Furthermore, the results demonstrate that the spatial distribution of NMIIB is strongly associated with the distribution of ezrin throughout the colony. Additionally, hiPSCs cultivated in mechanical barriers showed alterations in actin cytoskeletal organisation, with two distinct morphologies either displaying a fully formed cell-spanning ring or not. The formation of the cell-spanning ring was primarily observed in barriers with a lower stiffness of 25 MPa whereas a higher stiffness of 1 GPa led to fragmented cell-spanning rings in the majority of colonies. Finally, interfering with contractile tension resulted in early differentiation towards mesoderm and endoderm lineages in individual cells under self-renewal culture conditions. Based on these observations, three roles of the contractile tension generated by the cell-spanning ring were identified: (1) regulation of apicobasal polarity, (2) maintenance of colony integrity and (3) sustaining pluripotency.

In summary, the results indicate that the cell-spanning actomyosin ring is a major regulator of hiPSC colony morphology, enabling epithelial-like character and pluripotency maintenance. The structural resemblance to actomyosin cables described in embryonic epithelial tissue of other species suggest a potential role for the cell-spanning actomyosin ring in early human embryonic development. The obtained knowledge of biomechanical regulation can be used to improve stem cell-based models, gaining insights into human embryogenesis.

Zusammenfassung

Innerhalb der letzten Jahre wurde der mechanische Aspekt in der Pluripotenzregulierung immer deutlicher. Humane induzierte Stammzellen (hiPSZ) sind ein wertvolles und zugängliches Mittel, um das Zusammenspiel zwischen Zytomechanik und Regulierung der Pluripotenz *in vitro* zu untersuchen. Unter Standard Kultivierungsbedingungen weisen hiPSZ Kolonien zwei charakteristische Aktinstrukturen auf: Den bereits publizierten, sogenannte „actin fence“ und den hier beschriebenen zellübergreifenden Aktomyosinring. Aufgrund der Wichtigkeit von Zell-Zell-Interaktionen während der Pluripotenzdynamik *in vivo*, ist das Ziel dieser Arbeit die Aufgaben des zellübergreifenden Aktomyosinringes in den hiPSZ Kolonien zu definieren.

HiPSZ bilden an der apikalen Seite der Kolonie einen durchgängigen zellübergreifenden Aktomyosinring aus, welcher mit Nicht-muskulärem Myosin IIB (NMIIB) assoziiert ist. Dieser zellübergreifende Ring teilt die Kolonie in eine innere und äußere Population, wobei die innere Population ein ausgeprägtes Aktomyosin-Netwerk und eine Anreicherung der apikalen Marker Podocalyxin und Ezrin aufweist. Drei zentrale Ergebnisse zeigen die Bedeutung des zellübergreifenden Aktomyosinrings für die Koloniestruktur: (1) Er bildet sich unabhängig von Substrat oder Zelllinie, (2) er bildet sich auf weichem Substrat mit *in vivo*-ähnlichen Eigenschaften, und (3) er erneuert sich nach einer Strukturveränderung. Diese Ergebnisse weisen zusammen darauf hin, dass der zellübergreifende Aktomyosinring essenziell für die Koloniemorphologie ist. Des Weiteren zeigen die Ergebnisse, dass die räumliche Verteilung von NMIIB innerhalb der Kolonie mit der von Ezrin verknüpft ist. HiPSZ-Kolonien, die in mechanischen Barrieren kultiviert werden, zeigen Veränderungen in der Aktinzytoskelett-Anordnung mit zwei unterschiedlichen Morphologien: einem vollständigen oder fragmentierten zellübergreifenden Ring. Die Bildung eines vollständigen zellübergreifenden Rings wurde hauptsächlich bei Barrieren mit einer Steifigkeit von 25 MPa beobachtet, während eine höhere Steifigkeit von 1 GPa zu fragmentierten Ringen führte. Die Hemmung der Kontraktilität führte zur beginnenden Differenzierung in die mesodermale und endodermale Richtung. Der zellübergreifende Ring hat drei Hauptfunktionen (1) Regulierung der apikobasalen Polarität, (2) Erhalt der Kolonieintegrität und (3) Aufrechterhaltung der Pluripotenz.

Zusammengefasst deuten die Ergebnisse darauf hin, dass der zellübergreifende Aktomyosinring ein wichtiger Regulator der hiPSZ-Koloniemorphologie ist. Er erhält die epitheliale und pluripotente Charakteristik der hiPSZ. Die strukturelle Ähnlichkeit zu Aktomyosinkabeln in embryonalen Geweben anderer Spezies deutet auf eine mögliche Rolle in der frühen humanen Embryonalentwicklung hin. Dieses Wissen über die biomechanische Regulation kann zur Verbesserung stammzellbasierter Modelle und zum besseren Verständnis der humanen Embryogenese beitragen.

Content

1 Introduction

In the last years, many stem cell-based *in vitro* models were developed to shed light on the black box of human embryonic development (Shahbazi & Pasque, 2024). Even though a lot of knowledge was gained through studies in other organisms, particularly the mouse system, there are distinct limitations in transferring knowledge to the human system (Taniguchi et al., 2019). Thus, stem cell-based models using human pluripotent stem cells (hPSCs), including human embryonic stem cells (hESC) and human induced pluripotent stem cells (hiPSCs), provide a unique opportunity to recreate human development. Especially, the introduction of hiPSCs in 2007 enabled an advantageous and ethical alternative to experiments on the embryo or the usage of hESC (Takahashi et al., 2007). Their differentiation capacity, ability of self-renewal and easy accessibility makes them a valuable tool for fundamental research in developmental biology. In addition, they self-organize structures occurring *in vivo*, revealing the importance of mechanistic aspects of development (Taniguchi et al., 2017).

The present work aimed to elucidate the role of cytomechanics in regulating pluripotency of hiPSCs *in vitro*. In order to emphasize the connection between mechanical cues, cell morphogenesis and cell fate decisions, the following chapter introduces the concept of pluripotency, including the dynamic *in vivo* as well as molecular mechanism to maintain it *in vitro*. Additionally, proteins playing a crucial role in mechanobiological processes are described. Finally, actin cytoskeletal organisation associated with pluripotency maintenance in different pluripotent stem cells is introduced.

1.1 Early Embryonic Development and Pluripotency Dynamic *in Vivo*

The following process of human embryo development from day 0 to day 12 is described according to the review by Shahbazi and Pasque (Shahbazi & Pasque, 2024) (Figure 1). After fertilization, a series of cell divisions occur, resulting in a compact cluster of 16-32 cells, namely the morula. At this stage, cells are totipotent with the ability to differentiate into all cell types of both embryonic and extraembryonic tissue. As embryogenesis progresses, the differentiation potential of stem cells is gradually restricted. Based on position dependent cytomechanics and accumulation of transcription factors, cells self-sort into two distinct populations: outer cells become extraembryonic cells and inner cells become part of the inner cell mass (ICM). The latter population consists of pluripotent cells which possess the capacity to differentiate into all cell types of the germ layers: ectoderm, mesoderm and endoderm. The developed blastocyst is characterized by the outer layer of

trophectoderm (TE) surrounding a cavity and the ICM, located at one side. Until this stage, the developing embryo is covered by a glycoprotein layer known as the zona pellucida that is lost upon implantation into the endometrium. In the late blastocyst, after implantation, the ICM further divides into the epiblast and hypoblast, with the pluripotent epiblast disc at their contact point. Subsequently, the cells of the hypoblast extend to form the primitive yolk sac and the cells of the epiblast undergo lumenogenesis to form the amniotic cavity.

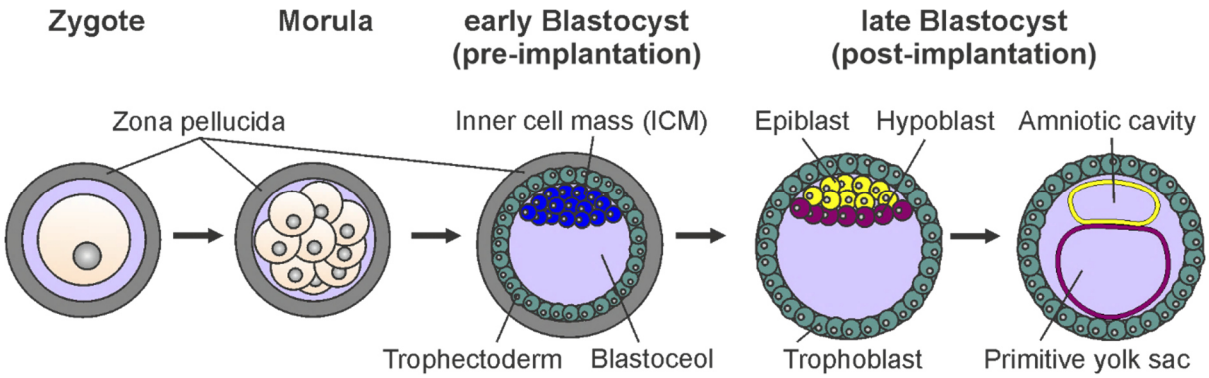

Figure 1: Early mammalian embryonic development

After fertilization, a series of cell divisions occur resulting in a firmly attached cluster of cells, the morula. As development progresses, the differentiation capacity is restricted from a totipotent state to a pluripotent state for the cells of the inner cell mass (ICM). Cells of the trophectoderm surrounding the ICM and the blastocoel become extraembryonic tissue. Upon implantation, the cells of the ICM further divide in the epiblast and hypoblast forming the amniotic cavity and the primitive yolk sac, respectively. Adapted from Shahbazi & Pasque, 2024.

The pluripotent cells of the ICM undergo a pluripotency transition during implantation and lumenogenesis (Shahbazi et al., 2017), emphasizing the interplay between morphological change and pluripotency regulation. The following process of epiblast rosette formation and lumenogenesis is described according to the 2019 published review by Taniguchi and colleagues (Taniguchi et al., 2019). At the beginning of the amniotic cavity formation, cells of the epiblast are unpolarized and in close contact to each other (Figure 2, left panel). They are in a naive pluripotent state, as the cells of the ICM, with the unlimited capacity to differentiate into all cell types of both somatic and germline lineages. Mediated by vesicle trafficking, the cells establish apicobasal polarity and arrange in a radial organisation (Figure 2, middle panel). The vesicles contain the apical marker Podocalyxin-like protein 1 (PODXL) that is transported to the apical membrane initiation site. At this site, a cyst-like structure forms, growing into the amniotic cavity (Figure 2, right panel). During this process, the pluripotent cells transition to a primed state, showing a more developmentally restricted potent state.

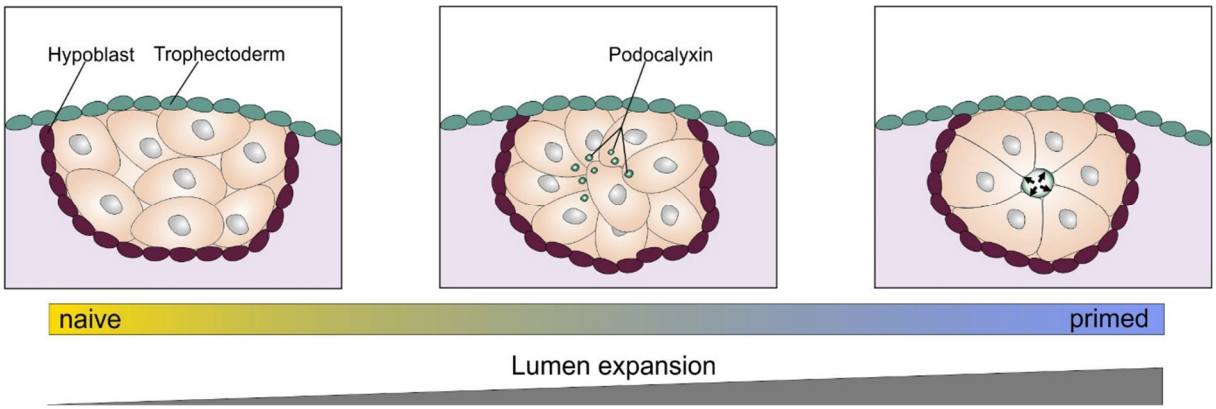

Figure 2: Epiblast rosette formation and lumenogenesis

After implantation of the blastocyst in the endometrium, pluripotent cells of the epiblast undergo a transitional shift from naive to primed pluripotency state. Initially, the cells are unpolarized and in close contact with each other. Signalling from the surrounding tissue together with vesicle transport of the apical marker podocalyxin mediates radial organisation and establishment of the cell polarity. Podocalyxin is transferred to the apical membrane initiation site, leading to a shared cyst-like structure in the centre. This lumen gives rise to the amniotic cavity of the epiblast. Adapted from Taniguchi et al., 2019.

The two distinct pluripotent states, naive and primed, are primarily characterized by studies performed in mice, as there are considerable variations across human studies (Huang et al., 2014). The *in vitro* counterparts representing these states are mESC for naive and mouse epiblast-derived stem cells (mEpiSC) for primed (Nichols & Smith, 2009). HPSCs, including hESCs and hiPSCs, share similar characteristics with mEpiSC and thus are classified as being in a primed state (Wu & Izpisua Belmonte, 2015). One of the main differences between the naive and the primed is the developmental state to contribute to chimaera formation (Mascetti & Pedersen, 2016). There are multiple molecular and functional differences between these states, including epigenetic factors like DNA hypomethylation, no X chromosome inactivation in female cells and a high single-cell cloning efficiency (Weinberger et al., 2016) for the naive state. However, in recent years, intermediate and formative PSC states have been described more frequently, highlighting the fluid transition between the pluripotent states (Yu et al., 2021).

1.2 The Pluripotency Gene Regulatory Network

As described in Section 1.1 the pluripotent stem cell state is highly dynamic *in vivo*. Isolation of ESCs and reprogramming of iPSCs provided the knowledge about molecular mechanisms in the maintenance of pluripotency (Takahashi & Yamanaka, 2006). In the following, the key players contributing to pluripotency regulation are highlighted.

1.2.1 Core Transcription Factors

Pluripotency is stabilized by a balanced expression of three core transcription factors; namely SRY-box 2 (SOX2), octamer-binding transcription factor 3/4 (OCT3/4) and NANOG (Li & Belmonte, 2017). The importance of these factors to pluripotency is evident during embryonic development as illustrated by the following examples. OCT3/4 and NANOG are expressed in cells of the ICM (Chambers et al., 2007; Schöler et al., 1989). For formation and development of the epiblast, NANOG and SOX2 are required, respectively (Avilion et al., 2003; Mitsui et al., 2003). Together, the three factors regulate an interconnected network of pluripotency genes, the pluripotency gene regulatory network (PGRN) (Li & Izpisua Belmonte, 2018). The transcriptional regulation occurs by genomic binding of the core factors facilitating the binding of additional transcription factors or altering the expression of pluripotency and lineage specific genes (Li & Izpisua Belmonte, 2018). Established early lineage specific markers for ectoderm, mesoderm and endoderm are for example SRY-box 1 (SOX1) , Brachyury and forkhead box A2 (FOXA2), respectively (Cai et al., 2006).

1.2.2 Signalling Pathways Maintaining Pluripotency

In addition to transcriptional regulation by the core transcriptions factors, other mechanisms including post-transcriptional regulation, epigenetic regulation and cellular signalling impact the delicate balance of pluripotency (Li & Belmonte, 2017). They are multiple extrinsic signalling pathways regulating pluripotency (Varzideh et al., 2023). Naive ground state, represented by mESCs *in vitro* is mainly maintained by the leukemia inhibitory factor (LIF) pathway, bone morphogenetic proteins (BMP) signalling and the canonical Wnt signalling pathway (Niwa et al., 1998; Ying et al., 2003). The stabilization of the primed state, including mEpiSCs, hESCs and hiPSCs, is mainly controlled by fibroblast growth factor (FGF) and transforming growth factor (TGF) signalling pathways (Figure 3) (Mossahebi-Mohammadi et al., 2020; Xiao et al., 2006). Given that the experiments of this study focus on hiPSCs, the signalling pathways supporting the primed state are described in the following.

The TGFβ/Activin/Nodal pathway directly controls pluripotency by interacting with the PGRN through NANOG (Vallier et al., 2009). As described by Itho and colleagues, the initiation is mediated by the ligand binding to the dimeric transmembrane receptors on the cell surface, followed by phosphorylation of SMAD proteins (Itoh et al., 2014). Subsequently, SMAD2/3 forms a complex with the coregulatory SMAD protein SMAD4 that is translocated into the nucleus to activate NANOG expression.

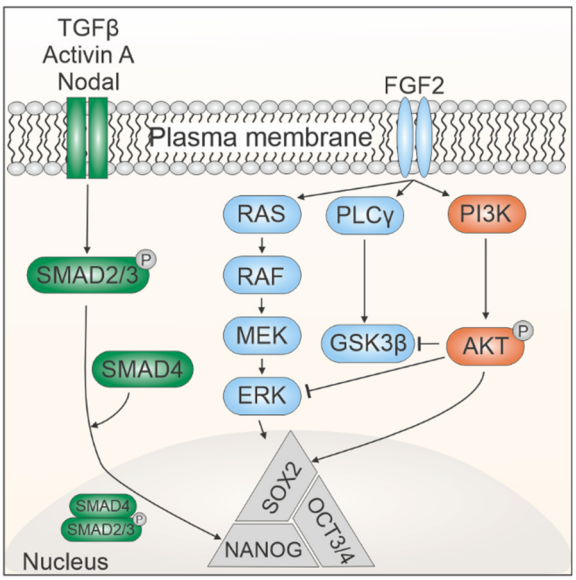

Figure 3: Key signalling pathways in primed state of pluripotency

The key signalling pathways maintaining primed pluripotency are the FGF and TGF pathways. The TGFβ/Activin/Nodal pathway influences the transcription of NANOG through a complex compiled of SMAD2/3 and SMAD4. The FGF pathway regulates pluripotency through three downstream pathways: MAPK/ERK, PLCγ and PI3/AKT. Each pathway as well as a crosstalk mechanism between the pathways regulate pluripotency gene expression by interaction with the core transcription factors. Adapted from Mossahebi-Mohammadi et al., 2020.

The second signalling pathway crucial for maintaining the primed pluripotent state is the FGF pathway (Mossahebi-Mohammadi et al., 2020). It has been shown that especially the binding of the ligand FGF2 to the receptor fibroblast growth factor receptor 1 (FGFR1) plays a crucial role in hiPSCs, activating three pathways downstream: Mitogen-activated protein kinase (MAPK)/extracellular signal-regulated kinase (ERK), Phospholipase C Gamma (PLCγ), and phosphatidylinositol-4,5-bisphosphate 3-kinase (PI3K)/AKT (Nakashima & Omasa, 2016). Especially, MAPK signalling was shown to play an essential role in maintaining primed pluripotency (Haghighi et al., 2018). After activation of RAS downstream of the cell surface receptor, a MAPK cascade is initiated where RAF, MEK and ERK are sequentially activated by phosphorylation (Zhang & Liu, 2002).

Subsequently, ERK is translocated to the nucleus, altering gene expression. PI3K/AKT also acts, downstream of FGF signalling, supporting the maintenance of pluripotency (Singh et al., 2012). The downstream activation of AKT leads to the inhibition of glycogen synthase kinase-3 (GSK3)β which contributes to PSC survival (Romorini et al., 2016). As developmental potential decreases, PI3K signalling increases, which is important for the transition into lineage specification (Mossahebi-Mohammadi et al., 2020). Activation of the PI3K/AKT pathway also regulates stemness by interaction with SOX2 (Schaefer & Lengerke, 2020). It is important to note that there are other signalling pathways, like Wnt/β catenin playing a role in maintaining pluripotency as well as a crosstalk mechanism between the pathways downstream of FGF signalling (Singh et al., 2012).

1.2.3 The Role of YAP in Stem Cell Fate

Another essential signalling pathway in regulation of stem cell survival and differentiation is the Hippo pathway (Figure 4) (Lian et al., 2010). The key components of the canonical pathway are mammalian STE20-like kinase 1/2 (MST1/2), protein salvador homologue 1 (SAV1), large tumour suppressor kinase 1/2 (LATS1/2), MOB kinase activators 1A and 1B (MOB1A/B), Yes-associated protein 1 (YAP), and WW-domain-containing transcription regulator 1 (TAZ) (Fu et al., 2022). The canonical signalling pathway is described according to the review by Fu and colleagues in 2022 (Fu et al., 2022). In general, the activated Hippo pathway initiates a kinase cascade where downstream MST1/2 and its scaffold protein SAV1 are activated by phosphorylation, which in turn subsequently phosphorylate LATS1/2 and its scaffold protein MOB1/2. The activated LATS1/2 phosphorylates and inactivates YAP and TAZ thus preventing the translocation of both transcriptional coactivators into the nucleus where they would interact with proteins of the transcriptional enhanced associated domain (TEAD) family. Upstream inactivation of the Hippo pathway by a phosphatase and kinase complex leads to the translocation of YAP/TAZ to the nucleus and activation of numerous target genes together with TEAD1-4 (Totaro et al., 2018). YAP/TAZ regulates the maintenance of pluripotency by interaction with the core pluripotency factors NANOG, OCT3/4 and SOX2, promoting their expression (Lian et al., 2010). In addition, the crucial role of YAP in hPSCs was highlighted for the generation of hiPSCs (Qin et al., 2014) as well as for inducing the transition to the naive state (Qin et al., 2016).

There are many upstream signals regulating the Hippo pathway, including cell polarity and mechanical cues (Fu et al., 2022). In response of an altered environment, such as stiffness of the environment, cell shape or cell-cell contact (Dasgupta & McCollum, 2019), cells can

adapt their gene expression in a process termed mechanotransduction (Dupont et al., 2011). Upon mechanical stimuli acting upstream to the Hippo signalling pathway, YAP/TAZ shuttles between inactivated cytoplasmic or activated nucleus location. For example, in dense cell cultures or cells grown on soft substrate, YAP/TAZ display cytoplasmic localisation, whereas isolated cells or cells growing on stiff substrate show nuclear localisation (Dupont et al., 2011). The external stimuli facilitate remodelling of the actin cytoskeleton and thereby alter the intrinsic cytomechanics (Walker et al., 2020). The mechanism behind the relation of mechanical forces by cytoskeletal components and YAP/TAZ activity is not yet well characterized (Driskill & Pan, 2023). However, it was proposed that mechanical forces generated by the cytoskeleton upon sensing, play a role in inhibition of LATS1/2 activity preventing YAP/TAZ phosphorylation (Wada et al., 2011).

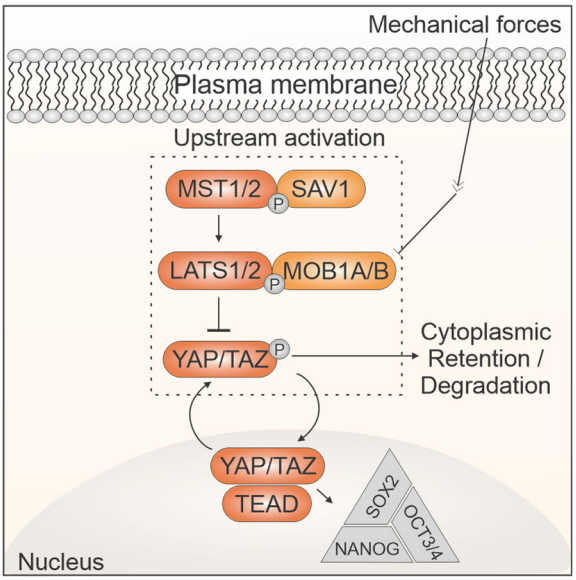

Figure 4: The Hippo signalling pathway

Activation of the Hippo signalling pathway is initiated by multiple upstream signals, including mechanical cues. The key components of the canonical pathway are indicated by the dotted square. In general, the upstream activation leads to sequential phosphorylation of MST1/2 and LATS1/2 and their respective scaffold proteins SAV1 and MOB1A/B. The activated LATS1/2 phosphorylates and inactivates the transcriptional coactivators YAP/TAZ thus preventing their translocation to the nucleus. YAP, together with TEAD proteins, regulate the expression of the core pluripotency transcription factors and play a crucial role in cell fate decisions. Adapted from Driskill & Pan, 2023

1.3 Cytomechanics

During early mammalian embryonic development, stem cells experience a series of mechanical cues driving cell fate decision (Vining & Mooney, 2017). These cues are applied externally by their surroundings, e.g. fluid flow, or are intrinsically generated by alteration in cytoskeletal architecture upon sensing mechanical signals in their environment. The mechanical signals are transferred to the cell by traction on the extracellular matrix (ECM) via anchoring complexes like focal adhesions or by cell-cell contact via cell junctions (Vining & Mooney, 2017). Especially in the early embryogenesis, the cell-cell signalling is dominant, but shifts to ECM-cell signalling in post-implantation embryos (Cosgrove et al., 2016). Following mechanical stimuli, the cell responds with alteration in cytoskeletal structure, changing cellular contractility (Weng et al., 2016).

1.3.1 Generation of Cellular Contractile Tension

Contractility is established by non-muscle myosin II (NMII) in association with actin filaments (Svitkina, 2018). The NMII motor protein is compiled of two heavy chains and two pairs of light chains, forming a hexameric structure (Figure 5) (Vicente-Manzanares et al., 2009). One pair of light chains are the essential light chains (ELC) and the other the myosin regulatory light chains (MRLC) which stabilize the conserved N-terminal motor domain of the heavy chains. The C-terminal rod domain of the heavy chain varies depending on the NMII isoform, namely NMIIA, NMIIB and NMIIC. In human, they are encoded by the three different genes, *MYH9*, *MYH10* and *MYH14*, respectively (Vicente-Manzanares et al., 2009). In addition to structural features, the three isoforms differ in functionality. While NMIIA is known to play a role during initiation of force generation, NMIIB is essential for stabilization and maintenance of contractile tension (Weißenbruch et al., 2021).

The activation of NMII is regulated by phosphorylation of the MRLC through several kinases, including the myosin light chain kinase and the Rho kinase, downstream of the Rho/Rho-associated protein kinase (ROCK) pathway (Matsumura, 2005; Vicente-Manzanares et al., 2009). Phosphorylation leads to a conformational change allowing motor activity. Phosphorylated NMII monomers polymerize to form bipolar minifilaments and exert contraction by sliding of antiparallel actin filaments (X. Liu et al., 2017; Shutova & Svitkina, 2018). The motor domain of the individual NMII monomers acts through an ATPase cycle (Vale & Milligan, 2000). NMII detaches from the actin filaments upon ATP binding. After ATP hydrolysis, NMII rebinds to actin and moving the actin filament upon phosphate release, causing the myosin power stroke. The remaining ADP is released,

leaving the NMII in the initial state of the cycle. The generated contractility varies in strength based on the organisation of the actomyosin system (Shutova & Svitkina, 2018), which is adapted after mechanosensing by the cell. The greatest contractile tension is exerted by aligned bundles of actin and NMII filaments as stress fibres or circular bundles. These two types of aligned bundles, are either associated with focal adhesions connecting the cell to the ECM or apply forces to the plasma membrane via mediators like the ezrin, radixin and moesin (ERM) proteins, respectively (Gardel et al., 2010; Schwayer et al., 2016).

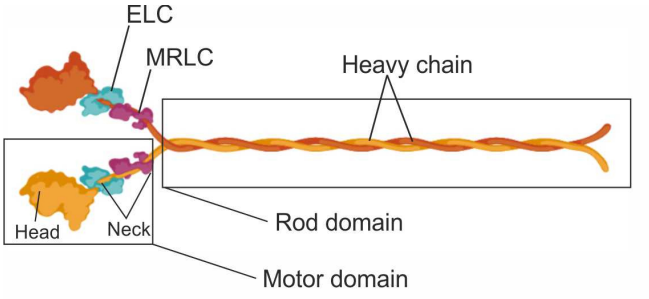

Figure 5: Hexameric structure of NMII molecule

The overall NMII structure consists of two heavy chains which are divided in a N-terminal motor domain and a C-terminal rod domain. Two pairs of light chains, the essential light chains (ELC) and the myosin regulatory light chains (MRLC), are associated with the motor domain. Activation of NMII is facilitated by phosphorylation of the MRLC. Adapted from Shutova & Svitkina, 2018. Created with BioRender.com.

1.3.2 Regulation of Cellular Membrane Tension

The ERM proteins play a crucial role in cell morphogenesis processes by acting as linker between the plasma membrane and the actin cytoskeleton (Arpin et al., 2011). Especially, ezrin is known to be prominent in early embryonic development, for example during the establishment of the apical domain in the 8-cell stage embryo (Louvet et al., 1996). The linkage of the actin cortex, a thin layer of an actin network right underneath the membrane, to the plasma membrane generates cortical membrane tension (Doherty & McMahon, 2008). This tension is regulated by switching between an active binding state and an inactive non-binding state of the linker proteins (Rouven Brückner et al., 2015). The structure of the ERM proteins is conserved, consisting of the globular N-terminal domain, the FERM domain, a linker region and the C-terminal domain (Fehon et al., 2010). After activation of ezrin by phosphorylation and phospholipid binding, the protein undergoes a conformational change enabling the binding of the FERM domain to the plasma membrane and the C-terminal domain to the actin filaments (Fievet et al., 2004). In the inactive state,

the ERM proteins are in a closed conformation, masking the membrane-binding and actin-binding sites of the N- and C-terminal domain (Figure 6A).

Besides the linkage of the underlying actin cytoskeleton to the membrane by ERM proteins, contractile tension generated by the actomyosin cortex contributes to regulation of membrane tension, in particular with myosin I (Mazerik & Tyska, 2012).

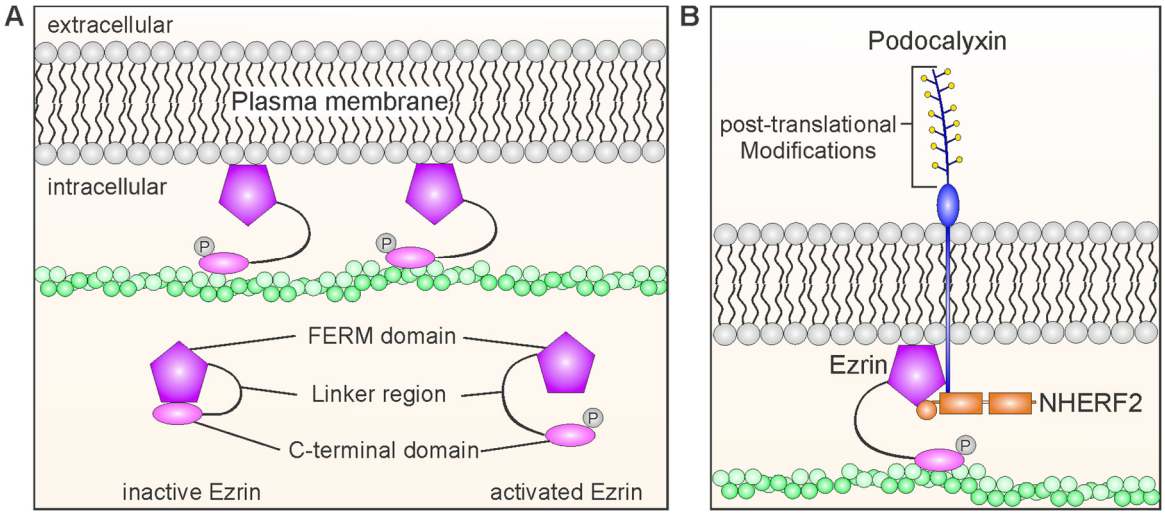

Figure 6: Structure and function of ezrin and podocalyxin

(A) Ezrin (magenta) functions as a crosslinker between plasma membrane and the actin cytoskeleton (green). Activation by phosphorylation initiates a conformational change allowing the FERM domain and the C-terminal domain of ezrin to bind to the plasma membrane and actin, respectively. Adapted from Fehon et al., 2010. **(B)** Podocalyxin (PODXL) (blue) is an integral transmembrane protein heavily modified at the extracellular domain. Together with ezrin and Na+/H+ exchanger regulatory cofactor 2 (NHERF2) (orange), PODXL forms a complex in specialized kidney epithelial cells to connect the actin cytoskeleton to the plasma membrane. Adapted from Takeda, 2003.

Another protein involved in the connection of the actin cytoskeleton to the plasma membrane is PODXL by either direct interaction with ezrin or mediated by the protein Na+/H+ exchanger regulatory cofactor 2 (NHERF-2) through its cytoplasmic domain (Figure 6B) (Fröse et al., 2018; Takeda, 2003). The PODXL-ezrin complex fulfils different roles in specific cell types. For example, in podocytes, terminally differentiated epithelial cells in the kidney, the complex ensures maintenance of the unique actin cytoskeleton architecture (Takeda, 2003). In carcinoma cells, the PODXL-ezrin complex enables metastatic formation by regulating the cytoskeleton dynamics (Fröse et al., 2018). Interestingly, PODXL is also highly expressed during human embryogenesis, for example in the epiblast rosette formation (Bedzhov & Zernicka-Goetz, 2014) described in Section

1.1 (Figure 2). In general, PODXL is an integral transmembrane carrier protein with many post-translational modifications like glycosylation, sialylation and sulfation (Nielsen & McNagny, 2009). This variety of post-translational modifications on the extracellular domain of PODXL are recognizable epitopes that serve as pluripotency surface markers with some defining hPSC pluripotency, like TRA-1-60, TRA-1-81 (Natunen et al., 2011; Schopperle & DeWolf, 2007). Upon differentiation of hPSCs, some surface markers are lost, however, PODXL itself serves as a pluripotency surface marker in other organisms (Kang et al., 2016). In addition to its role in characterizing pluripotency, a recent study highlighted the role of PODXL in maintaining pluripotency through regulating metabolic processes affecting pluripotency transcription factors (W.-J. Chen et al., 2023).

1.4 Apicobasal Polarity

Both proteins, ezrin and PODXL, are apical markers involved in promoting the establishment of apicobasal polarity (Bryant et al., 2014; Fehon et al., 2010). However, contractile tension generated by NMII is a driving factor through formation of cell junctions' complexes, especially adherence junctions (Heuzé et al., 2019). These junctions laterally link the cell to its neighbours and spatially separate it into an apical and basal domain (Buckley & St Johnston, 2022). On a molecular level, polarity and cell morphology is regulated by apicobasal polarity proteins specific for the apical and basolateral domain, respectively. Those specific proteins interact mutually antagonistic with each other, thus restricting apical or basal proteins to their respective domain (J. Chen & Zhang, 2013).

In general, the apical identity is defined by the atypical protein kinase C (aPKC), Par 6, cell division control protein 42 homolog (Cdc42) and the Crumbs complex (Figure 7) (Assémat et al., 2008; Bulgakova & Knust, 2009). First, aPKC binds Par6, forming a complex which is subsequently activated and recruited to the apical membrane by binding of Par3 and Cdc42 (Dong et al., 2020; Joberty et al., 2000; Lin et al., 2000; Nunes de Almeida et al., 2019; Suzuki et al., 2002). The Par6-aPKC complex additional binds the polarity protein Crumbs (CRB1-3) and its scaffold protein Stardust (Std), anchoring the complex to the plasma membrane (Buckley & St Johnston, 2022; Whitney et al., 2016). Apical polarity proteins, such as Crumbs, Cdc42 and Par3, play a crucial role in organizing the apical actin cytoskeleton (Buckley & St Johnston, 2022). Cdc42 directly influences activation of NMII through phosphorylation of the MRLC (Zihni et al., 2017). Crumbs possess FERM-binding motifs, which allows connection of Crumbs to the actin cytoskeleton (Margolis, 2018). The main components of the basolateral domain are Scribble, discs large and lethal giant larvae, together referred to as the Scribble complex.

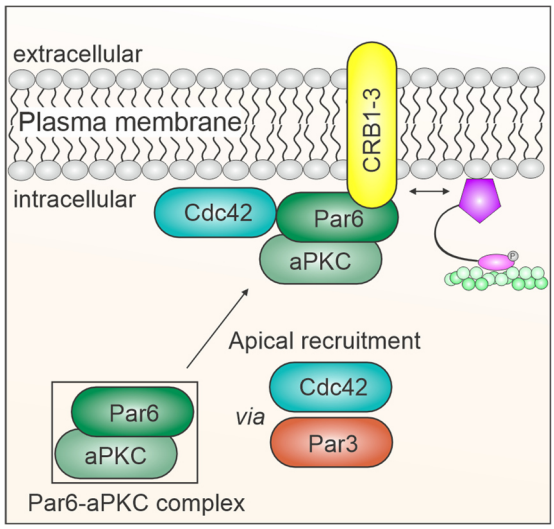

Figure 7: Apical domain structure

The apical domain is defined by a set of apical polarity proteins, mainly the atypical protein kinase C (aPKC), Par 6, Cdc42 and the Crumbs complex. Par6 and aPKC form a complex which is recruited to the apical plasma membrane via Par3 and Cdc42. Activation of the complex and anchoring to the apical membrane involves binding to Cdc42 and the Crumbs protein (CRIB1-3). Apical actin organisation is associated with multiple polarity proteins such as Crumbs through interaction with ERM proteins (magenta). Adapted from Buckley & St Johnston, 2022.

1.5 Cytoarchitecture in Pluripotent Stem Cells

Actomyosin contractility is essential for PSC colony architecture, including mESC and hPSC (S. Liu & Kanchanawong, 2022). In mESC, the actin cytoskeleton is organized as a meshwork, the actin cortex, with no prominent stress fibres or focal adhesions (Boraas et al., 2016; Xia, Yim, et al., 2019). Together with NMIIA, this 3D supracellular actomyosin cortex generates contractile tension and compression forces crucial for maintaining both colony integrity and pluripotency (Du et al., 2019; Xia, Lim, et al., 2019). In contrast to mESC colonies, hiPSC colonies display a position-dependent apicobasal polarity (Y. Kim et al., 2022), dividing the colony into a contact-free apical side and a basal side in contact with the ECM. Each side is characterized by a distinct actin cytoskeleton structure: the actin fence at the basal side and the cell-spanning actomyosin ring at the apical side (Figure 8). The actin fence was described in 2017 by Narva and her colleagues as a focal adhesion-dependent fence parallel to the colony edge (Narva et al., 2017). The actin filaments are organized as stress fibres enclosed by prominent focal adhesions (Figure 8, left panel) (Stubb et al., 2019). The cell-spanning actomyosin ring was first described by Dr. Sarah Bertels (Bertels, 2018). In contrast to the actin fence, the cell-spanning ring is a circumferential actin structure strongly associated with NMIIB, which connects neighbouring cells in the apical periphery (Figure 8, right panel). In addition, the apical side is characterized by an actomyosin network covering the cells encircled by the cell-spanning ring.

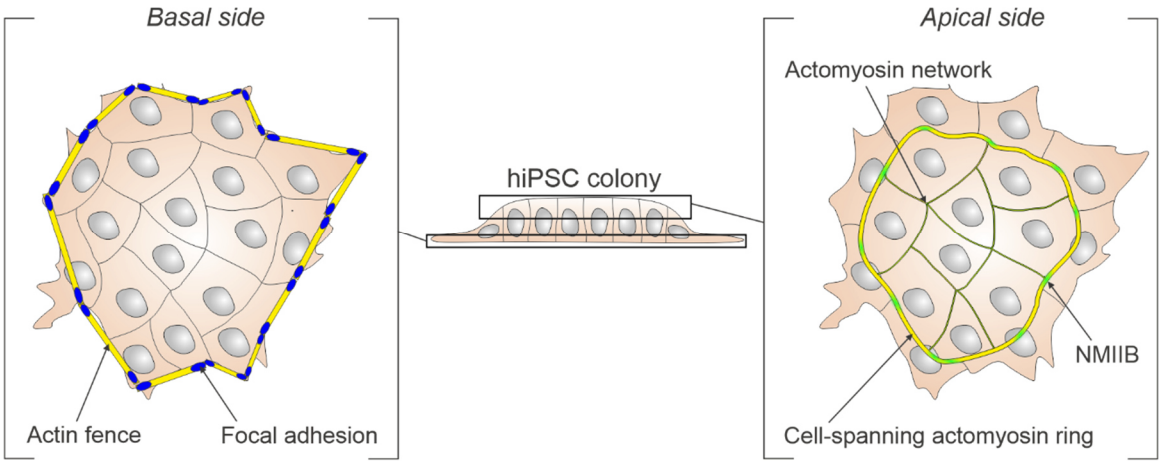

Figure 8: Actin cytoskeletal organisation in hiPSC colonies

Schematic diagram of the two distinct actin cytoskeleton structures in hiPSCs, the actin fence (left panel) and the cell-spanning actomyosin ring (right panel). The actin fence is located at the basal side of the colony, characterized by stress fibres flanked by prominent focal adhesions. In contrast, the cell-spanning actomyosin ring is a circumferential actin bundle at the apical side of the colony. It is strongly associated with the NMIIB isoform.

2 Motivation and Aim of the Thesis

In recent years, studies have highlighted the essential role of mechanical cues in mammalian embryogenesis and differentiation. PSCs, including mESCs and hiPSCs, are valuable tools for studying the interplay between cytomechanics and pluripotency regulation *in vitro.* In mESCs, representing the naive state of pluripotency, a unique actin cytoskeleton structure was described: The 3D supracellular actomyosin cortex, which plays a crucial role in both the maintenance of colony morphology and pluripotency. In hiPSC, representing the primed state, a functional pendant was introduced: The actin fence. This cytoskeletal structure highlights the impact of the cell's environment on cell fate decisions. However, mechanical signalling between neighbouring cells is also a crucial in the colony context and is not highlighted by the actin fence. The cell-spanning actomyosin ring connects neighbouring cells and thereby presumably enables signalling transfer between them. Given this characteristic, this study aims to elucidate the potential role of the cell-spanning ring as a major regulator of colony morphology and pluripotency in hiPSC colonies.

The role of contractile tension exerted by the cell-spanning ring was investigated in terms of colony morphology, and pluripotency regulation. In contrast to the mESC cytoskeleton structure, the cell-spanning ring in hiPSCs is strongly associated with NMII, especially with the isoform NMIIB. Thus, to illustrate the formation and dynamics of the cell-spanning ring via live cell imaging, a green fluorescent protein (GFP)-NMIIB reporter line was generated using Clustered Regularly Interspaced Short Palindromic Repeats (CRISPR)/Cas9 at first. Previous studies have shown the impact of pharmacological perturbance of contractility on the overall colony morphology. To investigate the specific role of the NMIIB isoform in maintenance of colony morphology, a partial NMIIB knock out was performed in hiPSC colonies. Additionally, to examine the contribution of the cell-spanning actomyosin ring to colony morphology, a defined 2.5D microenvironment acting as a mechanical barrier was fabricated using direct laser writing.

Finally, the influence of different cytomechanics on pluripotency regulation was investigated. In mESCs, membrane tension was shown to drive cell fate decisions. Thus, proteins associated with generating cortical membrane tension in hiPSC colonies were identified. Colonies were treated with inhibitors interfering with either contractile tension or cortical membrane tension. Subsequently, immunostaining of early differentiation markers was conducted to observe spontaneous differentiation.

3 Materials and Methods

3.1 Materials

In the following part, all materials are listed which were used for conducting this work.

3.1.1 Chemicals and Compounds

Table 1: Substances

Substance	**Supplier** **Product number**	**Final concentration**
β-Mercaptoethanol	Sigma Aldrich M6250	5 %
(−)-Blebbistatin	Sigma Aldrich B0560	10 µM
Bovine serum albumin (BSA)	Sigma Aldrich A4503	5 %
Cell Lysis Buffer (10X)	Cell Signaling Technology 9803	1x
Dimethylsulfoxid (DMSO)	Sigma Aldrich #D2650-5X5ML	N/A
DMEM (Dulbecco's Modified Eagle Medium)	PAN-Biotech GmbH #P04-03590	N/A
DMEM/F12 + GlutaMAX (1X)	Gibco #10565-018	N/A
dNTPs	Biozym #331520	10 mM each
Doxycyclin hyclate	Sigma-Aldrich, Inc. #D9891	1 µg/ml
DreamTaq buffer	ThermoFisher Scientific #EP0702	1x
DreamTaq DNA Polymerase	ThermoFisher Scientific #EP0702	5 U/µl
Dynabeads™ Protein G	ThermoFisher Scientific 10003D	~30 mg/ml
Ezrin Inhibitor, NSC668394	Sigma Aldrich 341216	10 µM
Geltrex™ LDEV-Free, hESC-Qualified, Reduced Growth	FisherScientific 11612149	1 %

Factor Basement Membrane Matrix		
Irgacure819	Ciba AG #024475001PS04	2 %
iMatrix-511	Nippi #381-07363	2.4 µg/ml
KnockOut Serum Replacement (KSR)	ThermoFisher Scientific #10828010	20 %
Lipofectamine™ Stem Transfection Reagent	Thermo Fisher Scientific STEM00003	N/A
Matrigel® hESC-Qualified Matrix	Corning Incorporated #354277	1%
mTeSR™ Plus Basal Medium	STEMCELL Technologies Inc. #05826	80%
mTeSR™ Plus 5x Supplement	STEMCELL Technologies Inc. #05827	20%
Mowiol	Merck #475904	20 %
Normocin	InvivoGen #ant-nr-1	50 µg/ml
Paraformaldehyde (PFA)	Merck #30525-89-4	4 %
Penicillin/Streptomycin (P/S)	Gibco #15140-122	1 %
Pentaerythrit-triacrylat (PETA)	Sigma-Aldrich #246794	
Phosphate Buffered Saline w/o Ca^{2+} and Mg^{2+}	Pan Biotech #P04-36500	N/A
Phosphate Buffered Saline with Ca^{2+} and Mg^{2+}	Corning #21-030-CVR	N/A
ReLeSR™	STEMCELL Technologies Inc. #5872	N/A
Sulfo-SANPAH	ThermoFisher Scientific #22589	5 mg/ml
Tetramethylethylendiamin (TEMED)	Roth #2367.3	1 %

SuperSignal™ West Pico PLUS Chemiluminescent Substrate	Thermo Fisher Scientific #34580	N/A
Triton-X	Carl Roth #3051.1	0.1 %
TrypLE™ Select Enzyme (1X), without phenol red	Gibco™ ThermoFisher Scientific #12563011	N/A
Y27632 (ROCK inhibitor)	STEMCELL Technologies Inc. #72304	10 µM

3.1.2 Buffers and Solutions

Table 2: Buffers and solutions

Name	**Ingredients**	**Final concentration**
Cytoskeleton extraction buffer (CEB)	EGTA	1 mM
	Magnesium chloride	1 mM
	PIPES	0.1 mM
	Triton X-100	0.5 % (w/v)
F12 medium	F12 powder	10.6 g/L
	Sodiumcarbonate ($NaHCO_3$)	1.18 g/L
	pH 6.5 to 6.7	
	after sterile filtration pH 7	
Freezing medium	mTeSR Plus	70 %
	KSR	20 %
	DMSO	10 %
	ROCK inhibitor (Y27632)	10 µM
	Doxycyclin	1 µg/ml
	Normocin	50 µg/ml
Laemmli buffer 10x	Tris	0.25 M
	Glycine	1.92 M
	SDS	1 %
	pH 8.3	
Matrigel coating solution	DMEM/F12	99 %
	Matrigel	1 %
PBS-T	Triton X-100	0.1 %
	PBS	99.9 %

	pH 7.4	
Post-FACS recovery medium	Conditioned sterile mTeSR : mTeSR	1:1
	Human recombinant bFGF	10 ng/ml
	Doxycyclin	1 µg/ml
	Normocin	50 µg/ml
	ROCK inhibitor (Y27632) (day 1 after FACS)	10 µM
RCA cleaning solution	Milli-Q water	150 ml
	30% H_2O_2 aq.	30 ml
	28% NH_3 aq.	30 ml
Rinse medium	DMEM : F12	1:1
SDS buffer (2x)	SDS	5 % (w/v)
	Glycerol	5 % (v/v)
	Tris-HCL	125 mM
	Bromophenol blue	0.01 % (w/v)
	β-Mercaptoethanol	5% (v/v)
Skim milk solution	PBS-T	95 %
	Skim milk powder	5%
Vinyltrimethoxysilane solution	Toluene	195 ml
	Vinyltrimethoxysilane	5 ml
Western blot buffer	Glycine	146.5 mM
	Tris	19.8 mM
	Methanol	25%

3.1.3 Antibodies

Table 3: Primary antibodies

Antigen	Host species Type	Supplier	Stock concentration	Dilution
Brachyury	Goat, polyclonal IgG	R&D Systems, #AF2085	0.2 mg/ml	1:200
hEzrin	Rabbit, monoclonal IgG	R&D Systems, #MAB7239-100	0.5 mg/ml	1:200
hEzrin	Rabbit, monoclonal IgG	Abcam, #ab40839	0.791 mg/ml	2µg (Co-IP)
HNF-3β/FOXA2	Goat, polyclonal IgG	R&D Systems, #AF2400	0.2 mg/ml	1:200
SOX1	Rabbit, polyclonal IgG	Abcam, #ab87775	1 mg/ml	1:200
SOX2	Mouse, monoclonal IgG	Abcam, #ab171380	1 mg/ml	1:200
NANOG	Rabbit, monoclonal IgG	Cell Signaling Technology, #4903S	11 µg/ml	1:200
NM Heavy Chain IIA	Rabbit, polyclonal IgG	BioLegend, #909801	1 mg/ml	1:500
NM Heavy Chain IIB	Rabbit, polyclonal IgG	BioLegend, #909901	1 mg/ml	1:500
OCT3/4	Mouse, monoclonal IgG	Santa Cruz, #sc-5279	0.2 mg/ml	1:100
hPodocalyxin	Goat, polyclonal IgG	R&D Systems, #AF1658-SP	0.2 mg/ml	1:200 (ICC) 2 µg (Co-IP)
YAP	Mouse, monoclonal IgG	Santa Cruz #sc-101199	0.1 mg/ml	1:300

Table 4: Secondary antibodies

Antigen	Conjugate	Host species	Supplier	Stock concentration	Dilution
Mouse IgG	Alexa 568	Donkey	Invitrogen, #A10037	2 mg/ml	1:200
Mouse IgG	Alexa 647	Goat	Life Technologies, #A21236	2 mg/ml	1:200
Mouse IgG	647	Donkey	Invitrogen, #A31571	2 mg/ml	1:200
Rabbit IgG	Alexa 568	Donkey	Invitrogen, #A10042	2 mg/ml	1:200
Rabbit IgG	Cy5	Donkey	Jackson Immunoresearch, #711-175-152	1.5 mg/ml	1:200
Diverse IgG (VeriBlot)	HRP	N/A	Abcam, #ab131366	0.04 g/ml	1:200

Table 5: Affinity probes

Antigen	Dye	Supplier	Stock concentration	Dilution
Actin (Phalloidin)	Alexa 488	Life Technologies, #A12379	300 units	1:200
Actin (Phalloidin)	Alexa 568	Life Technologies, #A12380	300 units	1:200
Actin (Phalloidin)	Alexa 647	Life Technologies, #A22287	300 units	1:100
DNA	DAPI	Roth, #6335	5 mg/ml	1:500

3.1.4 Plasmids and Primers

Table 6: Plasmids

Plasmid	Features	Supplied by
pMK-RQ_GFP-MYH10	Donor plasmid with homology arms and linker-GFP sequence for N-terminal tagging of human *MYH10*	Dr. Kai Weißenbruch
pX335-U6-Chimeric_BB-CBh-hSpCas9n(D10A): GFP-MYH10 – sgRNA2a	sgRNA against MYH10 (human), to induce single-strand nick (for paired single-strand nick approach)	Dr. Kai Weißenbruch
pX335-U6-Chimeric_BB-CBh-hSpCas9n(D10A): GFP-MYH10 – sgRNA2b	sgRNA against MYH10 (human), to induce single-strand nick (for paired single-strand nick approach)	Dr. Kai Weißenbruch
pSPCas9 (BB)-2A Puro V2.0 : MYH10-KO (T1)	sgRNA sequence against MYH10 (human) implemented	Dr. Kai Weißenbruch

Table 7: Primer sequences

Primer	Orientation	Sequence (5' → 3')	T_m
5'fwdr	sense	CCTCTGCTAGCCCTTTGTGA	57 °C
GFP rev	antisense	GATGTTGCCGTCCTCCTTGA	57 °C
MYH10 LHA	sense	GCAAACCCATCAGACAACCA	56 °C
MYH10 RHA	antisense	ATTCTCTGCCAACTCCACCA	56 °C

3.1.5 Microscopes and Devices

Table 8: Microscopes and objectives

Description	Manufacturer	Objective
AxioObserver Z1	Carl Zeiss	LD A-Plan 20x/0.35 EC Plan-Neofluar 40x/0.75
Axio Imager.Z1	Carl Zeiss	Achroplan 20x/0.5 w Ph2
LSM 800	Carl Zeiss	Plan-Apochromat 40x/1.4 Oil Plan-Apochromat 20x/0.8

Table 9: Devices

Description	Manufacturer	Application
Amersham Imager 600	GE Health Care	Documentation of gels and western blot membranes
Nanoscribe Photonic Professional	Nanoscribe	Fabrication of 2.5D substrates
Thermocycler PTC-200 DNA Engine Peltier Thermal Cycler	MJ Research	PCR amplification

3.2 Methods

3.2.1 Cultivation of hiPSCs

For this work, two fibroblast-derived hiPSC cell lines were used, namely D1 and 253G1. The hiPSC line D1 was kindly provided by the group of Prof. Dr. Jochen Utikal at the German Cancer Research Centre in Heidelberg. The cell line 253G1 was purchased from RIKEN Cell Bank in Japan.

Cell Culture Routine

To ensure pluripotency and enable growth of hiPSC colonies, hiPSCs were maintained in feeder-free conditions in mTeSR Plus medium at 37°C, 5% CO_2 in a humidified incubator. The culture medium was supplemented with Normocin and Doxycyclin in a final concentration of 1 µg/ml and 50 µg/ml, respectively. Cultivation and experiments were performed on Matrigel coated dishes or cover slips. Matrigel is a solubilized basement membrane solution composed of a variety of extracellular matrix proteins, including Laminin, Collagen IV, and growth factors. It is extracted from the Engelbreth-Holm-Swarm mouse sarcoma. Routine cultivation of hiPSCs included daily manual cleaning of hiPSC colonies by removing differentiated cells at the edge of the colonies and 3D cellular aggregates using a pipet tip. Afterwards, the colonies were washed three times with DMEM/F12, followed by adding new culture medium. To avoid 3D cellular aggregates and minimize the risk of spontaneous differentiation, the hiPSCs were passaged once per week. Prior to that, coating of 6-well plate with Matrigel was carried out by adding 1 ml of Matrigel and DMEM/F12 in a ratio of 1:100. The well plate was sealed with Parafilm and incubated for at least one hour at room temperature. The medium was aspirated from the well and exchanged with 2 ml of culturing medium for 24 h or 4 ml for 48 h. For passaging hiPSCs, colonies were picked manually and transferred into Matrigel-coated wells.

Seeding

Throughout this work, hiPSCs were seeded as colonies using ReLeSR or as single cells using TrypLE, depending on the need for the experiment. For seeding with ReLeSR, hiPSCs were washed once with PBS w/o Ca^{2+} and Mg^{2+} before adding 1 ml of ReLeSR to one 6-well for 30 sec. Next, ReLeSR was aspirated and the cells were incubated for 5 min at 37 °C. To loosen the cell adherence, the plate was tapped to the bench surface for roughly 30 sec. Afterwards, the cells were suspended in 2 ml mTeSR, supplemented with Normocin, and Doxycyclin, and transferred in a 15 ml reaction tube. Colonies were seeded in a ratio of 1:20. For single cell seeding, hiPSCs were also washed once with PBS w/o calcium and magnesium before adding 200 µl of TrypLE to one 6-well. After incubation for 3 min at 37 °C, cells were suspended in 3 ml mTeSR, transferred to a 15 ml reaction tube and centrifuged at 180 x g for 2 min. The collected cells were resuspended in 1 ml mTeSR supplemented with Normocin, Doxycyclin and 10 µM ROCK inhibitor (Y-27632) to enhance cell survival upon dissociation. After seeding, the cells were cultured for 48 h, with the culture medium being changed to mTeSR without ROCK inhibitor after 2 h. This allowed for actomyosin ring formation and prevented the priming effect of Y-27632 on hiPSCs (Maldonado et al., 2016). The seeding ratio was adjusted to the experimental set-up.

3.2.2 Immunocytochemistry

The standard immunostaining procedure of hiPSCs was conducted in a humidified chamber at RT. Detailed steps are listed in the following (Table 10).

Table 10: Steps for immunocytochemistry

Step	Solution	Duration
Washing	1x PBS with Ca^{2+} and Mg^{2+}	1x
Fixation	4 % PFA in PBS	10 min
Washing	1x PBS w/o Ca^{2+} and Mg^{2+}	Once
Permeabilization	PBST (0,1% Triton X-100 in 1x PBS)	3x5 min
Incubation Primary antibody	1% BSA in PBS Primary antibody (Table 3)	1 h
Washing	PBST	3x 5 min
Incubation Secondary antibody	1% BSA in PBS Secondary antibody (Table 4)	1 h
Washing	1x PBS w/o Ca^{2+} and Mg^{2+}	Once

Cleaning of coverslip	ddH_2O	Once
Mounting	Mowiol	Once

3.2.3 Co-Immunoprecipitation

To obtain cell lysates, D1 hiPSCs were seeded with ReLeSR one day prior to lysis. The cells were washed with PBS and incubated with 100 µl cytoskeleton extraction buffer for 1 min at RT. Subsequently, 200 µl of 1x cell lysis buffer were added and incubation occurred on ice for 5 min. HiPSCs were mechanically harvested using a cell scraper and centrifuged at 4 °C with 14000 rpm for 10 min. The supernatant was harvested and stored by -20 °C for further use.

In the first step of the Co-Immunoprecipitation (Co-IP), cell lysates were incubated overnight at 4 °C with 2 µg of either ezrin or PODXL antibody for pull-down. Next, the antibody-lysate solution was transferred into 1.5 ml reaction tubes containing magnetic beads and incubated for 2.5 h at 4 °C to allow adhesion of the antibodies to the beads. After incubation, the beads were washed three times with cold cell lysis buffer on ice, followed by adding 50 µl of 2x SDS buffer + 5% β-mercaptoethanol. The solution was boiled at 80 °C for 10 min and subsequently cooled for 10 min at RT. The supernatant was used for Western blot analysis.

Western Blot Analysis

5 % Gels for SDS-PAGE were prepared to analysis the Co-IP. The composition of the separation and stacking gel is shown in Table 11.

Table 11: Solutions for preparation of 5 % SDS gels

Separation Gel	**Stacking Gel**
8.1 ml ddH20	3.4 ml ddH20
3 ml Polyacrylamid	1 ml Polyacrylamide
3.75 ml Separation Gel Buffer	1.5 ml Stacking Gel Buffer
150 µl APS (10 %)	60 µl APS (10 %)
12 µl TEMED	15 µl TEMED

First, the separation gel was prepared and covered with isopropanol. After complete polymerization, the stacking gel was prepared. The final gel was loaded with the Co-IP samples and was run at 80 V with maximum Ampere for 15 min in 1x Laemmli buffer. Subsequently, the voltage was increased to 150 V for approximately 1 hour.

The blotting of the separated proteins to a methanol activated PVDF membrane occurred at 150 mA and maximum voltage for 2 hours on ice. For detection of the proteins, the membrane was treated according to following steps described in Table 12. Finally, the visualisation was performed by the Amersham Imager 600.

Table 12: Steps for protein detection in western blots

Step	Solution	Duration / Temperature
Blocking	5 % skim milk solution	1 h / RT
Primary antibody	Antibody (Table 3) in 5 % skim milk solution	Overnight / 4 °C
Washing	PBS-Tween 20	3x15 min / RT
Secondary antibody	Antibody (Table 4) in 5 % Skim milk solution	2 h /RT
Washing	PBS-Tween 20	3 x 15 min / RT
Washing	PBS	3 x 10 min / RT
Detection	Thermo Scientific™ SuperSignal™ West Pico PLUS Chemiluminescent Substrate	3-5 min / RT

3.2.4 Generation and Validation of hiPSC Reporter Line

To generate a hiPSC line with endogenous homozygous GFP-tagged NMIIB, a paired Cas9D10 nickase plasmid-based approach by Koch and colleagues was performed using the D1 cell line (Koch et al., 2018). The donor sequence for homology-directed repair template consisted of two homology arms (each 800 bp) framing the GFP sequence (717 bp) and a linker sequence (24 bp). Since the nickase Cas9 was used, paired gRNAs were introduced in the cells, one cutting the sense and one cutting the antisense strand.

Lipofection

Firstly, hiPSCs were seeded as single cells in Matrigel coated 12-wells and cultivated for 24 h (see Section 3.2.1 Seeding). Prior to transfection, fresh medium supplemented with 10 µM ROCK inhibitor was added to the cells. The donor plasmid and the two plasmids containing Cas9D10A and the sgRNAs (see Table 6) were introduced into the cells by lipofection. The transfection was conducted according to the manufacture's protocol for Lipofectamin stem transfection reagent. The amount of used DNA was in total 1 µg per 12-well, 500 ng of the donor plasmid and 250 ng of sgRNA plasmid each. The transfection solution was incubated for 24 h before being changed to regular mTeSR culture medium for an additional 24 h. The obtained heterogenous cell culture of transfected and

untransfected-cells was pre-selected by adding puromycin in a concentration of 5 µg/ml, removing cells that didn't incorporate the donor plasmid.

For the partial NMIIB knockout experiments, the same transfection protocol was conducted with minor adjustments. D1 GFP-NMIIB cells were transfected 2 h after seeding as single cells to prevent the formation of the cell-spanning actomyosin ring.

Fluorescence-Activated Cell Sorting (FACS)

The transfected cells were maintained as described in Section 3.2.1 Cell Culture Routine or adapted to single cell passaging until harvesting for fluorescence-activated cell sorting (FACS). Firstly, ROCK inhibitor and DAPI in a final concentration of 10 µM and 10 µg/ml, were added to the cells and incubated for one hour at 37°C. Cells were harvested using TrypLE and were filtered through a 35 µm mesh cell strainer. After centrifugation, cells were resuspended in FACS buffer. FACS was performed by the FACS Core Facility at the Heidelberg University Hospital.

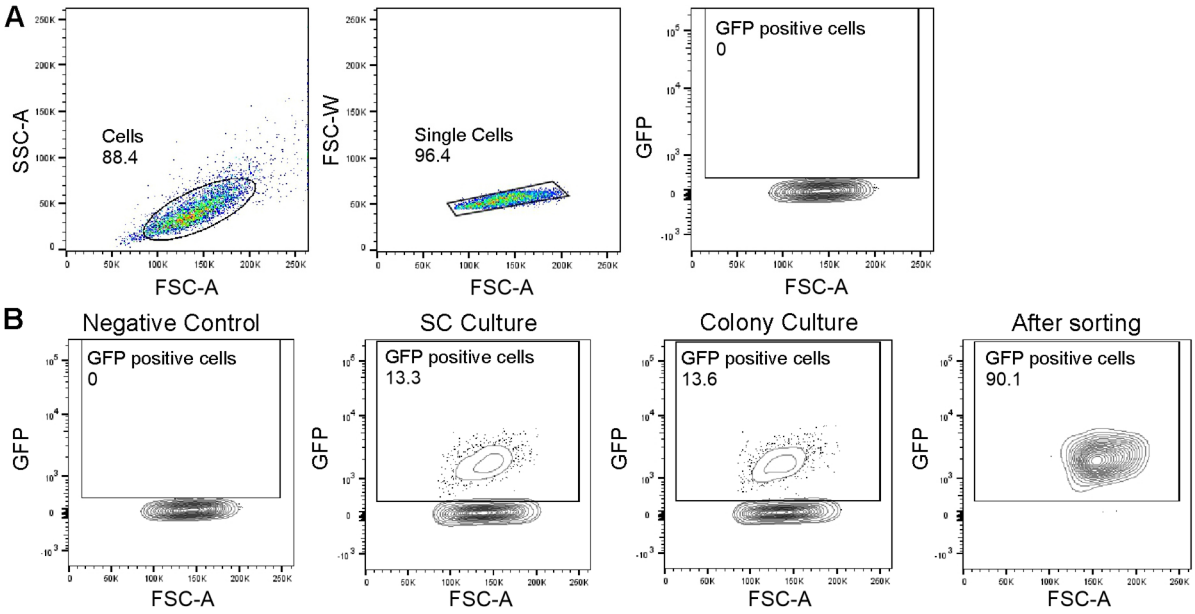

Figure 9: FACS of genome-edited hiPSCs

Transfected cells were cultivated as single cells or clumps until FACS. Untransfected D1 cells were used as a negative control. **(A)** Gateway strategy is depicted for the negative control. The plot shows the side-scatter (SSC) area versus the forward-scatter (FSC) area to gate for live hiPSCs (left plot). The plot in the middle displays the FSC area versus FSC pulse width to identify singlets. Based on the negative control, the background signal was used to define the gates for the GFP+ cells accordingly (indicated by the black polygon). The numbers within the plot indicate the percentage of cells, single cells and GFP positive cells, respectively. **(B)** The plots show, from left to right, the intensity of GFP for cells of the negative control, cells passaged as single cells, cells passaged in colonies and all selected GFP+ cells after sorting. Cells were sorted into 96-well plates to obtain single cell clones. Images were kindly compiled by Chiara Windsor, Heidelberg University Hospital.

Untransfected D1 cells were used as a negative control to define the background signal (Figure 9). Selected cells were sorted as bulk in a 24-well plate or as single cells in a 96-well plate containing post FACS-recovery medium, for expansion.

Junction Polymerase Chain Reaction and Sequencing

To analyse which single cell clones were homozygously and correctly tagged with GFP, junction PCR followed by Sanger sequencing was performed. For that, genomic DNA (gDNA) of hiPSCs cultivated in a 6-well was extracted as described in the following.

gDNA Extraction

First, hiPSCs were washed once with PBS w/o Ca^{2+} and Mg^{2+} followed by adding 500 µl of DNA lysis buffer. Using a cell scraper, the cells were detached from the 6-well and transferred to a 1.5 ml reaction tube. After incubation for 1 h at 56 °C and subsequently 10 min at 95 °C, the cell lysate was centrifuged for 5 min at 10000 x g. To purify the gDNA, ethanol precipitation was performed. For that, 10% volume of the gDNA in the form of sodium acetate and 110% in the form of ice-cold isopropanol were added to the supernatant and mixed thoroughly before storing the mixture at -20 °C for 30 min. To collect the DNA, centrifugation was conducted at 17000 x g for 30 min at 4 °C, followed by washing the pellet with 1 mL ice-cold ethanol. This step was repeated until the pellet occurred transparent. Finally, the ethanol was aspirated and the pellet was left to dry for 5 min at RT, before dissolving it in nuclease-free water at RT.

Polymerase Chain Reaction (PCR)

For amplification of gDNA, DreamTaq polymerase was used. Two primer sets were needed to (1) validate the correct insertion of the GFP tag and (2) check for homo- or heterozygously tagged NMIIB. The used primers, PCR mixes and cycling conditions are shown in Table 7, Table 13 and Table 14, respectively. The PCR products were transferred to a 1 % agarose gels, containing 0.005 % ROTI® GelStain, and run at 85 V. For documentation, the Amersham Imager 600 was used.

Table 13: Reaction mix for PCR

Component	Volume	Final concentration
DreamTaq Buffer	5 µl	1x
dNTPs	1 µL	0.2 mM
Primer, each	1 µL	0.2 µM
DNA	X	0.2 ng/µL
DreamTag Polymerase	0.25 µL	0.025 U/µL
H_2O	Add to 50 µL	

Table 14: Cycling sequence for PCR reaction mixes

Step	Temperature	Time	Cycles
Initial Denaturation	98 °C	30 sec	1
Denaturation	98 °C	10 sec	
Annealing	See Table 7	30 sec	35
Elongation	72 °C	30 sec /kb	
Final Elongation	72 °C	5 min	1
Storage	4 °C	forever	

The amplified DNA was extracted from the gel for Sanger sequencing. For that, the desired fragments were cut out and were treated with the Monarch PCR & DNA Cleanup Kit (New England Biolabs, #T1030S/L), according to the manufacture's protocol. Purified samples were sent to Eurofins for sequencing and the results were analysed using CLC Viewer.

3.2.5 Live Cell Imaging

To observe the formation and dynamics of cytoskeleton structures associated with NMIIB, live cell imaging (LCI) was performed using the D1 GFP-NMIIB reporter line. For that, the AxioObserver Z1 microscope equipped with an incubation chamber was used. Cells were seeded as clumps in petri dishes with a glass bottom (MatTek Corporation, 35 mm, No.1.5) or on gridded glass coverslips glued in a petri dish with PDMS (ibidi, #10816). In both cases, the surfaces were coated with Matrigel prior to seeding. Imaging occurred after 2 h in the incubator to allow the cells to adhere to the surface. To observe formation of cytoskeleton structures, cells on the petri dishes with glass bottom were imaged every 20 min as long as possible.

To investigate the dynamics of the cell-spanning actomyosin ring, cells on the gridded glass coverslips were imaged at three time points: (1) 2 h after seeding, (2) after treating the cells with either 10 µM Blebbistatin or DMSO for 6 h, and (3) after cultivating the cells without Blebbistatin or DMSO for an additional 16 h. Between the acquisition time points, cells were kept in the incubator. Based on the morphology of the actomyosin cell-spanning ring at the three time points, colonies were classified into one of three categories (Figure 10). The first category displays an intact, continuous visible myosin ring at the apical side of the colony. The second category shows one discontinuation in the ring, thus being slightly disturbed. The third category is called disturbed and describes a myosin ring with multiple interruptions. Only colonies classified as intact at the initial time point were included in the experiments. Since NMIIB is accumulated in the intersections of the cell-spanning actomyosin ring, immunostaining with Phalloidin was performed after the LCI to verify a continuous ring.

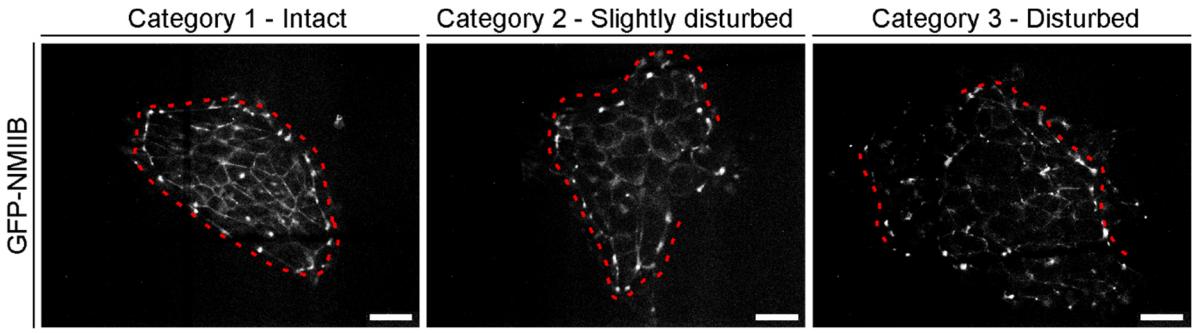

Figure 10: Morphology of cell-spanning actomyosin ring corresponding to the three categories

D1 GFP-NMIIB were imaged and classified at the start of the experiment, after 6 h of inhibitor treatment and after 16 h of cultivation without inhibitor. Each category is characterized by the appearance of the actomyosin ring, indicated by the dotted red line. Colonies belonging to the first category display a continuous ring. The second and third categories show a disturbance in the ring to varying degrees, namely one interruption for category two and multiple for category three. Scale bar: 50 µm.

3.2.6 Fabrication of 2D βCD-Ad Gels

βCD-Ad gels with a stiffness of 2 kPa were produced during a research stay at the Center for Integrative Medicine and Physics, Institute for Advanced Study, Kyoto University. First, round cover slips with a diameter of 30 mm were cleaned using the modified RCA method (Hillebrandt & Tanaka, 2001) to allow silanisation with vinyltrimethoxysilane solution overnight. The gels were prepared as described previously (Linke et al., 2024) with minor alternations. In detail, 89.2 mg 6-acrylamido–βCD (βCD-AAm), 15.4 mg adamantane-

acrylamide (Ad-AAm) and 416.6 mg acrylamide (AAm) were used. To allow adhesion of 253G1 hiPSCs, iMatrix-511 was covalently bound to the gel surface using a Sulfo-SANPAH photo-crosslinker. The cells were seeded as single cells at a density of $0.6x10^5$ cells/ gel. Cultivation on the gels occurred for 48 h at 37 °C, with a medium change after 2 hours to mTeSR without ROCK inhibitor and a medium change after 24 hours.

3.2.7 Fabrication of 2.5D Scaffolds

The 2.5D scaffolds, called mechanical barriers in this work, were fabricated using direct laser writing (DLW). DLW is a two-photon lithography process where a liquid photoresist is polymerised due to the absorption of two photons by a photoinitiator. For that, a femtosecond-pulsed laser is focused into the photoresist using a high N.A. objective.

The mechanical barriers were produced using one of two photoresists, namely Pentaerythritol triacrylate (PETA) or acrylate-functionalized canola oil (oil ink). Oil ink based mechanical barriers were provided by Clara Vazquez-Martel from the Institute for Molecular Systems Engineering and Advanced Materials, Heidelberg University.

Laser Writing Procedure

First, silanisation of 22 mm x 22 mm coverslips was performed to achieve a better adhesion of the printed 2.5D scaffolds. For that, coverslips were cleaned with isopropanol and blow-dried with nitrogen before plasma activation for 10 min. Afterwards, the pre-treated coverslips were stored in a solution of 1 mM 3-methacryloxypropyltrimethoxysilane and toluen for 1 h to allow the silanisation process. Finally, the coverslips were washed with ddH2O and blow-dried.

The job file containing the blueprint and writing parameters of the mechanical barriers was designed using Blender and DeScribe. For writing the scaffolds, a 63x oil immersion objective N.A. 1.4 was used and the writing parameters were set to 60 % laser power and a speed of 12500 µm/s for PETA based scaffolds. The silanised coverslips were placed into a sample holder and a droplet of the photoresist was added before the writing process. Multiple samples could be written in one sitting. After the writing process was finished, the scaffolds were developed in 1:1 isopropanol and acetone overnight to remove unpolymerised photoresist monomers.

The mechanical properties of the barriers written with PETA or oil ink were characterized by Clara Vazquez-Martel. For that, nanoindentation was performed on a Bruker Hysitron TI 980 Nanoindenter equipped with a BioXR transducer with a long shaft and adiamond Berkovich tip. The elastic modulus and the hardness values of the photoresists were measured in a dry state and after 24-hour storage in cell culture medium. Measurements of elastic modulus were used to calculate the Young's modulus, depicted in Figure 11. PETA has a Young's modulus of approximately 1 GPa when used in cell culture experiments. The oil ink has a Youngs modulus of 20 MPa under the same conditions.

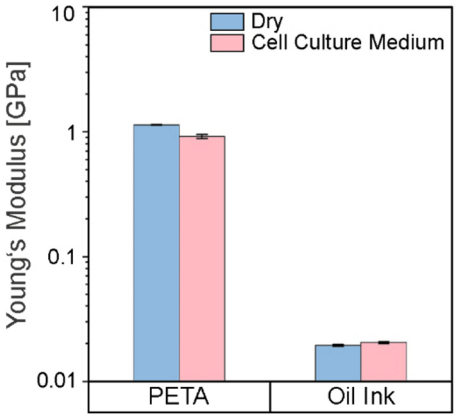

Figure 11: Young's modulus of PETA and oil ink

The mechanical properties of the scaffolds, written with either PETA or oil ink, were characterized by Clara Vazquez-Martel, IMSE and AM, Heidelberg University. For that, nanoindentation was performed to measure elastic modulus in a dry state and after submerging written structures in cell culture medium for 24 h. The results were used to calculate the Young's modulus for each condition. The Young's moduli applicable in cell experiments were 1 GPa for PETA and 20 MPa for oil ink, respectively.

Cultivation in Mechanical Barriers

To enhance cell viability, the scaffolds were washed twice with isopropanol and three times with PBS for 10 min each, prior to Matrigel coating. Single cell seeding of D1 GFP-NMIIB hiPSCs was conducted according to steps described in Section 3.2.1 in a 1:5 ratio. Seeded cells were incubated for 48 h at 37 °C with a medium change after 2 h to mTeSR without ROCK inhibitor and a medium change after 24 h. After immunostaining, colonies cultivated in mechanical barriers were classified into one of two categories, depending on the appearance of the NMIIB filaments associated with the cell-spanning actomyosin ring. If the GFP-NMIIB signal displayed a ring-like structure, colonies were classified as category one. The second category was characterized by scattered NMIIB filaments forming no or a partwise ring-like structure.

3.2.8 Inhibitor Treatments

The impact of cytomechanics on pluripotency regulation was tested by inhibitor treatments. To perturb the contractile tension or the cortical membrane tension, 10 µM Blebbistatin or ezrin inhibitor was added, respectively. As a control, colonies were treated with DMSO in parallel with the inhibitor treatments. The inhibitors were added to the media 2 h after clump seeding and incubated for 24 h before immunostaining with pluripotency markers or early differentiation markers. The experiments with ezrin inhibitor were performed by a student under supervision.

3.2.9 Image Processing, Quantitative Analysis and Statistics

Microscope images of immunostaining were acquired using a confocal laser scanning microscope LSM800 with the Zen blue imaging software (Zeiss). Image processing was conducted using Fiji by ImageJ. Representative images were adjusted in contrast and brightness, while images used for analysis of intensity measurements remained unprocessed. Unspecific fluorescence signal of the background was subtracted by measuring the mean intensity of the background at four different positions outside the colonies. The mean value of these four measurements was subtracted from the mean fluorescence intensity measured for the protein of interest (POI). 3D reconstructions of immunostainings were generated using the software Imaris (Oxford instruments). Compilation of figures was carried out with CorelDraw Graphics Suite 2022 (Corel Corporation).

Analyses of the results as well as statistical tests were performed in Excel (Office 365, Microsoft) or Origin 2022b (OriginLab). The p-values are depicted as $p \leq 0.05$ = *, $p \leq 0.01$ = ** and $p \leq 0.001$ = ***. The number of individual experiments is represented by N and the number of individual colonies of one experiment is represented in n.

Calculation of Transcription Factor Ratios

To measure the mean fluorescence intensity of transcription factors, a mask of the cell nuclei was created using a threshold on the DAPI channel, followed by using the “Fill holes” and Watershed separation plugin of Fiji (Figure 12A). Next, the particles were analysed to select regions of interest (ROI) for the individual nuclei. The particle size was restricted to 25 – 450 µm. ROIs selecting cells undergoing mitosis or apoptosis were excluded. In the last step, the defined ROIs were used to measure the mean fluorescence intensity of the respective transcription factor to calculate the ratio. To analyse the difference in transcription factors between the inner and outer populations, actin staining was used to determine the region that is encircled by the actomyosin ring (Figure 12B) Based on that outline, the cell nuclei were selected for the inner or outer population.

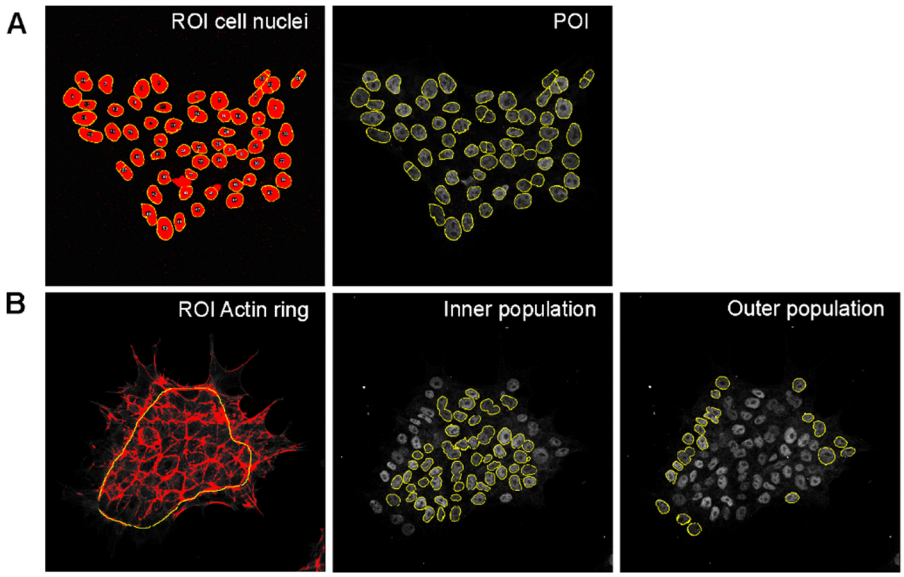

Figure 12: Quantification of transcription factors fluorescence intensities

The mean intensity of early differentiation markers, pluripotency markers and YAP was measured in ROIs defined by the DAPI signal. **(A)** The area covered by DAPI was used to define ROIs for the individual cell nuclei to measure the desired protein of interest (POI). **(B)** To determine which cell belongs to the inner or outer population, actin staining is used to specify the outline of the cell-spanning actomyosin ring.

Quantification of Proteins in z Direction

To evaluate the distribution of apical markers in the z direction, optical sections of hiPSC colonies were obtained with a section distance of 1 µm.

For measurements of PODXL distribution, two ROIs at different height positions in the colony were defined: (1) at the basal side of the colony, attached to the substrate and (2) at the position of the cell-spanning actomyosin ring. The ROIs were selected by using the actin staining as described above. A fold change of mean intensity at position (2) with respect to the value of position (1) was calculated, showing the increase or decrease of PODXL at an apical position.

A ROI matching the size of the barrier was selected to quantify ezrin distribution within colonies cultivated in mechanical barriers. The mean intensity of ezrin within this ROI was then measured for all 25 optical sections, corresponding to the height of the barrier. The intensity values for each colony were normalized from 0 to 1, followed by averaging all curves belonging to the same category. This was performed for mechanical barriers written with PETA or oil ink, respectively.

4 Results

HiPSCs self-organise actin cytoskeletal structures, which exert in association with NMII cellular contractility. These two structures are the previous-published actin fence and the here described cell-spanning actomyosin ring. The forces generated by the actin fence at the basal side of the colonies are well described by Narva and colleagues (Narva et al., 2017). The here presented work characterises the cell-spanning actomyosin ring, which is located at the apical side of hiPSC colonies. Furthermore, it investigates the influence of contractile tension generated by NMIIB on both hiPSC morphology and pluripotency regulation. In the following sections, the results of the individual experiments are described, revealing the central role of the cell-spanning actomyosin ring in hiPSC colonies.

4.1 Apical Actomyosin Organisation in hiPSC Colonies

The apical side of hiPSC colonies is characterized by a continuous cell-spanning actomyosin ring, which divides the cells into an inner and outer population as observed during preliminary work (Genthner, 2020). The cells of the inner population display a network of pronounced actin fibres. Immunostainings of NMII isoforms show co-localisation with the actin cytoskeleton (Figure 13).

NMIIB is strongly associated with the actin network covering the apical side and the actin ring. Accumulation of NMIIB is especially prominent in the ring, displaying an alternating pattern of NMIIB cluster (Figure 13, upper panel, zoom in). In contrast, NMIIA is not restricted to the localisation of the actin network and ring but is also distributed throughout the colony (Figure 13, bottom panel).

To assess the general relevance of the cell-spanning actomyosin ring in colony architecture, hiPSCs of the fibroblast-derived cell line 253G1 were cultivated on the protein coating iMatrix-511, a standard PSC culture matrix consisting of recombinant laminin-511 E8 fragments. The colony displays an evident actomyosin ring on the margin as seen for hiPSCs of the D1 cell line (Figure 14A, Figure 13). In addition, during a supervised master thesis, it was confirmed that the cell-spanning ring is also self-organized by peripheral blood-derived hiPSCs (A. Fischer, 2022). Collectively, these observations reveal that the cell-spanning actomyosin ring is formed independently of the hiPSC cell line or used protein coating.

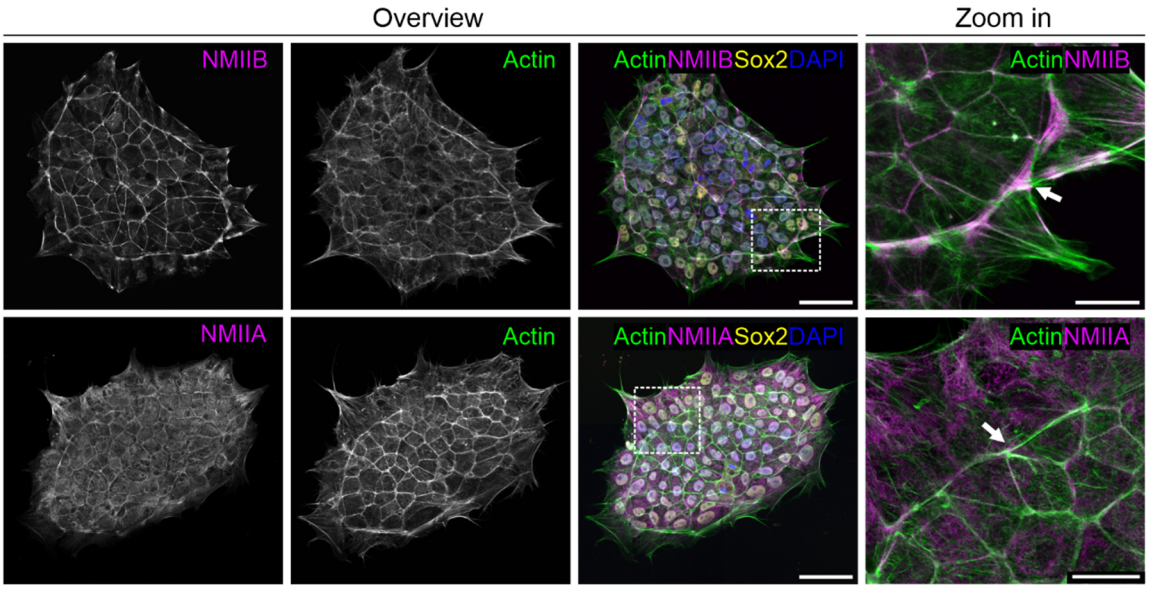

Figure 13: NMIIB is associated with the cell-spanning actomyosin ring

D1 hiPSCs were cultivated for 24 h and subsequently immunostained for the isoforms NMIIA and NMIIB (magenta), actin (green), SOX2 (yellow) and nuclei (blue). NMII is associated with the cell-spanning ring and the actin network covering the apical side of hiPSC colony. The isoform NMIIB primarily co-localises with these structures, whereas NMIIA is also present throughout the colony. The magnified area reveals an alternating accumulation pattern of NMIIB along the actin ring. The area of magnification is indicated by the white dotted polygon. Scale bar overview: 50 µm, zoom in: 15 µm.

To demonstrate that the contractile tension exerted by the actomyosin ring may also play a role in the *in vivo* situation, hiPSCs were cultivated on 2kPa soft βCD-Ad gels (Figure 14B). This value refers to the stiffness that cells in the ICM experience in the early embryo. The immunostaining of colonies cultivated on the gel shows that an actomyosin ring is visible, however the co-localisation of NMIIB with the actin stress fibres is not as prominent as on the glass control (Figure 14B, indicated with a red dotted line). Instead, NMIIB is also located throughout the colony (Figure 14B, bottom panel).

Taken together, the results reveal that the cell-spanning ring forms independently of cell line, matrix composition or substrate stiffness, indicating that it is a conserved cytoskeletal structure in hiPSCs.

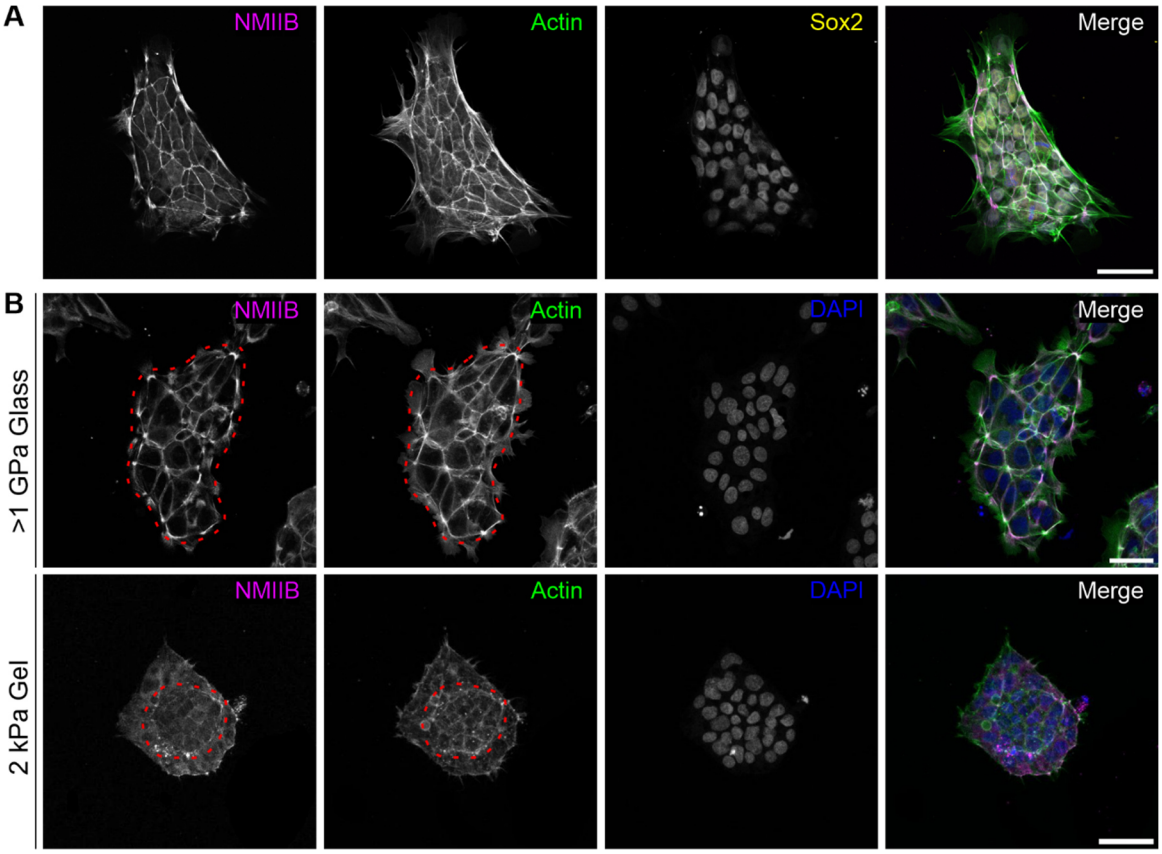

Figure 14: The cell-spanning ring is a conserved cytoskeleton structure in hiPSCs

HiPSCs of the cell line 253G1 were cultivated on iMatrix-511 and immunostained. The observed cellular components are NMIIB (magenta), actin (green), SOX2 (yellow) and nuclei (blue). **(A)** 253G1 colony displays a characteristic actomyosin ring, connecting cells in the periphery. **(B)** HiPSCs were cultivated on glass coverslips or 2kPa gels, both coated with i-Matrix-511. The immunostaining shows that colonies self-organise actomyosin rings independent of substrate stiffness. However, stress fibres are more prominent on the glass substrate. In addition, NMIIB localisation is not restricted to the actin ring but is rather distributed throughout the colony. Scale bar (A) and (B): 50 µm.

4.2 Dynamics of the Cell-Spanning Actomyosin Ring

To further characterize the cell-spanning actomyosin ring and determine the dynamics of the cytoskeleton structure, LCI was performed. As previously presented, the NMIIB isoform is strongly associated with the actin ring. Thus, a GFP-NMIIB reporter line was generated as described in Section 3.2.4.

After FACS, isogenic D1 GFP-NMIIB clones were analysed to identify candidates with the correct insertion of the GFP tag for use in LCI experiments. First, the localisation of the fusion protein was validated via immunostaining. The cells show an endogenous GFP-NMIIB signal that is overlapping with the signal of the NMIIB antibody staining (Figure 15A). The actin channel shows a characteristic network of actin fibres that co-localise with the NMIIB signal, both for the GFP-NMIIB and the NMIIB antibody staining.

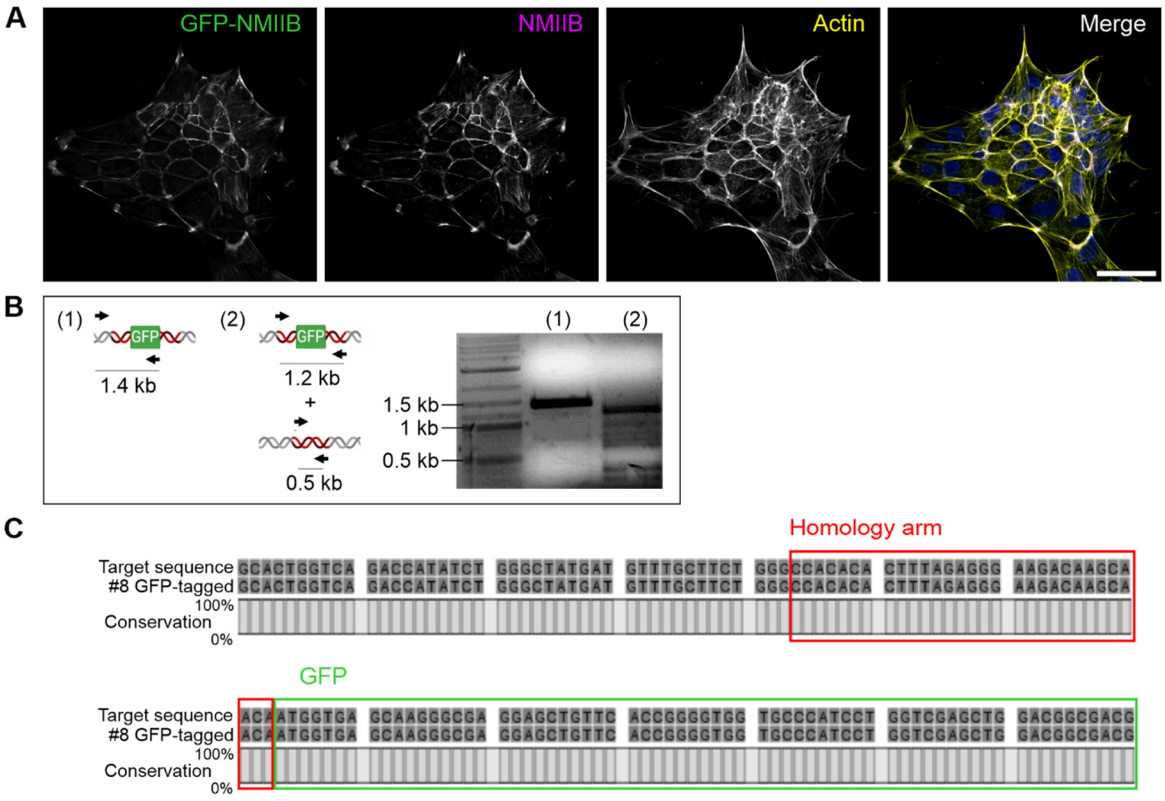

Figure 15: Generation and validation of D1 GFP-NMIIB reporter line

(A) Immunostaining of NMIIB displays an overlapping signal with the endogenous GFP-NMIIB signal. The merge channel highlights the association between NMIIB and actin. **(B)** Junction PCR was conducted to test the integration of GFP into the correct locus, as well as to determine whether all alleles were tagged. For this, two primer sets were used, and their binding sites are illustrated in the scheme on the left. **(C)** Sanger sequencing at the target site. The sequences of tagged NMIIB in clone 8 were aligned to the target sequence, including the homology arm and GFP sequence. The red box and green box indicate the correct insertion of the homology arm and GFP tag, respectively, in the genome. Scale bar (A): 50 µm.

Junction PCR with two sets of primers was conducted, to test the correct integration of GFP into the NMIIB locus as well as if all alleles were tagged (Figure 15B). The first set binds outside the left homology arm, in the genomic locus, and inside the fluorescent tag. A correct insertion is shown by a band with a size of 1.4 kb. The second set binds in both flanking homology arms, thus resulting in one or two PCR products, depending on whether the tagging is heterozygous or homozygous. The results indicate that a correct homozygous insertion of the GFP sequence was successful for clone 8 (Figure 15B). Subsequently, Sanger sequencing for this clone was performed. Alignment analysis of D1 GFP-NMIIB clone 8 with the target sequence shows a correct insertion of the donor template in the genome without introducing any mutations at the insertion site (Figure 15C). Clone 8 was identified as a successful candidate and was thus used for further experiments.

Next, to observe the formation of the cell-spanning actomyosin ring, the validated GFP-NMIIB clone 8 was used in LCI experiments. To allow cell adhesion, hiPSCs were seeded as clumps and incubated for 2 h before starting imaging. Previous immunocytochemical experiments indicated that hiPSCs self-organize the cell-spanning ring within 6 h after seeding. Prolonged light exposure during imaging can lead to cell structure alterations and cell damage to the point of apoptosis, a phenomenon termed phototoxicity (Icha et al., 2017). The sensitivity to phototoxicity is thereby cell-type specific.

During LCI it was observed that hiPSCs demonstrate high sensitivity to phototoxicity. Observation of the cell-spanning ring formation required an imaging time of multiple hours, with an interval of 20 minutes. Therefore, acquisition settings were preliminarily determined to ensure cell viability, including cell culture medium and type of fluorescence microscopy techniques. The results demonstrated that the microscope technique was the major determinant for cell viability. Imaging with wide-field epifluorescence in the apical plane of the colonies allowed for the longest imaging time without inducing apoptosis. The LCI confirmed that in most instances, the formation of the ring occurred within 6 h after seeding, as shown in Figure 16.

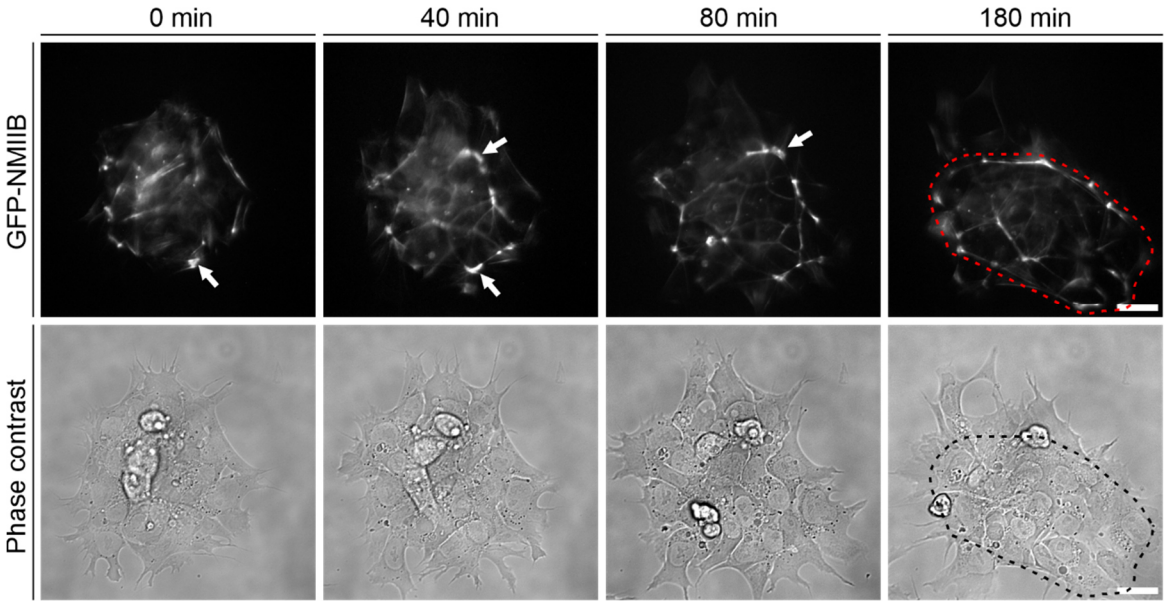

Figure 16: Formation of the cell-spanning actomyosin ring in a hiPSC colony

D1 GFP-NMIIB cells were seeded as clumps and incubated for 2 h before LCI. Images were acquired every 20 min. The upper panel shows the endogenous GFP-NMIIB signal 0 min, 40 min, 80 min and 180 min after starting LCI. The lower panel depicts the corresponding colony outline in phase contrast. Scale bar: 25 µm.

In the beginning, NMIIB is accumulated in multiple spots in the periphery of the colony, appearing as randomly organized filaments (Figure 16, indicated by arrows). After 40 minutes, the accumulation of NMIIB in the initial spots is increasing and new spots occur. Over time, with increasing cultivation time, the filaments appear more bundled, resulting in pronounced stress fibres. The characteristically distinct actomyosin network at the apical side of the colony also becomes evident. The formed cell-spanning ring, indicated by NMIIB filaments orientated in a ring-like structure (Figure 16, indicated by dotted red outline), is continuously growing and reorganised due to cell mitosis, adhesion and migration of cells into the periphery. The latter is nicely displayed in phase contrast images of the colony (Figure 16, bottom panel). A remodelling of the cell-spanning ring could also be observed during non-apoptotic blebbing of the colony.

Previous experiments with the myosin inhibitor Blebbistatin showed that the fracturing of the cell-spanning actomyosin ring leads to a loss in characteristic colony morphology. As demonstrated by the results of LCI, the cell-spanning ring is undergoing continuous re-organisation. This leads to the hypothesis that the perturbation of the actomyosin ring is reversible. To test whether this hypothesis holds true, D1 GFP-NMIIB colonies were seeded on gridded coverslips and incubated for 16 h before imaging. The gridded surface served to keep track of the colonies over the course of the experiment, since imaging

occurred at three specific time points. First, at the beginning of the experiment, second, after 6 hours of treatment with either Blebbistatin or DMSO, and third, after a 16-hour washout of the chemical compounds by cultivating the cells without them. Based on the morphology of NMIIB filaments, the colonies were classified into one of three categories: intact, slightly disturbed and disturbed. The classification into the three categories was conducted according to the criteria described in Section 3.2.5.

Figure 17A displays the morphological changes of an example colony at the specified three time points. The GFP-signal shows an initial intact NMIIB ring-like structure with clustered accumulations of NMIIB (Figure 17A, upper panel). The overall colony morphology is characteristic of hiPSCs, namely tight-packed cells with a few cell protrusions by cells in the periphery (Figure 17A, bottom panel). After Blebbistatin treatment for 6 h, the ring structure of NMIIB filaments is disturbed and the overall colony integrity is lost (Figure 17A). This is demonstrated by the spread morphology of cells, especially in the periphery, and the greater distance between cell nuclei (Figure 17A, bottom panel). Upon the removal of Blebbistatin, followed by a 16-hour cultivation, hiPSCs reorganize the cell-spanning actomyosin ring (Figure 17A, upper panel indicated by the red dotted line) and, in large part, regain their colony integrity. To verify the continuous characteristic of the actomyosin ring, immunostaining for actin was performed illustrating an intact cell-spanning ring without perturbation after washout (Figure 17B, indicated by the red dotted line). The quantification demonstrated that treatment with 10 µM Blebbistatin for 6 h leads to disturbance of the myosin ring in varying degrees, while the colonies treated with DMSO as a control show no effect. After the washout, over 60 % of the colonies display an intact ring-like structure. There is no significant difference compared to the control group, indicating that the approximately 40 % of colonies showing a slightly disturbed NMIIB ring may be the result of image acquisition rather than an inability to restore the cell-spanning ring.

The quantitative evaluation validates the observation that perturbation of the actomyosin network is reversible and thus support the hypothesis that the cell-spanning actomyosin ring is a highly dynamic cytoskeletal structure (Figure 17C).

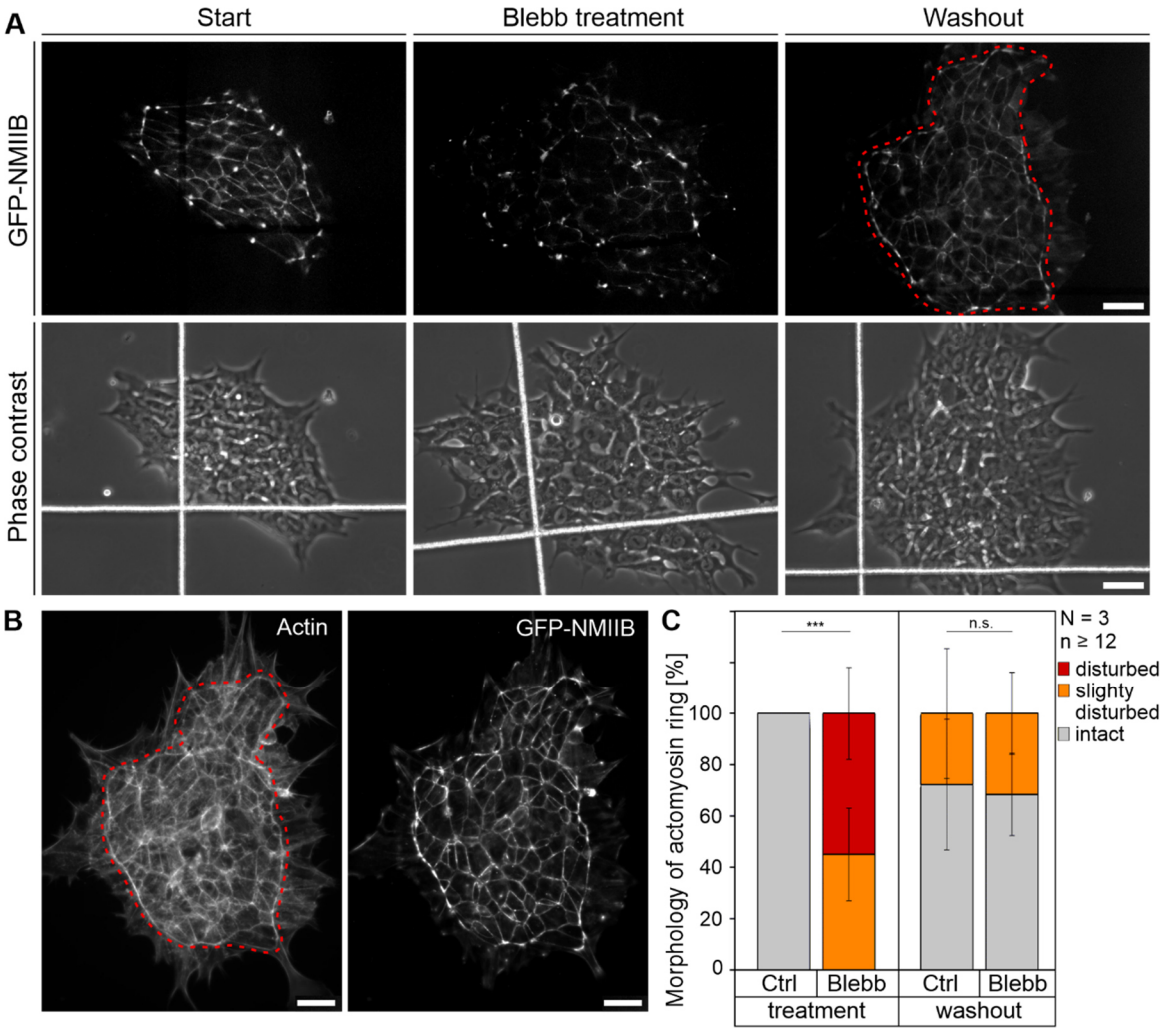

Figure 17: Re-establishment of the actomyosin ring after Blebbistatin treatment

D1 GFP-NMIIB hiPSCs were seeded as clumps on a gridded coverslip and incubated for 16 h before imaging. **(A)** A representative colony to illustrate morphological changes throughout the experiment is depicted. The GFP signal shows the organisation of the NMIIB filaments whereas the phase contrast shows the overall colony morphology. **(B)** Immunostaining of the representative colony after the washout to verify the continuous actomyosin ring. **(C)** Quantification of categories describing the morphology of the actomyosin ring. X^2-test was performed. Scale bar (A), (B): 50 µm.

In summary, these findings demonstrate that the cell-spanning actomyosin ring is a self-organized, highly dynamic cellular structure undergoing constant re-organisation. This ability to adapt and re-establish after perturbation suggests the importance of the cell-spanning ring in hiPSC colony architecture.

4.3 Contractile Tension Regulates Apical Identity in hiPSCs

It was shown in previous studies that hiPSCs exhibit a position-dependent apicobasal polarity that divides the cells of a colony into an inner and outer population (Genthner, 2020; Y. Kim et al., 2022). The inner population is characterized by an enrichment of the apical marker ezrin and thus being suggested as a potential mediator between the plasma membrane and the cell-spanning actomyosin ring.

4.3.1 Interaction of Podocalyxin and Ezrin

In kidney podocytes, PODXL is known to interact with ezrin building a complex that stabilizes the unique cell-type specific cytoskeletal structure (Orlando et al., 2001). To test whether PODXL also plays a role in hiPSCs cellular architecture and together with ezrin anchors the cell-spanning actomyosin ring, immunostaining of PODXL and ezrin was conducted.

The results demonstrate that PODXL is located in the area that is encircled by the cell-spanning actin ring (Figure 18A, upper panel indicated by white arrow). No PODXL accumulation is observed when actin fibres are not organized in a ring (Figure 18A, bottom panel). Immunostaining of PODXL and ezrin confirms co-localisation of both proteins within the actin ring (Figure 18B). To quantify the apical localisation of PODXL, the mean fluorescence intensity of the fluorescence signal was measured apical, at the position of the actin ring, and basal, near the substrate. The calculated fold change demonstrates that PODXL intensity is approximately five times higher at the position of the cell-spanning ring with respect to the signal measured near the substrate (Figure 18C). Ezrin signal also increases from the basal to the apical side of the colony. The data for ezrin was obtained during a preceding work (Genthner, 2020). The co-localisation indicates that PODXL and ezrin form a complex, as shown in podocytes, stabilizing the actomyosin ring. To verify a direct interaction between the two proteins, co-immunoprecipitation was performed (Figure 18D). Co-precipitation of PODXL and ezrin demonstrated some sort of complex formation of the proteins. A co-precipitate is only feasible when a pulldown is performed with PODXL and Western blotting analysis for ezrin. To verify the specificity of the obtained results, a pulldown with a human IgG instead of a specific antibody targeting PODXL or ezrin was conducted, resulting in no co-precipitate. As a positive control, ezrin was used for pulldown and analysing.

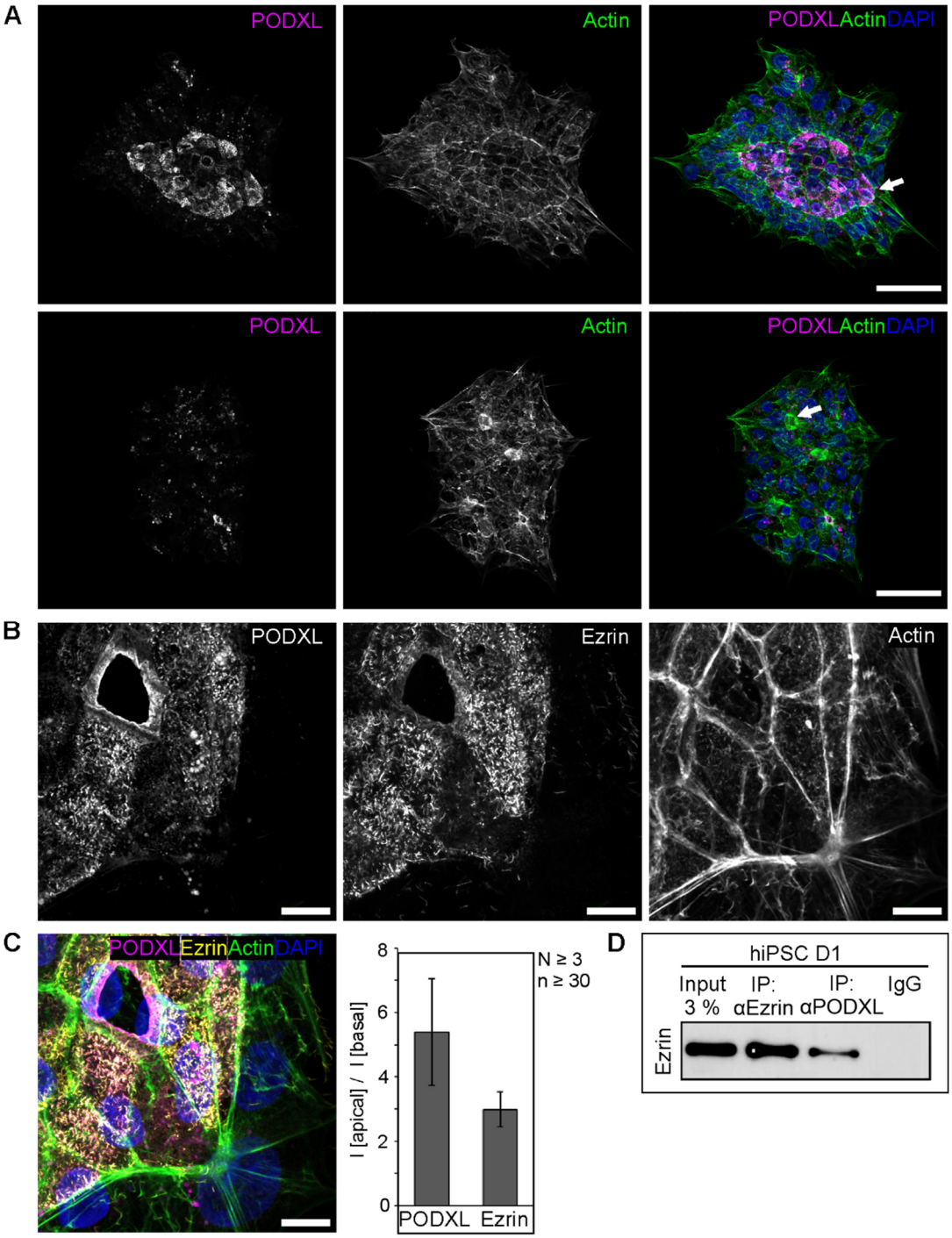

Figure 18: Co-localisation of apical marker ezrin and PODXL

D1 hiPSCs were cultivated for 24 h, following immunostaining or cell lysis for immunoprecipitation. Cellular components are PODXL (magenta), actin (green), ezrin (yellow) and nuclei (blue). **(A)** Immunostaining shows that PODXL is accumulated and restricted to the area encircled by the cell-spanning actin ring, indicated by the white arrow in the upper panel. PODXL signal displays no enrichment when the actin ring is not visible. **(B)** Ezrin and PODXL co-localise in the area defined by the cell-spanning actin ring. **(C)** The calculated fold changes demonstrate an increase of PODXL and ezrin intensity at the apical side of the colony. **(D)** Co-IP of PODXL and ezrin. Immunoprecipitation with an antibody against PODXL results in detecting ezrin in Western blot analysis. An unspecific human IgG leads to no precipitate. For reference, the initial cell lysate that was used for co-IP and was also analysed by Western blot. Scale bar (A): 50 µm; (B), (C): 10 µm.

The immunoprecipitation with PODXL yields a lower amount of precipitate compared to the initial cell lysate used for the co-IP (Figure 18D, referred to as input). This demonstrates that ezrin is only partially associated with PODXL in a complex which aligns with the observations of the immunostaining, showing ezrin located in lamellipodia (Figure 18B), but not PODXL.

4.3.2 Apical Ezrin Localisation Depends on NMIIB Distribution

Thus far, the results of immunostainings demonstrate that an ezrin-PODXL complex is associated with the cell-spanning actomyosin ring. It is discussed in the literature that cortical membrane tension exerted by ezrin, and contractile tensions, generated by actomyosin organisation, are interdependent (Diz-Muñoz et al., 2013). To assess whether this is also the case in hiPSC colonies, a partial NMIIB knockout (KO) was introduced using CRISPR/Cas9 in D1 GFP-NMIIB reporter line, followed by immunostaining to quantitatively analyse ezrin localisation. As a control group, cells were transfected without the genetic target.

Colonies from the control group displayed a characteristic hiPSC colony morphology, namely a cell-spanning actomyosin ring and a position dependent apical polarisation (Figure 19A, upper panel). Immunostaining of the transfected colonies displays a partial NMIIB KO, which is visualized by a lack of GFP-NMIIB signal (Figure 19A, bottom panel). The sporadic localisation of GFP-NMIIB throughout the colony results in a fragmented cell-spanning ring and scattered NMIIB filaments with no visible organisation. The lack of a cell-spanning ring is also highlighted by the actin staining. In addition, the colonies exhibit no characteristic continuous area enriched in ezrin, but rather multiple ezrin accumulations co-located with the fragments of the actomyosin ring or NMIIB filaments. To further analyse the distribution of ezrin, 3D reconstructions of the immunostaining were generated (Figure 19C). Upon closer observation of two areas where ezrin is accumulated (Figure 19B), it becomes apparent that apically located ezrin can only be found when it is associated with the cell-spanning actomyosin ring (Figure 19C, yellow box, indicated by white arrows). Contrary, ezrin associated with scattered NMIIB filaments, shows no apical localisation, but is present throughout the colony. This is evident by the localisation of ezrin underneath the nuclei (Figure 19C, red box, indicated by white arrows). To investigate the dependency of apical ezrin accumulation on actomyosin contractility exerted by NMIIB, the relative area covered by ezrin was measured and compared between control samples and colonies with partial NMIIB KO. The quantitative analysis demonstrates that the continuous area of apical enriched ezrin is significantly smaller in the colonies with partial NMIIB KO (Figure

19D). The mean area covered by ezrin in transfected colonies is approximately 25 %, whereas for colonies in the control group, it is approximately 40 %.

In summary, the results indicate that two forces are generated in hiPSC colonies, namely cortical membrane tension exerted by the PODXL-ezrin complex and contractility-dependent tension generated by the cell-spanning actomyosin ring. Furthermore, the partial NMIIB KO highlights the apparent necessity of contractile tension to establish position-dependent apical polarisation.

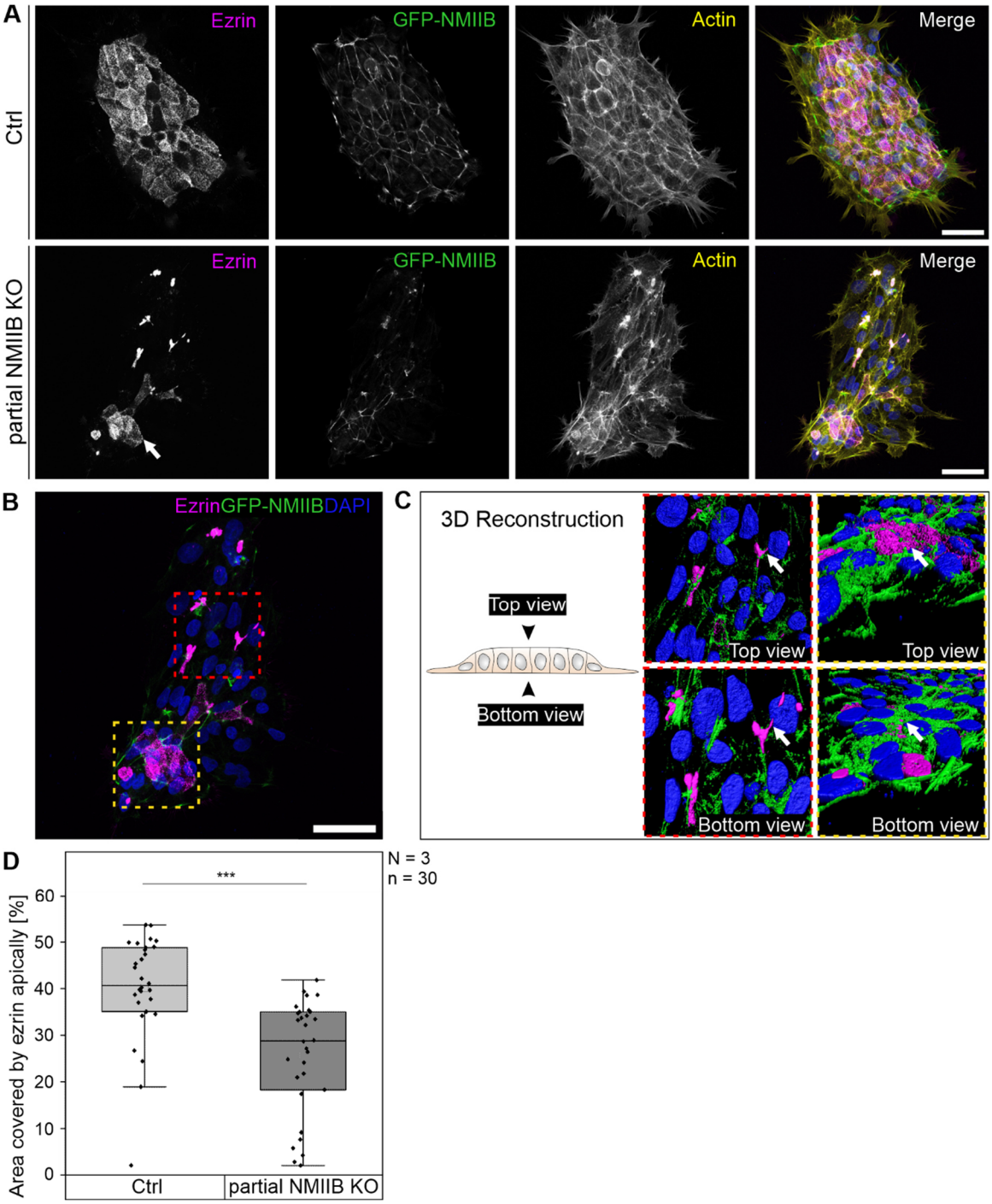

Figure 19: Partial NMIIB KO in D1 GFP-NMIIB reporter line

Ezrin (magenta), actin (yellow) and nuclei (blue). **(A)** Immunostainings of transfected D1 GFP-NMIIB hiPSCs and untransfected controls. Untransfected cells show a characteristic colony morphology (upper panel). Colonies with a partial NMIIB KO display a fragmented actomyosin ring and scattered NMIIB filaments. Ezrin is accumulated at localisations of the fragmented ring (bottom panel, indicated by the white arrow). **(B)** Areas used for 3D reconstruction are highlighted by boxes. **(C)** 3D visualisation shows that ezrin is exclusively apically located within fragments of the actomyosin ring (yellow box). **(D)** Quantitative analysis of the relative area covered by ezrin apically. In partial NMIIB KO colonies, the relative area covered by ezrin enrichment decreases significantly. Statistical significance was evaluated by a two-tailed t-test. Scale bar (A), (B): 50 µm.

4.4 Mechanical Barriers Impact hiPSC Colony Architecture

Experiments with the myosin inhibitor Blebbistatin as well as a partial NMIIB KO demonstrated that the contractility exerted by NMIIB is important for polarity establishment as well as maintaining colony integrity. Several studies have shown the influence of external cues by the microenvironment on apical polarisation and cytoskeletal organisation. To investigate the role of NMIIB in providing mechanical stability, a 2.5D scaffold was fabricated by DLW to serve as a mechanical barrier, potentially compensating for the tension generated by contractility.

4.4.1 Influence of Mechanical Barriers on Actomyosin Organisation

The mechanical barriers were written with either PETA or oil ink as a photoresist to alter the stiffness of the cells microenvironment. Based on the used photoresist, the mechanical barriers have a Young's modulus of approximately 1 GPa or 20 MPa, respectively. An array of 8x8 mechanical barriers with 200 µm distance between the structures was produced on each coverslip using PETA or oil ink (Figure 20A). Visualisation by scanning electron microscopy (SEM) from top and side view shows that the features of the mechanical barriers are equal, independent of the used photoresist (Figure 20B).

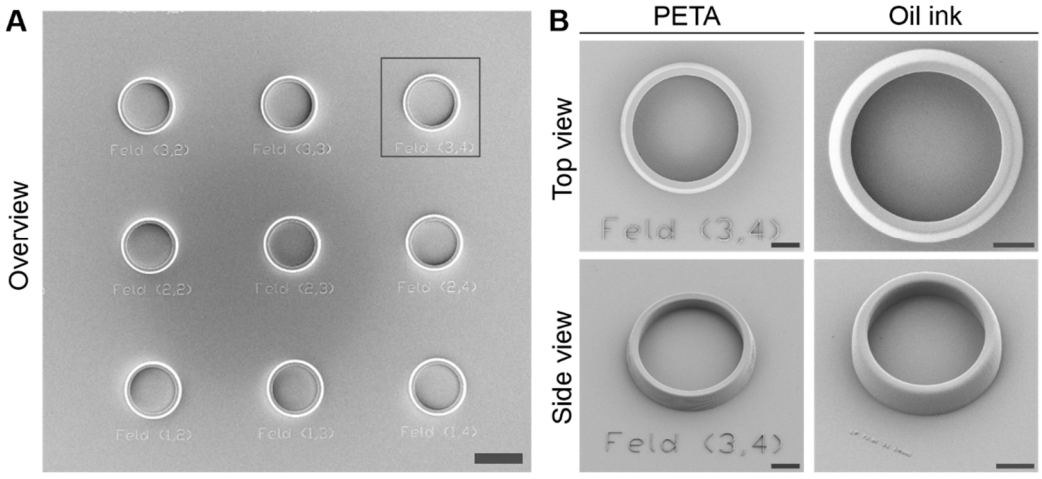

Figure 20: Scanning electron micrographs of direct laser written mechanical barriers

(A) Overview of the mechanical barriers. An array of 8x8 scaffolds was fabricated. (**B)** Mechanical barrier written with PETA or oil ink, respectively. The top and side views illustrate that the barriers are equal in appearance, regardless of the photoresist. The mechanical barriers written with oil ink were kindly provided by Clara Vazquez-Martel, IMSE and AM Heidelberg University. Scale bar (A): 100 µm; (B): 25 µm. The SEM images were taken by Clara Vazquez Martel, IMSE and AM, Heidelberg University.

The inner diameter of the mechanical barrier is approximately 100 µm, allowing seeded single hiPSCs to form colonies spanning the whole entity of the scaffold within 48 h of cultivation (Figure 21A). During the 48 h, hiPSCs further divide and self-organize in a tightly packed colony composed of radially aligned cells. LCI of the GFP-NMIIB signal shows a cluster of NMIIB signal in the centre of the colony (Figure 21A, GFP-NMIIB channel indicated by white arrow). For closer observation of the cytoskeletal organisation in response to external cues from the microenvironment, immunostaining of hiPSCs was performed. Colonies cultivated in mechanical barriers, independent of the photoresist, display two distinct colony morphologies (Figure 21B). The first category is defined by an evident cell-spanning actomyosin ring with restricted ezrin enrichment, as seen in 2D cultivation. The second category is characterized by scattered NMIIB filaments and the lack of a continuous cell-spanning ring in the periphery (Figure 21B, indicated by white arrows). Ezrin is restricted to the area covered by NMIIB filaments. In both categories, actin fibres are not organized in a network structure at the apical side of the colony as observed on a flat surface, but rather appear as an accumulation co-localised with ezrin (Figure 21B, actin channel indicated by white arrows). HiPSCs which were cultivated in the mechanical barriers maintained their pluripotent character, even if the colonies were classified in category two (Figure 21C, indicated by white arrows). This was verified by immunostaining with the pluripotency marker SOX2. Classification shows that approximately 30 % of colonies cultivated in mechanical barriers written with PETA display a morphology of category one (Figure 21D). The majority, approximately 70 %, are classified as category two. A reverse trend is observed for colonies cultivated within oil ink-derived mechanical barriers.

In conclusion, the results demonstrate that the microenvironment has an impact on the cytoskeleton architecture of hiPSC colonies. The requirement for self-organizing a cell-spanning actomyosin ring presumably depends on the stiffness provided by the microenvironment. A higher stiffness of 1 GPa by PETA favours the occurrence of scattered NMIIB filaments, whereas a lower stiffness of 20 MPa by the oil ink leads to the majority of colonies displaying a continuous cell-spanning actomyosin ring. These observations suggest that the microenvironment, providing the necessary stability, can compensate the role of NMIIB in maintaining colony integrity.

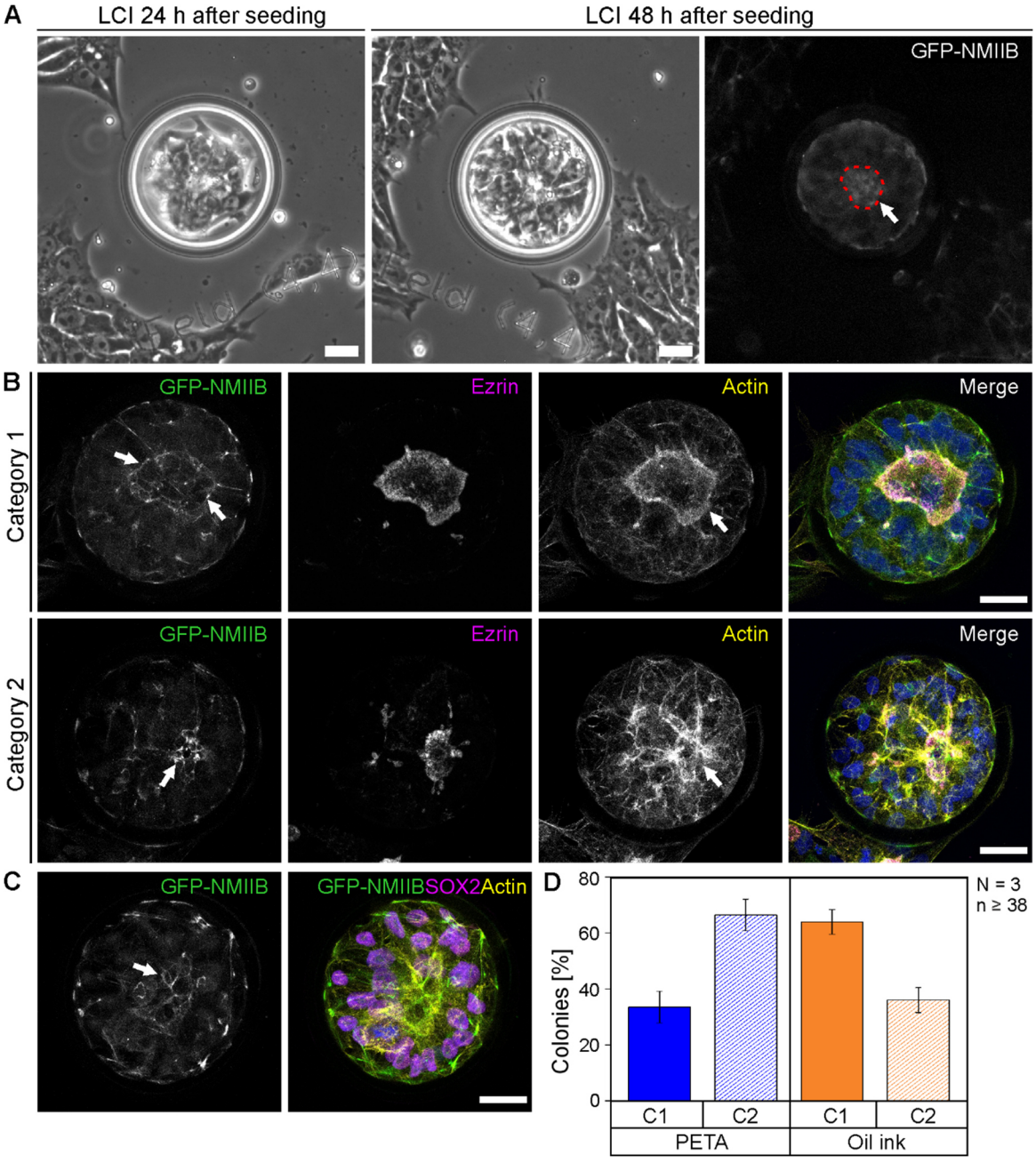

Figure 21: Cultivation in mechanical barriers alters the hiPSC colony architecture

D1 GFP-NMIIB were seeded as single cells and cultivated for 48 h, followed by immunostaining. Ezrin is visualized in magenta, actin in yellow and nuclei in blue. **(A)** HiPSCs were cultivated for 48 h to allow the cells to form colonies, filling in the space within the scaffolds. NMIIB cluster in the centre is indicated by the white arrow. **(B)** Based on the morphology of the NMIIB organisation, colonies were classified into one of two categories. The first is defined by an evident cell-spanning actomyosin ring with restricted ezrin enrichment. The second category is characterized by scattered NMIIB filaments without a continuous cell-spanning ring in the periphery. **(C)** Immunostaining of the pluripotency marker SOX2, visualized in magenta, verifies that hiPSCs cultivated in scaffolds maintain their pluripotent character. **(D)** Classification of the morphology demonstrates that cultivation in PETA-based barriers favour the occurrence of category two, whereas in oil ink-based barriers it is category one. Scale bar (A)-(C): 25 µm.

4.4.2 Influence of Mechanical Barriers on Ezrin Distribution

The results demonstrate that the stiffness of the mechanical barriers affects the cytoskeletal organisation of hiPSC colonies. To assess the impact of this effect on apicobasal polarisation, ezrin distribution throughout the colony in x- and y direction in different z planes was evaluated as described in Section 3.2.9.

First, the planar distribution was determined by calculating the relative area covered by ezrin with respect to the inner area of the scaffolds. As colonies spanning the entire scaffold were used, the area encircled by the barrier served as the reference (Figure 22A). For category one, approximately 20 % of the colony is covered by ezrin on average. There is no significant difference in average coverage between colonies of category one cultivated in PETA-derived or oil ink-derived mechanical barriers. The data for category two supports the previous finding of category-specific morphology, regardless of the used photoresist. In contrast to colonies in category one, the average coverage by ezrin is reduced by half for colonies in category two. This significantly decreased area covered by ezrin supports the results in Section 4.3.2, indicating a dependency of apical polarisation on contractility tension generated by NMIIB.

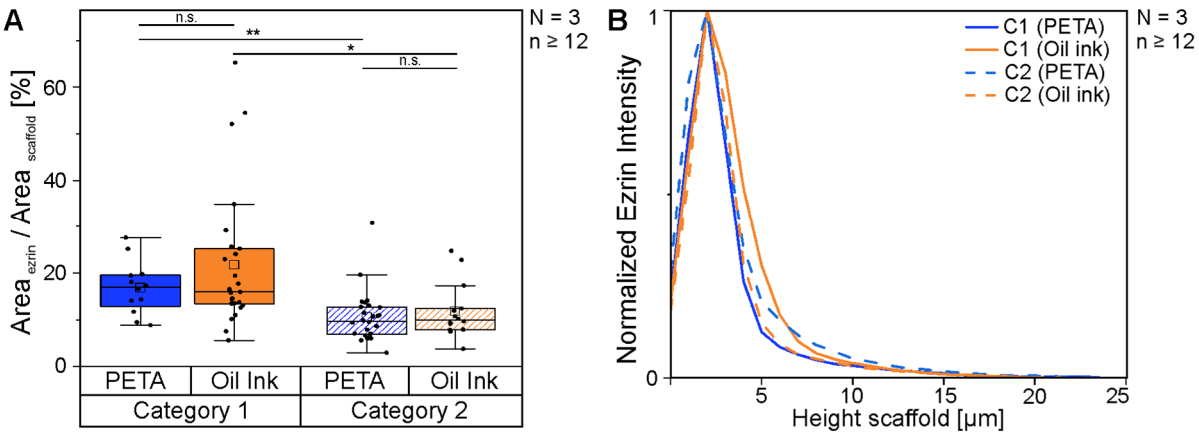

Figure 22: Cultivation in mechanical barriers impacts ezrin distribution

Ezrin distribution in colonies of either category one or two was evaluated. In addition, the potential influence of the two different photoresists on the ezrin localisation pattern was tested. **(A)** The graph shows the relative area covered by ezrin with respect to the inner area of the scaffold. A significant decrease in the area covered by ezrin in colonies of category two compared to colonies of category one is observed. The results demonstrate that the morphology of the categories is specific, independent of the used photoresist. The data was tested using a two-tailed t-test. **(B)** Ezrin throughout the colony in the z plane is visualised by a curve representing the normalized ezrin intensity plotted against the height of the scaffold. No significant difference between the curves for the two categories or depending on the photoresist is observed. The curve shows an incline with a peak at a height of 2 µm. Statistical significance was tested by the Kolmogorov-Smirnoff-test.

To visualise ezrin distribution throughout the z plane, normalized ezrin intensity is plotted against the height of the scaffold (Figure 22B). The curves show an increase in ezrin with the highest signal at a height of 2 µm. This is the position, the cell-spanning actomyosin ring was typically observed in a colony growing in a monolayer, indicating the role of ezrin as a linker between the ring and the plasma membrane. Subsequently, the ezrin signal decreases up to a height of 8 µm. This data aligns with the observed average height of approximately 8 µm for a colony under standard culture conditions. Ezrin distribution curves for colonies in categories one and two display the same progression, illustrating no significant difference in ezrin distribution across categories or scaffold materials. Statistical significance was tested by the Kolmogorov-Smirnoff-test. The curve illustrates that the highest occurrence of ezrin is at the position of the continuous or NMIIB filaments, corresponding to the categories one or two, respectively. This suggests a primary apical localisation of ezrin in colonies cultivated in mechanical barriers. Interestingly, an ezrin signal is observed at the bottom of the scaffold. This initially detected ezrin signal at the basal side of the colony is presumably due to the localisation of ezrin in lamellipodia.

In summary, the results demonstrate that the reorganisation of the cytoskeletal architecture in response to the external cues of the microenvironment has an impact on apical polarisation. However, this influence is restricted to the planar distribution of ezrin, illustrated by a decrease in ezrin-enriched area in colonies without a continuous cell-spanning actomyosin ring. The effect is congruent with the observations in Section 4.3.2, stressing the dependency of establishing apical polarisation by contractility tension exerted by NMIIB in association with actin. Taken together, these observations suggest that a mechanical barrier with a high stiffness can substitute the role of the cell-spanning actomyosin ring in maintaining integrity, however, it apparently cannot regulate apical polarisation.

4.5 Mechanical Regulation of Pluripotency in hiPSC Colonies

Recently, the interplay between the cellular architecture of pluripotent stem cells, cellular mechanics and pluripotency has been highlighted in the literature (S. Liu & Kanchanawong, 2022). So far, the results demonstrate that hiPSCs have a distinctive cytoskeleton architecture essential for maintaining colony integrity and epithelial character, defined by the established apicobasal polarity. Furthermore, the cell-spanning actomyosin ring divides the colony into an inner and outer population, with the inner population experiencing more mechanical cues, namely cortical membrane tension exerted by the PODXL-ezrin complex and contractility tension generated by the cell-spanning actomyosin ring. To study the influence of cytomechanics on pluripotency in hiPSCs, two experiments were conducted.

4.5.1 Distribution of Transcription Factors in hiPSC Colonies

First, to test whether there is a difference between the inner and outer populations regarding pluripotency regulation, immunostaining was performed for the pluripotency marker NANOG and YAP, a mechanotransducer and transcriptional regulator of the pluripotency network.

NANOG and YAP are both located within the nuclei of cells belonging to the inner population and to the outer population (Figure 23A). The mean intensities of NANOG or YAP were measured and averaged separately for cells in the inner and outer population of colonies. The classification of the cells into one of the populations was based on the location of the cell-spanning actomyosin ring, as illustrated in Figure 23B. The analysis demonstrated a significantly lower YAP intensity in the outer population compared to the inner population. The higher amount of nuclear YAP in cells of the inner population aligns with the higher mechanical cues these cells experience due to the cortical membrane tension and the contractile tension. No significant difference in NANOG intensity was observed between the two cell populations.

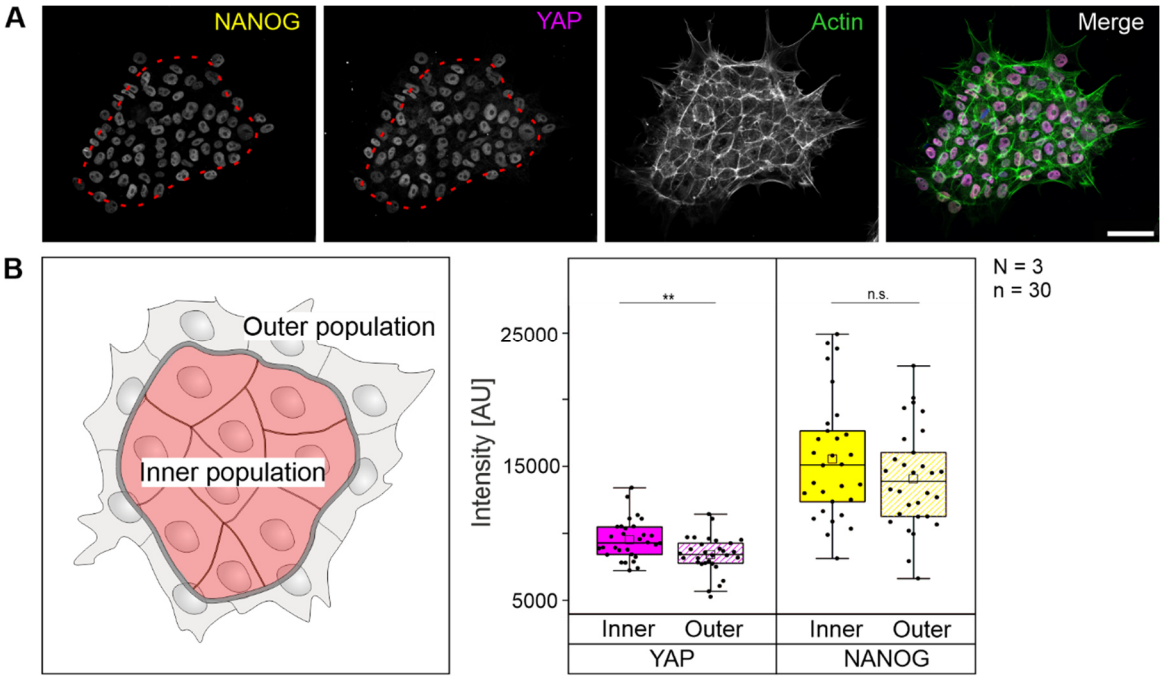

Figure 23: Distribution of NANOG and YAP across hiPSCs within the colony

D1 hiPSCs were cultivated for 24 h, followed by immunostaining of NANOG (yellow), YAP (magenta) and actin (green). **(A)** Immunostaining illustrates the localisation of the pluripotency marker NANOG and the mechanotransducer YAP across all nuclei in the colony. The population is divided by the characteristic cell-spanning actomyosin ring in the inner and outer populations indicated by red dotted line. Scale bar: 50 µm **(B)** Mean fluorescence intensities of NANOG and nuclear YAP in inner or outer cell populations. For each colony, cells were classified as inner or outer cell, and their intensities were averaged separately. The data represents the average intensities of 30 colonies. Statistical analysis was conducted by two sample t-test.

4.5.2 Influence of Cytomechanics on Pluripotency

For the second experiment, colonies were treated with inhibitors perturbing either contractility or cortical membrane tension to assess the impact of cytomechanical properties on pluripotency regulation. The inhibitor treatments were conducted as described in Section 3.2.8, followed by immunostaining for early differentiation markers. One representative marker was selected for each of the three germ layers, namely Brachyury for mesoderm, FOXA2 for endoderm and SOX1 for ectoderm.

The contractile tension of the cell-spanning actomyosin ring was perturbed by the inhibitor Blebbistatin. Immunostaining displays that upon prolonged treatment with Blebbistatin for 24 h, the distinctive cytoskeleton structure of hiPSCS colonies is lost (Figure 24A). No actin organisation as a ring-like structure is visible, but rather accumulations of actin. In addition, the actin staining shows that the characteristic tightly packed morphology of hiPSC colony is loosened, illustrated by an increased emergence of cellular protrusions. To assess the effect of interfering with contractility on the ratio of transcription factors in hiPSCs, a ratio was calculated for the intensity of each early differentiation marker to the pluripotency marker in the nuclei. The graph illustrates this ratio either colony-wise or for single cells (SC). A ratio above 1 indicates cells entering early differentiation (Figure 24B-D, indicated by the red line). For the mesodermal marker Brachyury, as well as for the ectodermal marker FOXA2, the evaluation shows that isolated cells enter early differentiation upon treatment with Blebbistatin (Figure 24B, C). In contrast, no cells entering differentiation in neural ectodermal fate, represented by SOX1, are observed (Figure 24D). Colony-wise, no substantial shift in the mean ratio of transcription factors is visible for any of the differentiation markers, demonstrating that spontaneous differentiation is restricted to individual cells within the colony rather than affecting the entire colony (Figure 24E). However, statistical analysis shows a significant difference in mean variation between treated colonies and the control, indicating an alteration of transcription factor composition within hiPSCs upon perturbation of contractile tension.

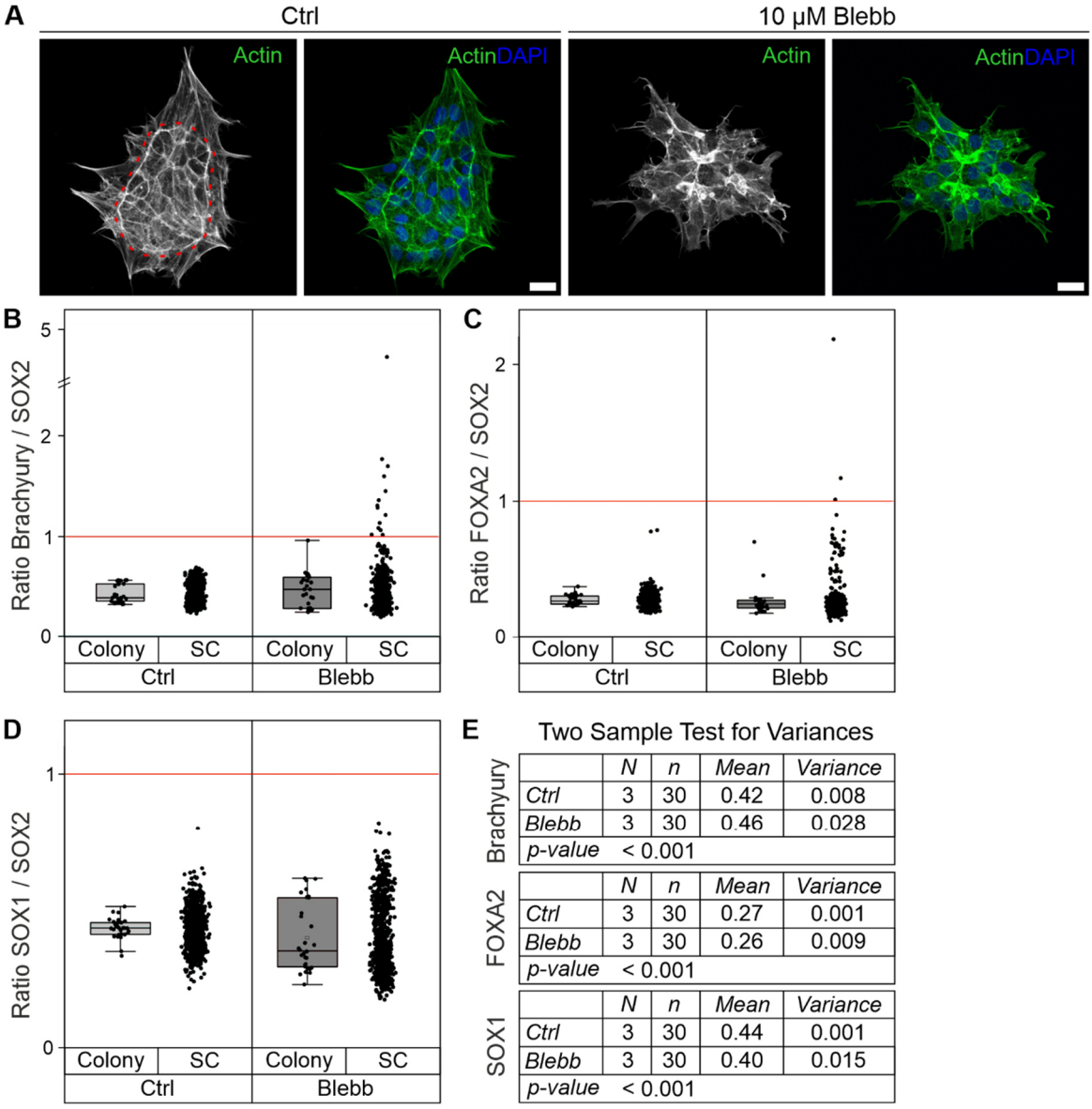

Figure 24: Interfering with contractile tension results in differentiation

HiPSCs were treated with Blebbistatin to perturbate the contractility tension generated by the cell-spanning actomyosin ring. Subsequently, immunostaining of actin (green), nuclei (blue), SOX2 and one of three early differentiation markers, namely Brachyury, FOXA2 and SOX1, was conducted. **(A)** Immunostaining of actin shows the cytoskeleton structure representative of control and treated colonies. Control colonies display a continuous actin ring, indicated by a red dotted line. Treated colonies show no ring-like actin organisation, but rather accumulations. Scale bar: 25 µm. **(B)-(D)** The graph illustrates the ratio of differentiation marker to pluripotency marker, either colony-wise or for single cells (SC). A ratio above 1 indicates cells entering early differentiation in mesoderm, endoderm and ectoderm, as shown by Brachyury, FOXA2 and SOX1, respectively. Spontaneous differentiation in mesodermal and endodermal fate is observed for single cells. **(E)** Statistical analysis was performed by two sample tests for variances. The results show a significant difference in mean variation between the control and treated samples, demonstrating an effect on transcription factor composition within hiPSCs after Blebbistatin treatment.

In some cases, the mean transcription factor ratios revealed a shift of the ratio in favour to SOX2, especially in the evaluation for the ectodermal marker SOX1 (Figure 25). Based on this observation, the influence of contractile tension on the pluripotency gene regulatory network was also evaluated. For that, a fold change was calculated, illustrating the difference in mean intensity measured for NANOG, SOX2 and OCT3/4 in Blebbistatin treated colonies with respect to the control group. The graph demonstrates a significant increase in SOX2 signal in Blebbistatin treated cells compared to the control group, however, no significant alterations for NANOG and OCT3/4. An increase in SOX2 intensity suggests an alteration of the balanced PGRN, thus leading to differentiation. Based on the literature, upregulation of SOX2 promotes early neuroectodermal fate (Sarkar & Hochedlinger, 2013).

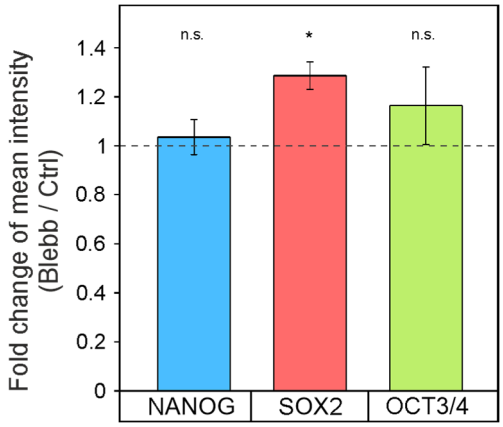

Figure 25: Blebbistatin treatment increases SOX2 mean fluorescence intensity

HiPSCs were treated with Blebbistatin to perturbate the contractility tension generated by the cell-spanning actomyosin ring. Immunostaining of NANOG, SOX2 and OCT3/4 was performed, followed by intensity measurements to calculate a fold change of intensity measured in treated colonies with respect to the untreated control group. The graph shows a significant increase in SOX2 intensity in Blebbistatin treated cells compared to the control group. The other two components of the PGRN, NANOG and OCT3/4, display no significant differences.

In addition to contractile tension, the influence of cortical membrane tensions on pluripotency regulation was tested using an ezrin inhibitor, hindering the connection between actin cytoskeleton and plasma membrane. Interfering with the cortical membrane tension results in a partwise fragmented cell-spanning actin ring (Figure 26A, indicated by the red dotted outline). However, compared to the Blebbistatin treated cells, the effect of the ezrin inhibitor is less pronounced, with the overall colony integrity being maintained. The smaller effect is also apparent in the evaluation of the transcription factor ratios. The graphs show that one cell depicts a ratio above 1, thus entering endodermal differentiation (Figure 26C). For the other differentiation markers, no event of spontaneous differentiation is observed (Figure 26B and D). The mean values of the transcription factors display a negligible difference between colonies of control and treated samples, similar to evaluations in Blebbistatin treated cells. However, statistical analysis shows no significant difference in the mean variances between control and ezrin inhibitor treated colonies for any of the differentiation markers (Figure 26D). This observation suggests no effect of perturbing the cortical membrane tension on pluripotency regulation.

In summary, the inhibitor treatment experiment revealed an impact of cytomechanics on pluripotency regulation. Immunostainings and evaluation of transcription factor ratios clearly demonstrate the importance of contractile tension, generated by the cell-spanning actomyosin ring, in maintaining both the cytoskeleton architecture and pluripotent character of hiPSCs. Although the culture medium used for the experiments provided the cells with crucial components, like FGF, to sustain pluripotency, spontaneous differentiation in Blebbistatin treated cells is observed, suggesting the crucial role of mechanical regulation in cell fate decisions.

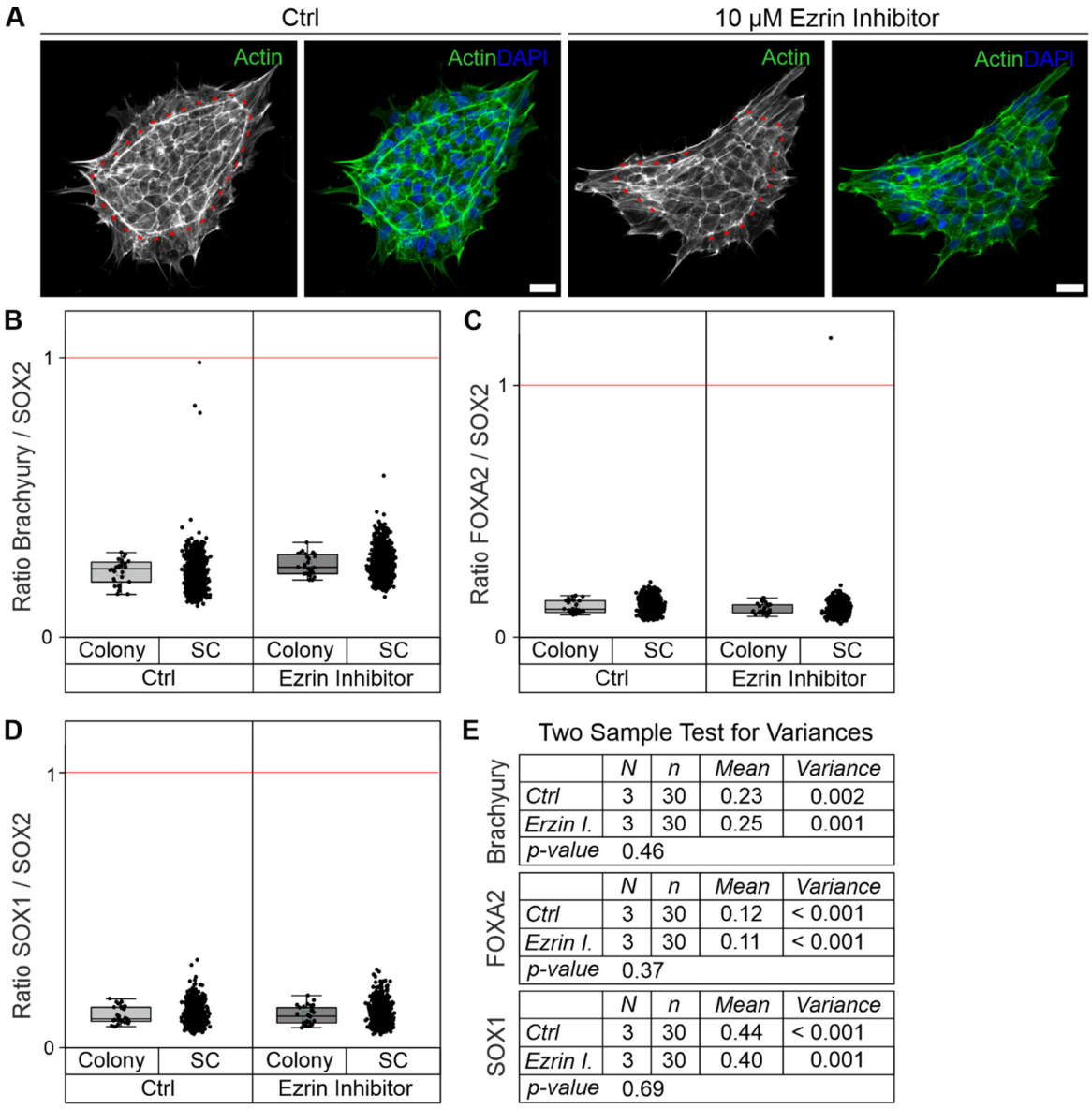

Figure 26: Interfering with cortical membrane tension showed no effect on pluripotency

HiPSCs were treated with an ezrin inhibitor to perturbate the cortical membrane tension generated by ezrin-actin binding. Subsequently, immunostaining of actin (green), nuclei (blue), SOX2 and one of three early differentiation markers, namely Brachyury, FOXA2 and SOX1, was conducted. **(A)** Immunostaining of actin shows the cytoskeleton structure representative of control and treated colonies. Control colonies display a continuous actin ring, whereas treated colonies show a fragmented actin ring, indicated by red dotted lines. Scale bar: 25 µm. **(B)-(D)** The graph illustrates the ratio of differentiation marker to pluripotency marker, either colony-wise or for single cells (SC). A ratio above 1 indicates cells entering early differentiation in mesoderm, endoderm and ectoderm, as shown by Brachyury, FOXA2 and SOX1, respectively. Spontaneous differentiation in endodermal fate is observed for one single cell. **(E)** Statistical analysis was performed by two sample tests for variances. The results show no significant difference in mean variation between the control and treated samples, indicating no effect on transcription factor composition within hiPSCs after ezrin inhibitor treatment.

5 Discussion

Pluripotency is maintained by several molecular mechanisms, including transcriptional, epigenetic and metabolic regulation. The influence of cytomechanics on pluripotency regulation has been increasingly highlighted in recent years. *In vitro*, hiPSCs self-organise an apically-located actomyosin structure connecting neighbouring cells, the cell-spanning actomyosin ring. Based on the importance of cell-cell interactions and transfer of intrinsic mechanical forces *in vivo,* the objective of this work was to elucidate the role of the cell-spanning actomyosin ring as a major regulator in hiPSC colonies.

The results of the present work demonstrate that the contractile tension, exerted by the NMIIB isoform, is a key regulatory mechanism in hiPSC colonies through performing three important tasks: (1) Regulation of apicobasal polarity, (2) Maintenance of colony integrity, and (3) Sustaining pluripotency. In the following chapter, the formation and roles of the cell-spanning ring are discussed. Moreover, the contribution of the actin fence and the cell-spanning ring to pluripotency *in vitro* is highlighted. Finally, a potential role of the cell-spanning ring in post-implantation human embryonic development is discussed.

5.1 Characterisation of the Cell-Spanning Actomyosin Ring in hiPSCs

To study the nature of the cell-spanning actomyosin ring, it was important to gain knowledge about the formation and dynamics. Given the strong association of NMIIB with the cell-spanning ring, a GFP-NMIIB reporter line was generated using CRISPR/Cas9.

LCI of hiPSC colonies shortly after seeding revealed that formation occurs through a stepwise accumulation of NMIIB at multiple spots in the periphery of the colony resulting in prominent fibres (Figure 16). Simultaneously, an apical network of NMIIB associated actin fibres becomes evident (Figure 16). Interestingly, in Drosophila salivary placode cells, a circumferential actomyosin cable at the apical-lateral level is formed, similar to the cell-spanning ring in hiPSCs (Röper, 2012). In salivary gland cells, this actomyosin cable is assembled through the anisotropic localisation of the apical polarity marker Crumbs which is driven by homophilic interactions between neighbouring cells. Membrane areas with high levels of Crumbs lead to an increased dissociation rate constant of Rok, the homolog of ROCK in Drosophila, potentially through a Cdc42-regulated kinase (Sidor et al., 2020). In contrast, low levels of Crumbs allow for the accumulation of Rok which activates NMIIB through phosphorylation of the RLC.

Another characteristic that the cell-spanning actomyosin ring in hiPSCs and the actomyosin cable in Drosophila cells have in common is the ability to adapt and re-

establish after perturbation. Laser ablation performed in the study of Röper and colleagues demonstrated that the actomyosin cable is under high tension and its fracturing is quickly repaired. This aligns with the results in Section 4.2. showing that the fracturing of the cell-spanning ring is reversible after NMIIB inhibition (Figure 17C). Recently, the formation of multicellular actomyosin cables associated with the specific isoform NMIIB was also demonstrated in chick and mouse lens placode (Houssin et al., 2020).

In conclusion, these similarities suggest that the cell-spanning ring structurally resembles the actomyosin cables described in developmental epithelial tissues throughout different species.

5.2 Podocalyxin-Ezrin Complex Anchors the Cell-Spanning Actomyosin Ring

The role of the actomyosin cables in epithelial tissue is to drive morphogenesis by apical constriction of the tissue (Houssin et al., 2020). In hiPSC colonies, no apical constriction resulting in bending of the hiPSC colony is observed. What hinders this process in hiPSCs *in vitro*? One proposed idea could be a stabilizing effect through a PODXL-ezrin complex, which is known to maintain the cytoskeletal structure in kidney podocytes (Orlando et al., 2001). To test whether PODXL and ezrin form a complex in hiPSCs, immunostaining and co-immunoprecipitation were conducted.

The results demonstrated that ezrin and PODXL are both present in the area defined by the cell-spanning actomyosin ring (Figure 18B) and are apically located (Figure 18C). The successful co-precipitation of PODXL and ezrin revealed an interaction between both proteins and the formation of a complex (Figure 18D). In the literature, ezrin links transmembrane proteins like PODXL to the actin cytoskeleton, which is crucial to maintain a cell type specific structural integrity (Wegner et al., 2010). In zebrafish embryonic epithelial tissue (Chouhan et al., 2024) myosin-mediated contractility is a dominant force as it is in hiPSCs (S. Liu & Kanchanawong, 2022). To maintain epithelial integrity, a delicate balance of contractility and tension is required. In the zebrafish model the counteracting force to contractile tension is proposed to be cortical membrane tension generated by ezrin (Chouhan et al., 2024). The interdependency of cortical membrane tension and contractile tension is an accepted concept (Diz-Muñoz et al., 2013). In the study by Chouhan and colleagues, the results suggest that the relaxing influence of ezrin in cooperation with E-Cadherin-mediated adhesion seems essential for mechanical stability of the tissue (Chouhan et al., 2024). Both proteins, ezrin and E-cadherin, are present in hiPSC colonies (Y. Kim et al., 2022; Narva et al., 2017) and are localised in the central area of the colonies, where presumable high contractility generated by NMIIB is

exerted. This observation lends support to the hypothesis that ezrin counteracts the contractility of the cell-spanning actomyosin ring and hinders apical constriction *in vitro*.

Taken together, the formation of a PODXL-ezrin complex in hiPSCs was verified through co-immunoprecipitation. The role of both proteins, PODXL and ezrin, in maintaining structural integrity in different systems supports the hypothesis that the PODXL-ezrin complex maintains the structure of the cell-spanning actomyosin ring in hiPSC colonies.

5.3 Contractile Cell-Spanning Ring Regulates Apicobasal Polarity in hiPSCs

HiPSCs inherit an epithelial-like character, illustrated in particular through distinct apical and basal domains (Y. Kim et al., 2022; Zorzan et al., 2020). Studies have shown that the establishment and maintenance of apicobasal polarity is interactively controlled by actin cytoskeleton and polarity markers in epithelial cells (Buckley & St Johnston, 2022). To study the influence of NMIIB on apicobasal polarisation in hiPSCs, a partial NMIIB KO was introduced.

The results demonstrated that the partial NMIIB KO in hiPSC colonies resulted in a fragmented cell-spanning ring and scattered NMIIB filaments with no visible organisation (Figure 19A). Moreover, apical ezrin accumulation was not restricted to one continuous area but was rather diffused and co-localised with the fragments of the actomyosin ring or NMIIB filaments (Figure 19A). The area covered by the apical marker ezrin was significantly reduced in colonies with partial NMIIB KO compared to the control (Figure 19D). Thus, indicating the necessity of contractile tension to establish the characteristic apicobasal polarisation. This assumption is supported by the results in Section 4.3.2, which demonstrate a correlation between the absence of a fully formed cell-spanning ring and a reduced area covered by ezrin (Figure 22A). Furthermore, the literature highlights the role of NMII to mediate morphological changes, such as establishment of polarity through spatial distribution and organisation of actin into bundled structures (Buckley & St Johnston, 2022). Additionally, NMII is known to control apicobasal polarity through regulating formation and maturation of adherence junction in mammalian epithelial cells (Heuzé et al., 2019). However, epithelial polarity is known to be controlled by multiple factors. Cellular polarity is established by cytoskeletal components, which in turn are indirectly regulated by polarity proteins, such as Crumbs (Buckley & St Johnston, 2022; Röper, 2012). This relationship between the regulation of actomyosin activity and apical polarity proteins is still under investigation.

To summarise, the spatial distribution of NMII strongly correlates with ezrin accumulation, thus indicating a role of the cell-spanning actomyosin ring in regulating apicobasal polarity.

5.4 Contractile Cell-Spanning Ring Maintains Colony Integrity in hiPSC

Several studies have highlighted that a tight colony morphology is needed for complete pluripotency (S. Liu & Kanchanawong, 2022). To investigate the role of NMIIB in providing mechanical stability, a 2.5D scaffold was fabricated by DLW to serve as a mechanical barrier, potentially compensating for the tension generated by contractility.

In Blebbistatin treatment experiments inhibiting myosin activity, phase contrast images show an increased emergence of cell protrusions (Figure 17A, phase contrast). Additionally, colonies with a partial KO specifically targeting NMIIB also demonstrate a loosened colony morphology, defined by visible greater distance between individual cell nuclei (Figure 19A, merge channel). The association of the cell-spanning ring to maintain integrity is supported by diverse studies about collective migration, including epithelial cells and neural crest cells (Reffay et al., 2014; Shellard et al., 2018). Here, contractile tension exerted by supracellular actomyosin cables hinder the formation of protrusions and initiation of new leader cells.

Cultivation of hiPSC colonies in 2.5D scaffolds, the mechanical barriers, resulted in an altered organisation of cytoskeletal components. The influence of a ring culture system to the actomyosin organisation was also demonstrated by a recent study (M.-H. Kim et al., 2023). The cells displayed a radial alignment and NMIIB clusters appeared in the centre (Figure 21A, GFP-NMIIB channel). The presence of the mechanical barrier could not consistently enforce the formation of the actomyosin ring or induce its loss, as it could be observed that colonies either displayed the cell-spanning actomyosin ring or not (Figure 21B). However, it was observed that growth in the mechanical barriers prevented actin organisation in fibres like under standard cultivation conditions (Figure 13 and Figure 21B). More importantly, it was assessed that the formation of the cell-spanning actomyosin ring was dependent on the barrier's stiffness. In lesser stiff barriers of 20 MPa the colonies tended to form the cell-spanning ring while in stiff barriers of 1 GPa the formation of a cell-spanning ring was uncommon (Figure 21D). This observation leads to the hypothesis that contractility forces exerted by the cell-spanning ring are strong and the barrier needs to have a high stiffness to act as a replacement. One may argue that hiPSCs are not mechanically sensitive enough to sense changes in stiffness in a range of a high Young's modulus between MPA and GPa, since the surrounding tissue of stem cells *in vivo* is in a kPa range (Gu et al., 2022). However, other studies have shown the sensitivity of hiPSCs

to substrate stiffness in MPa range, resulting in alteration of epithelial and cytoskeletal organisation (Llewellyn et al., 2024). In detail, the experiments revealed that hiPSCs cultivated on soft substrate display alterations in junction formation and disrupted epithelial integrity. These effects were observed on substrates with stiffness in the MPa and kPa range, compared to standard cultivation substrates with a stiffness in the GPa range. It is important to note that the study by Llewellyn and colleagues was performed on a flat substrate whereas the mechanical barriers used in this study only apply a mechanical cue to the edge cells of the colony.

The results reveal a change in cytoskeletal organisation and decrease of area covered by the apical marker ezrin (Figure 21B and Figure 22A) in category 2. The distribution of ezrin throughout the colony in z level is not altered between the categories. However, it can be hypothesized that the edge cells touching the walls of the barrier initiate the formation of an internal apical domain as seen in the implantation of the blastocyst (Figure 2, Section 1.1). This is accompanied with a translocation of apical markers from an external localisation to the new internal apical membrane initiation site and could explain the reduction of area covered by ezrin. It can be assumed that with a prolonged cultivation time the barriers would initiate growth in multiple cell layers leading to a complete formation of an internal apical domain and ultimately the formation of a lumen. The capacity of hPSC colonies to form a cyst-like structure when cultivated in a 3D ECM microenvironment was shown in another work published in 2017 (Taniguchi et al., 2017).

In conclusion, the results show that cultivation in mechanical barriers alters the actin cytoskeletal organisation and accumulation of apically located ezrin in hiPSCs. Depending on the stiffness of the barriers, the majority of hiPSCs did not display a fully formed cell-spanning actomyosin ring. Thus, the findings in this work suggest that the microenvironment needs to have a specific stiffness to replace the exerted contractile tension and maintain colony integrity.

5.5 Contractile Cell-Spanning Ring Sustains Pluripotency in hiPSCs

So far, the results highlight the role of the cell-spanning actomyosin ring in regulating the epithelial-like character, including the apicobasal polarity and integrity. The epithelial-like cells of the inner population experience two cytomechanical cues, the contractile tension of actomyosin and cortical membrane tension by the PODXL-ezrin complex. To study a potential position dependent influence of cytomechanics in hiPSC colonies, immunostaining for pluripotency regulating transcription factors was conducted.

The results showed the localisation of the pluripotency marker NANOG and transcriptional regulator YAP in each cell nucleus of the colony (Figure 23A). However, the inner population of hiPSC colonies show a stronger signal for YAP compared to the outer population (Figure 23B), highlighting the heterogeneity of hPSCs colonies described in the literature (Hayashi et al., 2019). The higher amount of YAP in nuclei of the inner cell population is presumably caused by the autonomous mechanical force generated by actomyosin. YAP/TAZ activity was shown to be controlled through sensing of myosin-mediated tension at focal adhesions but, more interestingly, in adherence junctions (Elosegui-Artola et al., 2016; Takeichi, 2014). Regulation of YAP/TAZ through contractile tension at adherence junctions was shown to be cell density dependent (Dasgupta & McCollum, 2019). At low densities, contractile tension promotes YAP/TAZ activity, whereas high cell densities lead to YAP/TAZ inhibition. In this study, hiPSCs were seeded at low densities, allowing small colony formation, which aligns with the conditions favouring YAP/TAZ activation through contractile tension-dependent signalling at adherence junctions. However, the mechanism of YAP/TAZ regulation via the actin cytoskeleton is still not clear and includes multiple regulators via the canonical as well as noncanonical pathways.

To study the influence of the cytomechanics on pluripotency maintenance in hiPSCs, inhibitor treatments interfering with the either contractile or cortical membrane tension were conducted. Subsequently, the occurrence of spontaneous differentiation was illustrated by immunostaining of early differentiation marker.

Interfering with the cortical membrane tension by ezrin inhibition for 24 hours had minor effect on the actin cytoskeleton and no effect on the ratio of pluripotency marker and early differentiation markers (Figure 26). Contrary to previous publications, the results presented in this work indicate that the cortical membrane tension has no influence on pluripotency regulation. In mESCs, membrane tension was reported to mediate regulation of pluripotency (De Belly et al., 2021) and changes in cortical membrane tension can impact the membrane tension (Sakamoto et al., 2023). Since no effect was seen in the present

experiments, it can be assumed that the effect of membrane tension is restricted to late-stage naive pluripotency but has no influence in primed pluripotent cells.

The inhibition of NMII for 24 h revealed that interfering with contractile tension heavily impacts the cytoskeletal organisation and results in spontaneous differentiation (Figure 24). Recent studies have disclosed epithelial integrity as a key factor in regulating pluripotency (Legier et al., 2023). As discussed previously in Section 5.3 and 5.4, the contractile tension of the cell-spanning ring is proposed to maintain the epithelial-like character of hiPSCs, including polarity and integrity. Thus, it can be hypothesised that the cell-spanning ring is also a major regulator for pluripotency. Early differentiation signs were monitored in individual cells, positive for the mesodermal marker Brachyury, as well as for the ectodermal marker FOXA2 (Figure 24B and 24C). This aligns with the findings that epiblast cells maintained *in vitro* tend to differentiate towards mesoderm/endoderm direction. (Hayashi et al., 2019). Furthermore, Legier and colleagues reported an enhanced differentiation potential of hiPSCs in mesodermal direction in differentiation assays upon epithelial disruption (Legier et al., 2023). In this work, Blebbistatin treatment to perturb the contractile tension led to spontaneous differentiation and significantly increased SOX2 intensity (Figure 25), even under self-renewal culture conditions. Thus, altering the composition of the three core transcription factors NANOG, SOX2 and Oct3/-4 in the nucleus. These data are in contrast to the results of Legier and colleagues showing no effect on stemness identity by disruption of epithelial integrity, but influence on cell fate acquisition (Legier et al., 2023). This discrepancy can be potentially explained by two factors. First, the epithelial disruption was introduced by downregulation of Glypican-4, a cell surface protein and regulator of growth factor signalling (Legier et al., 2023). This downregulation resulted in hiPSC colonies with areas of abnormal tight junction organisation. In contrast, inhibition of NMII in this study led to an overall loss in cytoskeletal organisation (Figure 24A). Thus, it can be hypothesised that the degree of disruption is decisive for promoting differentiation. The second explanation, the influence of epithelial disruption on the core pluripotency factors, was tested using quantitative reverse transcription PCR (RT-qPCR). This method analyses an average expression level across all hiPSCs and thus doesn't demonstrate cell-to-cell variations. The results of this work highlighted that spontaneous differentiation is restricted to individual cells within the colony rather than affecting the entire colony. Consequently, a method for gene expression analysis focusing on individual cells should be performed, such as single-cell RT-qPCR and single-cell sequencing (Kashima et al., 2020; Ma et al., 2021). These methods can generate insight into cell-specific expression alterations, demonstrating a more accurate representation of the heterogeneous hiPSC population.

But how does contractile tension regulate pluripotency? Based on the literature and the presented results, it can be speculated that multiple aspects are accountable for that. Firstly, signalling pathways regulating primed pluripotency are affected. Legier and his colleagues propose that epithelial integrity, which is maintained by contractile tension, restricts morphogen sensing by controlling the accessibility of receptors on cell surfaces. This regulation, in turn, modulates the binding of ligands of the TGF signalling pathway and thereby its activity. Secondly, the epithelial integrity enables the apical localisation of the PODXL-ezrin complex as shown in this study. This complex was described to affect activity of the downstream signalling pathways MAPK and PI3K of the FGF pathway in cancer cells (Sizemore et al., 2007). Furthermore, it was proposed that PODXL itself regulates pluripotency via metabolic pathways in hiPSCs (W.-J. Chen et al., 2023).

Taken together, the results show that hiPSC colonies display a heterogeneity in YAP and NANOG distribution presumable because of the position dependent mechanical cues that are experienced. Perturbation of contractile tension results in early differentiation in mesoderm and endoderm direction. This leads to the assumption that tight and polarized morphology of hiPSC colonies is a key determinant in sustaining pluripotency.

5.6 Actin Fence or Cell-Spanning Actomyosin Ring: What is the Key Regulator?

As mentioned in Section 1.5 the different states of pluripotency naive and primed represented by mESCs and hPSCs *in vitro* have distinct actomyosin organisations. HiPSC colonies exhibit two distinct autonomous actomyosin structures, the actin fence and the cell-spanning ring. Both structures exert high actomyosin contractility which was shown to be a major mechanism in maintaining colony morphology and pluripotency. In the following, the actin structures are compared regarding structural features and influence on overall colony architecture.

Whereas the ventral stress fibres of the actin fence are presumably associated with the NMIIA isoform (Narva et al., 2017; Naumanen et al., 2008), the cell-spanning actomyosin ring is strongly associated with NMIIB (Figure 13, upper panel). The distinct roles of the isoforms are congruent with the association with the respective actin structure. NMIIA contributes to stress fibre formation and focal adhesion maturation facilitating cell-matrix signalling transfer, as seen in the basal located focal-adhesion dependent actin fence (Narva et al., 2017; Naumanen et al., 2008; Tojkander et al., 2012). In the cell-spanning ring, both isoforms, NMIIA and NMIIB are present as presented by the immunostaining (Figure 13), however NMIIB is evidently accumulated in the cell-spanning ring and the associated apical actin network. In general, NMIIA initiates cellular tensions and NMIIB

facilitates prolonged stable force generation (Weißenbruch et al., 2021). In addition, NMIIB is required to ensure spatial stability of the junctions and co-locates with the adhesion protein E-cadherin, essential for cell-cell contact (Heuzé et al., 2019; Mège & Ishiyama, 2017). Collectively, these NMIIB specific roles support the stability-providing characteristic nature of the cell-spanning ring and the associated actin network.

Both actin structures, the actin fence and the cell-spanning actomyosin ring were observed independently of the cell line, substrate stiffness or protein coating (Figure 14) (Narva et al., 2017). However, the immunostaining of hiPSC colonies on 2 kPa soft substrates illustrates that the NMIIB signal associated with the self-organized actomyosin ring is not as prominent as on stiff substrates (Figure 14B). Alterations in the structure on soft substrates were also demonstrated for the actin fence (Narva et al., 2017). Collectively, these findings reveal that both structures are essential for hiPSC colonies. However, the literature shows that hiPSC colony morphology on soft substrates strongly depends on apical cell-cell interactions, which are reinforced (Gerardo et al., 2019). This is demonstrated by the presence of apical Vinculin.

HiPSC colonies are divided into inner and outer population that differ in morphology, mechanical features and gene expression as shown in the present work (Figure 18 and Figure 23) and supported by another recent study (Y. Kim et al., 2022). This work proposes that each population relies on one of the two actin structure to maintain pluripotency *in vitro*. The outer population presumably relies on the force generated through focal adhesions, which are essential for mechanosensing. These large focal adhesions are proposed to correlate with pluripotency based on a force-directed signalling in focal adhesions (Narva et al., 2017). Contrarily, the inner population presumably relies on the contractile tensions generated by the cell-spanning actomyosin ring, regulating pluripotency in different ways as discussed in Section 5.5.

To sum up, both actin structures were shown to be essential for colony morphology and pluripotency regulation. Based on the heterogeneous nature of hiPSC colonies, this work proposes a position-dependent regulation of the inner and outer population through the actin fence and the cell-spanning actomyosin ring, respectively.

5.7 The Cell-Spanning Actomyosin Ring in Human Embryogenesis

In vivo, cell-ECM and cell-cell signalling interactions are essential during early human embryogenesis. The formation of the epiblast and transition of pluripotency is initiated, amongst other factors, through successful implantation in the endometrium highlighting the role of matrix-cell-coupling for pluripotency dynamic. This is in particular relevant in the human system, where implantation occurs at the site of the ICM localisation until fully embedded, in contrast to the mouse system where the ICM is located opposite to the implantation site (Aplin & Ruane, 2017; Knöfler et al., 2019). During epiblast formation in the mouse system, cells of the ICM are in close contact to each other. YAP accumulates in the eventual epiblast, where it is proposed to promote expression of SOX2 and NANOG. This process divides the population into highly pluripotent epiblast cells and neighbouring cells with lower capacity for pluripotency, which eventually differentiate towards primitive endoderm, becoming the hypoblast (Driskill & Pan, 2023). This classification in two distinct populations during epiblast formation, is resembled in the *in vitro* situation, where the cell-spanning ring divides the colony into an inner and outer population (Figure 23B). Here, the cells of the inner population also display a higher amount of nuclear YAP. Thus, it can be hypothesised that the inner and outer populations represent highly pluripotent epiblast cells and neighbouring cells primed to become primitive endoderm, respectively *in vitro*. This assumption is supported by the results in Section 5.5, demonstrating that spontaneous differentiation in mesoderm and endoderm direction occurs after losing restriction by the cell-spanning actomyosin ring (Figure 24).

How can insights from *in vitro* actin cytoskeleton architecture studies improve our understanding of cytoskeletal dynamics during human embryogenesis? The epiblast rosette formation and lumenogenesis of the amniotic cavity are not well described in human embryonic development due to ethical constraints in investigation of embryos after implantation (Shahbazi & Pasque, 2024). It is known that epiblast cells form a pseudostratified epithelial tissue, the pluripotent epiblast disc (Shahbazi, 2020). The vesicle transport of PODXL is an initiator of radial organisation and lumen formation (Bryant et al., 2010). However, looking at morphogenesis of other epithelial tissues during embryonic development, the actomyosin cable revealed to be a major regulator in initiation of invagination (Houssin et al., 2020; Röper, 2012). The actomyosin cable forms at the onset of invagination and persists during lumen formation in mouse lens placode (Röper, 2012). It was proposed that the high contractility facilitates the centripetal movement and initial bending by apical constriction of the tissue, thus contributing to the initiation of invagination (Houssin et al., 2020).

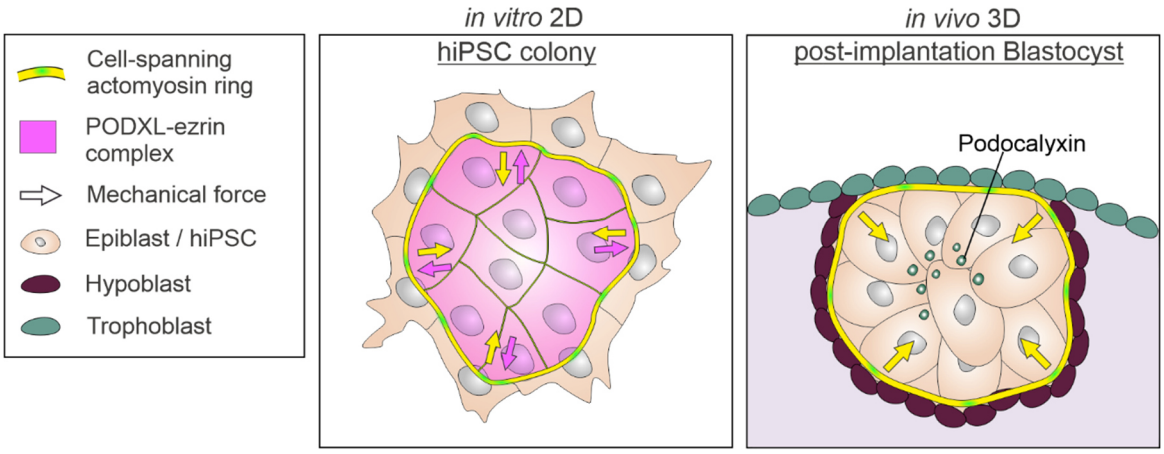

Figure 27: Model of the mechanical regulation by the cell-spanning actomyosin ring *in vivo*

Schematic illustrating that the contractile tension of the cell-spanning actomyosin ring is counteracted by the Podocalyxin (PODXL)-ezrin complex to maintain colony integrity and epithelial character of hiPSC colonies *in vitro*. The model proposes that *in vivo*, amniotic cavity formation is mediated by apical constriction of the pluripotent epiblast disc through the contractile tension generated by the cell-spanning ring and PODXL vesicle transport.

The structural resemblance of the actomyosin cable in lens placodes and the cell-spanning ring in hiPSC colonies was highlighted in Section 5.1. Because of this structural resemblance, this work proposes that the cell-spanning ring has the same function *in vivo* and is a mechanical regulator in human epiblast lumenogenesis. This hypothesis is supported by experiments performed in the mouse system, where mESCs showed that epiblast polarisation is presumably mediated by actomyosin-mediated constriction (Bedzhov & Zernicka-Goetz, 2014). Moreover, in a recent hPSC-based *in vitro* model it was shown that epiblast morphogenesis involves phosphorylated ERM proteins, PODXL and a ring-like organisation of actin (Oldak et al., 2023). This would mean that upon implantation, internal apical polarisation is initiated, mediated by a PODXL vesicle transport to the apical membrane initiation site and apical constriction through the cell-spanning actomyosin ring (Figure 27). Thus, it uncovers another potential mechanical aspect in human embryonic development and sheds light on the black box of human embryogenesis.

6 Conclusion and Outlook

The objective of this work was to elucidate the potential role of the cell-spanning ring as a major regulator in hiPSC colonies. In summary, it can be concluded that the crucial role of the cell-spanning actomyosin ring in maintaining both colony morphology and pluripotency was successfully demonstrated. The key findings and conclusions are summarised and the potential future approaches are described in the following.

The present work shows that the colony architecture, due to its heterogenic character relies on both actin cytoskeletal structures: the actin fence and the cell-spanning ring. However, the majority of cells in hiPSC colonies are in contact with and dependent on the contractile tension of the cell-spanning actomyosin ring. Additionally, the results demonstrated that the cell-spanning actomyosin ring is a preserved cytoskeletal structure in hiPSCs. Thus, it stresses the importance of the cell-spanning ring as a major regulator, which, to the best of my knowledge, has been neglected in models explaining pluripotency regulation in hiPSCs. To further verify the impact of the cell-spanning actomyosin ring, the exerted contractile tension should be measured by laser ablation.

The results of this work suggest that the cell-spanning ring regulates the epithelial character by establishing apicobasal polarity and maintaining colony integrity. Interfering with contractile tension leads to epithelial disruption and initiates early differentiation even under self-renewal cultivation conditions. This highlights the great influence of mechanical cues on pluripotency regulation and indicates the characteristic morphology of hiPSC colonies, maintained by the cell-spanning actomyosin ring, to be a key determinant in sustaining pluripotency. However, interfaces between the actin cytoskeleton and pluripotency regulation need to be addressed. Additionally, it is important to note that pluripotency regulation is facilitated by a complex network with different facets, including epigenetic modifications (Arthur et al., 2024), which need to be considered for creating an overall model of pluripotency regulation.

The structure of the cell-spanning actomyosin ring resembles the actomyosin cable described in embryonic mouse epithelial tissue *in vivo* where it mediates invagination and ultimately lumenogenesis (Houssin et al., 2020). To further verify this resemblance, immunostaining of Crumbs needs to be performed to determine if an anisotropic Crumb patterning, which is associated with actomyosin cable in Drosophila (Röper, 2012), is also present in hiPSCs. Because of this structural resemblance, this work proposes that the cell-spanning ring has a similar function *in vivo* and is a mechanical regulator in human epiblast lumenogenesis. However, to verify a potential role of the cell-spanning actomyosin ring in initiation of amniotic cavity formation, a transfer to a 3D system is required. One

approach could be to include the GFP-NMIIB reporter line in the current state-of-the-art post-implantation stem-cell-based embryo models with spatially organized morphogenesis (Oldak et al., 2023). However, this model is based on unmodified hESCs. To bypass ethical constraints associated with modifying hESCs due to their embryonic origin, induction of human naive pluripotency in hiPSC could be performed using the protocol by Fischer and colleagues (L. A. Fischer et al., 2022).

7 Bibliography

Aplin, J. D., & Ruane, P. T. (2017). Embryo–epithelium interactions during implantation at a glance. *Journal of Cell Science*, *130*(1), 15–22. https://doi.org/10.1242/jcs.175943

Arpin, M., Chirivino, D., Naba, A., & Zwaenepoel, I. (2011). Emerging role for ERM proteins in cell adhesion and migration. In *Cell Adhesion and Migration*. https://doi.org/10.4161/cam.5.2.15081

Arthur, T. D., Nguyen, J. P., D'Antonio-Chronowska, A., Matsui, H., Silva, N. S., Joshua, I. N., Aguiar, L. R., Arias, A. D., Benaglio, P., Berggren, W. T., Belmonte, J. C. I., Borja, V., Cook, M., DeBoever, C., Diffenderfer, K. E., Donovan, M. K. R., Farnam, K., Fujita, K., Garcia, M., … Frazer, K. A. (2024). Complex regulatory networks influence pluripotent cell state transitions in human iPSCs. *Nature Communications*, *15*(1), 1664. https://doi.org/10.1038/s41467-024-45506-6

Assémat, E., Bazellières, E., Pallesi-Pocachard, E., Le Bivic, A., & Massey-Harroche, D. (2008). Polarity complex proteins. *Biochimica et Biophysica Acta (BBA) - Biomembranes*, *1778*(3), 614–630. https://doi.org/10.1016/j.bbamem.2007.08.029

Avilion, A. A., Nicolis, S. K., Pevny, L. H., Perez, L., Vivian, N., & Lovell-Badge, R. (2003). Multipotent cell lineages in early mouse development depend on SOX2 function. *Genes & Development*, *17*(1), 126–140. https://doi.org/10.1101/gad.224503

Bedzhov, I., & Zernicka-Goetz, M. (2014). Self-Organizing Properties of Mouse Pluripotent Cells Initiate Morphogenesis upon Implantation. *Cell*, *156*(5), 1032–1044. https://doi.org/10.1016/j.cell.2014.01.023

Bertels, S. (2018). Maintaining stemness of human induced pluripotent stem cells by biochemically and geometrically defined growth substrates. *Dissertation*.

Boraas, L. C., Guidry, J. B., Pineda, E. T., & Ahsan, T. (2016). Cytoskeletal Expression and Remodeling in Pluripotent Stem Cells. *PLOS ONE*, *11*(1), e0145084. https://doi.org/10.1371/journal.pone.0145084

Bryant, D. M., Datta, A., Rodríguez-Fraticelli, A. E., Peränen, J., Martín-Belmonte, F., & Mostov, K. E. (2010). A molecular network for de novo generation of the apical surface and lumen. *Nature Cell Biology*, *12*(11), 1035–1045. https://doi.org/10.1038/ncb2106

Bryant, D. M., Roignot, J., Datta, A., Overeem, A. W., Kim, M., Yu, W., Peng, X., Eastburn, D. J., Ewald, A. J., Werb, Z., & Mostov, K. E. (2014). A Molecular Switch for the Orientation of Epithelial Cell Polarization. *Developmental Cell*, *31*(2), 171–187. https://doi.org/10.1016/j.devcel.2014.08.027

Buckley, C. E., & St Johnston, D. (2022). Apical–basal polarity and the control of epithelial form and function. *Nature Reviews Molecular Cell Biology*, *23*(8), 559–577. https://doi.org/10.1038/s41580-022-00465-y

Bulgakova, N. A., & Knust, E. (2009). The Crumbs complex: from epithelial-cell polarity to retinal degeneration. *Journal of Cell Science*, *122*(15), 2587–2596. https://doi.org/10.1242/jcs.023648

Cai, J., Chen, J., Liu, Y., Miura, T., Luo, Y., Loring, J. F., Freed, W. J., Rao, M. S., & Zeng, X. (2006). Assessing Self-Renewal and Differentiation in Human Embryonic Stem Cell Lines. *Stem Cells*, *24*(3), 516–530. https://doi.org/10.1634/stemcells.2005-0143

Chambers, I., Silva, J., Colby, D., Nichols, J., Nijmeijer, B., Robertson, M., Vrana, J., Jones, K., Grotewold, L., & Smith, A. (2007). Nanog safeguards pluripotency and

mediates germline development. *Nature*, *450*(7173), 1230–1234. https://doi.org/10.1038/nature06403

Chen, J., & Zhang, M. (2013). The Par3/Par6/aPKC complex and epithelial cell polarity. *Experimental Cell Research*, *319*(10), 1357–1364. https://doi.org/10.1016/J.YEXCR.2013.03.021

Chen, W.-J., Huang, W.-K., Pather, S. R., Chang, W.-F., Sung, L.-Y., Wu, H.-C., Liao, M.-Y., Lee, C.-C., Wu, H.-H., Wu, C.-Y., Liao, K.-S., Lin, C.-Y., Yang, S.-C., Lin, H., Lai, P.-L., Ng, C.-H., Hu, C.-M., Chen, I.-C., Chuang, C.-H., … Lu, J. (2023). Podocalyxin-Like Protein 1 Regulates Pluripotency through the Cholesterol Biosynthesis Pathway. *Advanced Science*, *10*(1), 2205451. https://doi.org/https://doi.org/10.1002/advs.202205451

Chouhan, G., Lewis, N. S., Ghanekar, V., Koti Ainavarapu, S. R., Inamdar, M. M., & Sonawane, M. (2024). Cell-size-dependent regulation of Ezrin dictates epithelial resilience to stretch by countering myosin-II-mediated contractility. *Cell Reports*, *43*(6), 114271. https://doi.org/10.1016/j.celrep.2024.114271

Cosgrove, B. D., Mui, K. L., Driscoll, T. P., Caliari, S. R., Mehta, K. D., Assoian, R. K., Burdick, J. A., & Mauck, R. L. (2016). N-cadherin adhesive interactions modulate matrix mechanosensing and fate commitment of mesenchymal stem cells. *Nature Materials*, *15*(12), 1297–1306. https://doi.org/10.1038/nmat4725

Dasgupta, I., & McCollum, D. (2019). Control of cellular responses to mechanical cues through YAP/TAZ regulation. *Journal of Biological Chemistry*, *294*(46), 17693–17706. https://doi.org/10.1074/jbc.REV119.007963

De Belly, H., Stubb, A., Yanagida, A., Labouesse, C., Jones, P. H., Paluch, E. K., & Chalut, K. J. (2021). Membrane Tension Gates ERK-Mediated Regulation of Pluripotent Cell Fate. *Cell Stem Cell*, *28*(2), 273-284.e6. https://doi.org/10.1016/j.stem.2020.10.018

Diz-Muñoz, A., Fletcher, D. A., & Weiner, O. D. (2013). Use the force: membrane tension as an organizer of cell shape and motility. *Trends in Cell Biology*, *23*(2), 47–53. https://doi.org/10.1016/j.tcb.2012.09.006

Doherty, G. J., & McMahon, H. T. (2008). Mediation, Modulation, and Consequences of Membrane-Cytoskeleton Interactions. *Annual Review of Biophysics*, *37*(1), 65–95. https://doi.org/10.1146/annurev.biophys.37.032807.125912

Dong, W., Lu, J., Zhang, X., Wu, Y., Lettieri, K., Hammond, G. R., & Hong, Y. (2020). A polybasic domain in aPKC mediates Par6-dependent control of membrane targeting and kinase activity. *Journal of Cell Biology*, *219*(7). https://doi.org/10.1083/jcb.201903031

Driskill, J. H., & Pan, D. (2023). Control of stem cell renewal and fate by YAP and TAZ. *Nature Reviews Molecular Cell Biology*, *24*(12), 895–911. https://doi.org/10.1038/s41580-023-00644-5

Du, J., Fan, Y., Guo, Z., Wang, Y., Zheng, X., Huang, C., Liang, B., Gao, L., Cao, Y., Chen, Y., Zhang, X., Li, L., Xu, L., Wu, C., Weitz, D. A., & Feng, X. (2019). Compression Generated by a 3D Supracellular Actomyosin Cortex Promotes Embryonic Stem Cell Colony Growth and Expression of Nanog and Oct4. *Cell Systems*, *9*(2), 214-220.e5. https://doi.org/10.1016/j.cels.2019.05.008

Dupont, S., Morsut, L., Aragona, M., Enzo, E., Giulitti, S., Cordenonsi, M., Zanconato, F., Le Digabel, J., Forcato, M., Bicciato, S., Elvassore, N., & Piccolo, S. (2011). Role of YAP/TAZ in mechanotransduction. *Nature*, *474*(7350), 179–183. https://doi.org/10.1038/nature10137

Elosegui-Artola, A., Oria, R., Chen, Y., Kosmalska, A., Pérez-González, C., Castro, N., Zhu, C., Trepat, X., & Roca-Cusachs, P. (2016). Mechanical regulation of a molecular clutch defines force transmission and transduction in response to matrix rigidity. *Nature Cell Biology*, *18*(5), 540–548. https://doi.org/10.1038/ncb3336

Fehon, R. G., McClatchey, A. I., & Bretscher, A. (2010). Organizing the cell cortex: The role of ERM proteins. In *Nature Reviews Molecular Cell Biology*. https://doi.org/10.1038/nrm2866

Fievet, B. T., Gautreau, A., Roy, C., Del Maestro, L., Mangeat, P., Louvard, D., & Arpin, M. (2004). Phosphoinositide binding and phosphorylation act sequentially in the activation mechanism of ezrin. *The Journal of Cell Biology*, *164*(5), 653–659. https://doi.org/10.1083/jcb.200307032

Fischer, A. (2022). Long-Term Cultivation of Human iPS Cells on a Defined Protein-Coated Substrate. *Master Thesis*.

Fischer, L. A., Khan, S. A., & Theunissen, T. W. (2022). *Induction of Human Naïve Pluripotency Using 5i/L/A Medium* (pp. 13–28). https://doi.org/10.1007/978-1-0716-1908-7_2

Fröse, J., Chen, M. B., Hebron, K. E., Reinhardt, F., Hajal, C., Zijlstra, A., Kamm, R. D., & Weinberg, R. A. (2018). Epithelial-Mesenchymal Transition Induces Podocalyxin to Promote Extravasation via Ezrin Signaling. *Cell Reports*, *24*(4), 962–972. https://doi.org/10.1016/j.celrep.2018.06.092

Fu, M., Hu, Y., Lan, T., Guan, K.-L., Luo, T., & Luo, M. (2022). The Hippo signalling pathway and its implications in human health and diseases. *Signal Transduction and Targeted Therapy*, *7*(1), 376. https://doi.org/10.1038/s41392-022-01191-9

Gardel, M. L., Schneider, I. C., Aratyn-Schaus, Y., & Waterman, C. M. (2010). Mechanical Integration of Actin and Adhesion Dynamics in Cell Migration. *Annual Review of Cell and Developmental Biology*, *26*(1), 315–333. https://doi.org/10.1146/annurev.cellbio.011209.122036

Genthner, E. (2020). Intracellular structures defining apical identity in human induced pluripotent stem cells. *Master Thesis*.

Gerardo, H., Lima, A., Carvalho, J., Ramos, J. R. D., Couceiro, S., Travasso, R. D. M., Pires das Neves, R., & Grãos, M. (2019). Soft culture substrates favor stem-like cellular phenotype and facilitate reprogramming of human mesenchymal stem/stromal cells (hMSCs) through mechanotransduction. *Scientific Reports*, *9*(1), 9086. https://doi.org/10.1038/s41598-019-45352-3

Gu, Z., Guo, J., Zhai, J., Feng, G., Wang, X., Gao, Z., Li, K., Ji, S., Wang, L., Xu, Y., Chen, X., Wang, Y., Guo, S., Yang, M., Li, L., Han, H., Jiang, L., Wen, Y., Wang, L., … Gu, Q. (2022). A Uterus-Inspired Niche Drives Blastocyst Development to the Early Organogenesis. *Advanced Science*, *9*(28). https://doi.org/10.1002/advs.202202282

Haghighi, F., Dahlmann, J., Nakhaei-Rad, S., Lang, A., Kutschka, I., Zenker, M., Kensah, G., Piekorz, R. P., & Ahmadian, M. R. (2018). bFGF-mediated pluripotency maintenance in human induced pluripotent stem cells is associated with NRAS-MAPK signaling. *Cell Communication and Signaling*, *16*(1), 96. https://doi.org/10.1186/s12964-018-0307-1

Hayashi, Y., Ohnuma, K., & Furue, M. K. (2019). *Pluripotent Stem Cell Heterogeneity* (pp. 71–94). https://doi.org/10.1007/978-3-030-11096-3_6

Heuzé, M. L., Sankara Narayana, G. H. N., D'Alessandro, J., Cellerin, V., Dang, T.,

Williams, D. S., Van Hest, J. C., Marcq, P., Mège, R.-M., & Ladoux, B. (2019). Myosin II isoforms play distinct roles in adherens junction biogenesis. *ELife*, *8*. https://doi.org/10.7554/eLife.46599

Hillebrandt, H., & Tanaka, M. (2001). Electrochemical Characterization of Self-Assembled Alkylsiloxane Monolayers on Indium−Tin Oxide (ITO) Semiconductor Electrodes. *The Journal of Physical Chemistry B*, *105*(19), 4270–4276. https://doi.org/10.1021/jp004062n

Houssin, N. S., Martin, J. B., Coppola, V., Yoon, S. O., & Plageman, T. F. (2020). Formation and contraction of multicellular actomyosin cables facilitate lens placode invagination. *Developmental Biology*, *462*(1), 36–49. https://doi.org/10.1016/j.ydbio.2020.02.014

Huang, K., Maruyama, T., & Fan, G. (2014). The Naive State of Human Pluripotent Stem Cells: A Synthesis of Stem Cell and Preimplantation Embryo Transcriptome Analyses. *Cell Stem Cell*, *15*(4), 410–415. https://doi.org/10.1016/j.stem.2014.09.014

Icha, J., Weber, M., Waters, J. C., & Norden, C. (2017). Phototoxicity in live fluorescence microscopy, and how to avoid it. *BioEssays*, *39*(8). https://doi.org/10.1002/bies.201700003

Itoh, F., Watabe, T., & Miyazono, K. (2014). Roles of TGF-β family signals in the fate determination of pluripotent stem cells. *Seminars in Cell & Developmental Biology*, *32*, 98–106. https://doi.org/10.1016/j.semcdb.2014.05.017

Joberty, G., Petersen, C., Gao, L., & Macara, I. G. (2000). The cell-polarity protein Par6 links Par3 and atypical protein kinase C to Cdc42. *Nature Cell Biology*, *2*(8), 531–539. https://doi.org/10.1038/35019573

Kang, L., Yao, C., Khodadadi-Jamayran, A., Xu, W., Zhang, R., Banerjee, N. S., Chang, C.-W., Chow, L. T., Townes, T., & Hu, K. (2016). The Universal 3D3 Antibody of Human PODXL Is Pluripotent Cytotoxic, and Identifies a Residual Population After Extended Differentiation of Pluripotent Stem Cells. *Stem Cells and Development*, *25*(7), 556–568. https://doi.org/10.1089/scd.2015.0321

Kashima, Y., Sakamoto, Y., Kaneko, K., Seki, M., Suzuki, Y., & Suzuki, A. (2020). Single-cell sequencing techniques from individual to multiomics analyses. *Experimental & Molecular Medicine*, *52*(9), 1419–1427. https://doi.org/10.1038/s12276-020-00499-2

Kim, M.-H., Kuroda, M., Ke, D., Thanuthanakhun, N., & Kino-oka, M. (2023). An in vitro culture platform for studying the effect of collective cell migration on spatial self-organization within induced pluripotent stem cell colonies. *Journal of Biological Engineering*, *17*(1), 25. https://doi.org/10.1186/s13036-023-00341-z

Kim, Y., Jang, H., Seo, K., Kim, J. H., Lee, B., Cho, H. M., Kim, H. J., Yang, E., Kim, H., Gim, J.-A., Park, Y., Ryu, J. R., & Sun, W. (2022). Cell position within human pluripotent stem cell colonies determines apical specialization via an actin cytoskeleton-based mechanism. *Stem Cell Reports*, *17*(1), 68–81. https://doi.org/https://doi.org/10.1016/j.stemcr.2021.11.005

Knöfler, M., Haider, S., Saleh, L., Pollheimer, J., Gamage, T. K. J. B., & James, J. (2019). Human placenta and trophoblast development: key molecular mechanisms and model systems. *Cellular and Molecular Life Sciences*, *76*(18), 3479–3496. https://doi.org/10.1007/s00018-019-03104-6

Koch, B., Nijmeijer, B., Kueblbeck, M., Cai, Y., Walther, N., & Ellenberg, J. (2018). Generation and validation of homozygous fluorescent knock-in cells using CRISPR-Cas9 genome editing. *Nature Protocols*. https://doi.org/10.1038/nprot.2018.042

Legier, T., Rattier, D., Llewellyn, J., Vannier, T., Sorre, B., Maina, F., & Dono, R. (2023). Epithelial disruption drives mesendoderm differentiation in human pluripotent stem cells by enabling TGF-β protein sensing. *Nature Communications*, *14*(1), 349. https://doi.org/10.1038/s41467-023-35965-8

Li, M., & Belmonte, J. C. I. (2017). Ground rules of the pluripotency gene regulatory network. *Nature Reviews Genetics*, *18*(3), 180–191. https://doi.org/10.1038/nrg.2016.156

Li, M., & Izpisua Belmonte, J. C. (2018). Deconstructing the pluripotency gene regulatory network. *Nature Cell Biology*, *20*(4), 382–392. https://doi.org/10.1038/s41556-018-0067-6

Lian, I., Kim, J., Okazawa, H., Zhao, J., Zhao, B., Yu, J., Chinnaiyan, A., Israel, M. A., Goldstein, L. S. B., Abujarour, R., Ding, S., & Guan, K.-L. (2010). The role of YAP transcription coactivator in regulating stem cell self-renewal and differentiation. *Genes & Development*, *24*(11), 1106–1118. https://doi.org/10.1101/gad.1903310

Lin, D., Edwards, A. S., Fawcett, J. P., Mbamalu, G., Scott, J. D., & Pawson, T. (2000). A mammalian PAR-3–PAR-6 complex implicated in Cdc42/Rac1 and aPKC signalling and cell polarity. *Nature Cell Biology*, *2*(8), 540–547. https://doi.org/10.1038/35019582

Linke, P., Munding, N., Kimmle, E., Kaufmann, S., Hayashi, K., Nakahata, M., Takashima, Y., Sano, M., Bastmeyer, M., Holstein, T., Dietrich, S., Müller-Tidow, C., Harada, A., Ho, A. D., & Tanaka, M. (2024). Reversible Host–Guest Crosslinks in Supramolecular Hydrogels for On-Demand Mechanical Stimulation of Human Mesenchymal Stem Cells. *Advanced Healthcare Materials*, *13*(10). https://doi.org/10.1002/adhm.202302607

Liu, S., & Kanchanawong, P. (2022). Emerging interplay of cytoskeletal architecture, cytomechanics and pluripotency. *Journal of Cell Science*, *135*(12), jcs259379. https://doi.org/10.1242/jcs.259379

Liu, X., Billington, N., Shu, S., Yu, S.-H., Piszczek, G., Sellers, J. R., & Korn, E. D. (2017). Effect of ATP and regulatory light-chain phosphorylation on the polymerization of mammalian nonmuscle myosin II. *Proceedings of the National Academy of Sciences*, *114*(32). https://doi.org/10.1073/pnas.1702375114

Llewellyn, J., Charrier, A., Cuciniello, R., Helfer, E., & Dono, R. (2024). Substrate stiffness alters layer architecture and biophysics of human induced pluripotent stem cells to modulate their differentiation potential. *IScience*, *27*(8), 110557. https://doi.org/10.1016/j.isci.2024.110557

Louvet, S., Aghion, J., Santa-Maria, A., Mangeat, P., & Maro, B. (1996). Ezrin Becomes Restricted to Outer Cells Following Asymmetrical Division in the Preimplantation Mouse Embryo. *Developmental Biology*, *177*(2), 568–579. https://doi.org/10.1006/dbio.1996.0186

Ma, J., Tran, G., Wan, A. M. D., Young, E. W. K., Kumacheva, E., Iscove, N. N., & Zandstra, P. W. (2021). Microdroplet-based one-step RT-PCR for ultrahigh throughput single-cell multiplex gene expression analysis and rare cell detection. *Scientific Reports*, *11*(1), 6777. https://doi.org/10.1038/s41598-021-86087-4

Maldonado, M., Luu, R. J., Ramos, M. E. P., & Nam, J. (2016). ROCK inhibitor primes human induced pluripotent stem cells to selectively differentiate towards mesendodermal lineage via epithelial-mesenchymal transition-like modulation. *Stem Cell Research*. https://doi.org/10.1016/j.scr.2016.07.009

Margolis, B. (2018). The Crumbs3 Polarity Protein. *Cold Spring Harbor Perspectives in Biology*, *10*(3), a027961. https://doi.org/10.1101/cshperspect.a027961

Mascetti, V. L., & Pedersen, R. A. (2016). Contributions of Mammalian Chimeras to Pluripotent Stem Cell Research. *Cell Stem Cell*, *19*(2), 163–175. https://doi.org/10.1016/j.stem.2016.07.018

Matsumura, F. (2005). Regulation of myosin II during cytokinesis in higher eukaryotes. *Trends in Cell Biology*, *15*(7), 371–377. https://doi.org/10.1016/j.tcb.2005.05.004

Mazerik, J. N., & Tyska, M. J. (2012). Myosin-1A Targets to Microvilli Using Multiple Membrane Binding Motifs in the Tail Homology 1 (TH1) Domain. *Journal of Biological Chemistry*, *287*(16), 13104–13115. https://doi.org/10.1074/jbc.M111.336313

Mège, R. M., & Ishiyama, N. (2017). Integration of Cadherin Adhesion and Cytoskeleton at Adherens Junctions. *Cold Spring Harbor Perspectives in Biology*, *9*(5), a028738. https://doi.org/10.1101/cshperspect.a028738

Mitsui, K., Tokuzawa, Y., Itoh, H., Segawa, K., Murakami, M., Takahashi, K., Maruyama, M., Maeda, M., & Yamanaka, S. (2003). The Homeoprotein Nanog Is Required for Maintenance of Pluripotency in Mouse Epiblast and ES Cells. *Cell*, *113*(5), 631–642. https://doi.org/10.1016/S0092-8674(03)00393-3

Mossahebi-Mohammadi, M., Quan, M., Zhang, J.-S., & Li, X. (2020). FGF Signaling Pathway: A Key Regulator of Stem Cell Pluripotency. *Frontiers in Cell and Developmental Biology*, *8*. https://doi.org/10.3389/fcell.2020.00079

Nakashima, Y., & Omasa, T. (2016). What Kind of Signaling Maintains Pluripotency and Viability in Human-Induced Pluripotent Stem Cells Cultured on Laminin-511 with Serum-Free Medium? *BioResearch Open Access*, *5*(1), 84–93. https://doi.org/10.1089/biores.2016.0001

Narva, E., Stubb, A., Guzman, C., Blomqvist, M., Balboa, D., Lerche, M., Saari, M., Otonkoski, T., & Ivaska, J. (2017). A Strong Contractile Actin Fence and Large Adhesions Direct Human Pluripotent Colony Morphology and Adhesion. *Stem Cell Reports*, *9*(1), 67–76. https://doi.org/10.1016/j.stemcr.2017.05.021

Natunen, S., Satomaa, T., Pitkanen, V., Salo, H., Mikkola, M., Natunen, J., Otonkoski, T., & Valmu, L. (2011). The binding specificity of the marker antibodies Tra-1-60 and Tra-1-81 reveals a novel pluripotency-associated type 1 lactosamine epitope. *Glycobiology*, *21*(9), 1125–1130. https://doi.org/10.1093/glycob/cwq209

Naumanen, P., Lappalainen, P., & Hotulainen, P. (2008). Mechanisms of actin stress fibre assembly. *Journal of Microscopy*, *231*(3), 446–454. https://doi.org/10.1111/j.1365-2818.2008.02057.x

Nichols, J., & Smith, A. (2009). Naive and Primed Pluripotent States. *Cell Stem Cell*, *4*(6), 487–492. https://doi.org/10.1016/j.stem.2009.05.015

Nielsen, J. S., & McNagny, K. M. (2009). The Role of Podocalyxin in Health and Disease. *Journal of the American Society of Nephrology*, *20*(8), 1669–1676. https://doi.org/10.1681/ASN.2008070782

Niwa, H., Burdon, T., Chambers, I., & Smith, A. (1998). Self-renewal of pluripotent embryonic stem cells is mediated via activation of STAT3. *Genes & Development*, *12*(13), 2048–2060. https://doi.org/10.1101/gad.12.13.2048

Nunes de Almeida, F., Walther, R. F., Pressé, M. T., Vlassaks, E., & Pichaud, F. (2019). Cdc42 defines apical identity and regulates epithelial morphogenesis by promoting apical recruitment of Par6-aPKC and Crumbs. *Development*, *146*(15).

https://doi.org/10.1242/dev.175497

Oldak, B., Wildschutz, E., Bondarenko, V., Comar, M.-Y., Zhao, C., Aguilera-Castrejon, A., Tarazi, S., Viukov, S., Pham, T. X. A., Ashouokhi, S., Lokshtanov, D., Roncato, F., Ariel, E., Rose, M., Livnat, N., Shani, T., Joubran, C., Cohen, R., Addadi, Y., … Hanna, J. H. (2023). Complete human day 14 post-implantation embryo models from naive ES cells. *Nature*. https://doi.org/10.1038/s41586-023-06604-5

Orlando, R. A., Takeda, T., Zak, B., Schmieder, S., Benoit, V. M., McQuistan, T., Furthmayr, H., & Farquhar, M. G. (2001). The Glomerular Epithelial Cell Anti-Adhesin Podocalyxin Associates with the Actin Cytoskeleton through Interactions with Ezrin. *Journal of the American Society of Nephrology*, *12*(8), 1589–1598. https://doi.org/10.1681/ASN.V1281589

Qin, H., Diaz, A., Blouin, L., Lebbink, R. J., Patena, W., Tanbun, P., LeProust, E. M., McManus, M. T., Song, J. S., & Ramalho-Santos, M. (2014). Systematic Identification of Barriers to Human iPSC Generation. *Cell*, *158*(2), 449–461. https://doi.org/10.1016/j.cell.2014.05.040

Qin, H., Hejna, M., Liu, Y., Percharde, M., Wossidlo, M., Blouin, L., Durruthy-Durruthy, J., Wong, P., Qi, Z., Yu, J., Qi, L. S., Sebastiano, V., Song, J. S., & Ramalho-Santos, M. (2016). YAP Induces Human Naive Pluripotency. *Cell Reports*, *14*(10), 2301–2312. https://doi.org/10.1016/j.celrep.2016.02.036

Reffay, M., Parrini, M. C., Cochet-Escartin, O., Ladoux, B., Buguin, A., Coscoy, S., Amblard, F., Camonis, J., & Silberzan, P. (2014). Interplay of RhoA and mechanical forces in collective cell migration driven by leader cells. *Nature Cell Biology*, *16*(3), 217–223. https://doi.org/10.1038/ncb2917

Romorini, L., Garate, X., Neiman, G., Luzzani, C., Furmento, V. A., Guberman, A. S., Sevlever, G. E., Scassa, M. E., & Miriuka, S. G. (2016). AKT/GSK3β signaling pathway is critically involved in human pluripotent stem cell survival. *Scientific Reports*, *6*(1), 35660. https://doi.org/10.1038/srep35660

Röper, K. (2012). Anisotropy of Crumbs and aPKC Drives Myosin Cable Assembly during Tube Formation. *Developmental Cell*, *23*(5), 939–953. https://doi.org/10.1016/j.devcel.2012.09.013

Rouven Brückner, B., Pietuch, A., Nehls, S., Rother, J., & Janshoff, A. (2015). Ezrin is a Major Regulator of Membrane Tension in Epithelial Cells. *Scientific Reports*, *5*(1), 14700. https://doi.org/10.1038/srep14700

Sakamoto, R., Banerjee, D. S., Yadav, V., Chen, S., Gardel, M. L., Sykes, C., Banerjee, S., & Murrell, M. P. (2023). Membrane tension induces F-actin reorganization and flow in a biomimetic model cortex. *Communications Biology*, *6*(1), 325. https://doi.org/10.1038/s42003-023-04684-7

Sarkar, A., & Hochedlinger, K. (2013). The sox family of transcription factors: versatile regulators of stem and progenitor cell fate. *Cell Stem Cell*, *12*(1), 15–30. https://doi.org/10.1016/j.stem.2012.12.007

Schaefer, T., & Lengerke, C. (2020). SOX2 protein biochemistry in stemness, reprogramming, and cancer: the PI3K/AKT/SOX2 axis and beyond. *Oncogene*, *39*(2), 278–292. https://doi.org/10.1038/s41388-019-0997-x

Schöler, H. R., Hatzopoulos, A. K., Balling, R., Suzuki, N., & Gruss, P. (1989). A family of octamer-specific proteins present during mouse embryogenesis: evidence for germline-specific expression of an Oct factor. *The EMBO Journal*, *8*(9), 2543–2550. https://doi.org/10.1002/j.1460-2075.1989.tb08392.x

Schopperle, W. M., & DeWolf, W. C. (2007). The TRA-1-60 and TRA-1-81 Human Pluripotent Stem Cell Markers Are Expressed on Podocalyxin in Embryonal Carcinoma. *Stem Cells*, *25*(3), 723–730. https://doi.org/10.1634/stemcells.2005-0597

Schwayer, C., Sikora, M., Slováková, J., Kardos, R., & Heisenberg, C.-P. (2016). Actin Rings of Power. *Developmental Cell*, *37*(6), 493–506. https://doi.org/10.1016/j.devcel.2016.05.024

Shahbazi, M. N. (2020). Mechanisms of human embryo development: from cell fate to tissue shape and back. *Development*, *147*(14). https://doi.org/10.1242/dev.190629

Shahbazi, M. N., & Pasque, V. (2024). Early human development and stem cell-based human embryo models. *Cell Stem Cell*, *31*(10), 1398–1418. https://doi.org/10.1016/j.stem.2024.09.002

Shahbazi, M. N., Scialdone, A., Skorupska, N., Weberling, A., Recher, G., Zhu, M., Jedrusik, A., Devito, L. G., Noli, L., Macaulay, I. C., Buecker, C., Khalaf, Y., Ilic, D., Voet, T., Marioni, J. C., & Zernicka-Goetz, M. (2017). Pluripotent state transitions coordinate morphogenesis in mouse and human embryos. *Nature*, *552*(7684), 239–243. https://doi.org/10.1038/nature24675

Shellard, A., Szabó, A., Trepat, X., & Mayor, R. (2018). Supracellular contraction at the rear of neural crest cell groups drives collective chemotaxis. *Science*, *362*(6412), 339–343. https://doi.org/10.1126/science.aau3301

Shutova, M. S., & Svitkina, T. M. (2018). Mammalian nonmuscle myosin II comes in three flavors. *Biochemical and Biophysical Research Communications*, *506*(2), 394–402. https://doi.org/10.1016/j.bbrc.2018.03.103

Sidor, C., Stevens, T. J., Jin, L., Boulanger, J., & Röper, K. (2020). Rho-Kinase Planar Polarization at Tissue Boundaries Depends on Phospho-regulation of Membrane Residence Time. *Developmental Cell*, *52*(3), 364-378.e7. https://doi.org/10.1016/j.devcel.2019.12.003

Singh, A. M., Reynolds, D., Cliff, T., Ohtsuka, S., Mattheyses, A. L., Sun, Y., Menendez, L., Kulik, M., & Dalton, S. (2012). Signaling Network Crosstalk in Human Pluripotent Cells: A Smad2/3-Regulated Switch that Controls the Balance between Self-Renewal and Differentiation. *Cell Stem Cell*, *10*(3), 312–326. https://doi.org/10.1016/j.stem.2012.01.014

Sizemore, S., Cicek, M., Sizemore, N., Ng, K. P., & Casey, G. (2007). Podocalyxin Increases the Aggressive Phenotype of Breast and Prostate Cancer Cells In vitro through Its Interaction with Ezrin. *Cancer Research*, *67*(13), 6183–6191. https://doi.org/10.1158/0008-5472.CAN-06-3575

Stubb, A., Guzmán, C., Närvä, E., Aaron, J., Chew, T.-L., Saari, M., Miihkinen, M., Jacquemet, G., & Ivaska, J. (2019). Superresolution architecture of cornerstone focal adhesions in human pluripotent stem cells. *Nature Communications*, *10*(1), 4756. https://doi.org/10.1038/s41467-019-12611-w

Suzuki, A., Ishiyama, C., Hashiba, K., Shimizu, M., Ebnet, K., & Ohno, S. (2002). aPKC kinase activity is required for the asymmetric differentiation of the premature junctional complex during epithelial cell polarization. *Journal of Cell Science*, *115*(18), 3565–3573. https://doi.org/10.1242/jcs.00032

Svitkina, T. (2018). The Actin Cytoskeleton and Actin-Based Motility. *Cold Spring Harbor Perspectives in Biology*, *10*(1), a018267. https://doi.org/10.1101/cshperspect.a018267

Takahashi, K., Tanabe, K., Ohnuki, M., Narita, M., Ichisaka, T., Tomoda, K., & Yamanaka, S. (2007). Induction of Pluripotent Stem Cells from Adult Human Fibroblasts by Defined Factors. *Cell*. https://doi.org/10.1016/j.cell.2007.11.019

Takahashi, K., & Yamanaka, S. (2006). Induction of Pluripotent Stem Cells from Mouse Embryonic and Adult Fibroblast Cultures by Defined Factors. *Cell*. https://doi.org/10.1016/j.cell.2006.07.024

Takeda, T. (2003). Podocyte cytoskeleton is connected to the integral membrane protein podocalyxin through Na + /H + -exchanger regulatory factor 2 and ezrin. *Clinical and Experimental Nephrology*, *7*(4), 260–269. https://doi.org/10.1007/s10157-003-0257-8

Takeichi, M. (2014). Dynamic contacts: rearranging adherens junctions to drive epithelial remodelling. *Nature Reviews Molecular Cell Biology*, *15*(6), 397–410. https://doi.org/10.1038/nrm3802

Taniguchi, K., Heemskerk, I., & Gumucio, D. L. (2019). Opening the black box: Stem cell-based modeling of human post-implantation development. In *Journal of Cell Biology*. https://doi.org/10.1083/jcb.201810084

Taniguchi, K., Shao, Y., Townshend, R. F., Cortez, C. L., Harris, C. E., Meshinchi, S., Kalantry, S., Fu, J., O'Shea, K. S., & Gumucio, D. L. (2017). An apicosome initiates self-organizing morphogenesis of human pluripotent stem cells. *Journal of Cell Biology*, *216*(12), 3981–3990. https://doi.org/10.1083/jcb.201704085

Tojkander, S., Gateva, G., & Lappalainen, P. (2012). Actin stress fibers – assembly, dynamics and biological roles. *Journal of Cell Science*. https://doi.org/10.1242/jcs.098087

Totaro, A., Panciera, T., & Piccolo, S. (2018). YAP/TAZ upstream signals and downstream responses. *Nature Cell Biology*, *20*(8), 888–899. https://doi.org/10.1038/s41556-018-0142-z

Vale, R. D., & Milligan, R. A. (2000). The Way Things Move: Looking Under the Hood of Molecular Motor Proteins. *Science*, *288*(5463), 88–95. https://doi.org/10.1126/science.288.5463.88

Vallier, L., Mendjan, S., Brown, S., Chng, Z., Teo, A., Smithers, L. E., Trotter, M. W. B., Cho, C. H.-H., Martinez, A., Rugg-Gunn, P., Brons, G., & Pedersen, R. A. (2009). Activin/Nodal signalling maintains pluripotency by controlling Nanog expression. *Development*, *136*(8), 1339–1349. https://doi.org/10.1242/dev.033951

Varzideh, F., Gambardella, J., Kansakar, U., Jankauskas, S. S., & Santulli, G. (2023). Molecular Mechanisms Underlying Pluripotency and Self-Renewal of Embryonic Stem Cells. *International Journal of Molecular Sciences*, *24*(9), 8386. https://doi.org/10.3390/ijms24098386

Vicente-Manzanares, M., Ma, X., Adelstein, R. S., & Horwitz, A. R. (2009). Non-muscle myosin II takes centre stage in cell adhesion and migration. *Nature Reviews Molecular Cell Biology*, *10*(11), 778–790. https://doi.org/10.1038/nrm2786

Vining, K. H., & Mooney, D. J. (2017). Mechanical forces direct stem cell behaviour in development and regeneration. *Nature Reviews Molecular Cell Biology*, *18*(12), 728–742. https://doi.org/10.1038/nrm.2017.108

Wada, K.-I., Itoga, K., Okano, T., Yonemura, S., & Sasaki, H. (2011). Hippo pathway regulation by cell morphology and stress fibers. *Development*, *138*(18), 3907–3914. https://doi.org/10.1242/dev.070987

Walker, M., Rizzuto, P., Godin, M., & Pelling, A. E. (2020). Structural and mechanical remodeling of the cytoskeleton maintains tensional homeostasis in 3D microtissues under acute dynamic stretch. *Scientific Reports*, *10*(1), 7696. https://doi.org/10.1038/s41598-020-64725-7

Wegner, B., Al-Momany, A., Kulak, S. C., Kozlowski, K., Obeidat, M., Jahroudi, N., Paes, J., Berryman, M., & Ballermann, B. J. (2010). CLIC5A, a component of the ezrin-podocalyxin complex in glomeruli, is a determinant of podocyte integrity. *American Journal of Physiology. Renal Physiology*, *298*(6), F1492-503. https://doi.org/10.1152/ajprenal.00030.2010

Weinberger, L., Ayyash, M., Novershtern, N., & Hanna, J. H. (2016). Dynamic stem cell states: Naive to primed pluripotency in rodents and humans. *Nature Reviews Molecular Cell Biology*, *17*(3), 155–169. https://doi.org/10.1038/nrm.2015.28

Weißenbruch, K., Grewe, J., Hippler, M., Fladung, M., Tremmel, M., Stricker, K., Schwarz, U. S., & Bastmeyer, M. (2021). Distinct roles of nonmuscle myosin II isoforms for establishing tension and elasticity during cell morphodynamics. *ELife*, *10*. https://doi.org/10.7554/eLife.71888

Weng, S., Shao, Y., Chen, W., & Fu, J. (2016). Mechanosensitive subcellular rheostasis drives emergent single-cell mechanical homeostasis. *Nature Materials*, *15*(9), 961–967. https://doi.org/10.1038/nmat4654

Whitney, D. S., Peterson, F. C., Kittell, A. W., Egner, J. M., Prehoda, K. E., & Volkman, B. F. (2016). Binding of Crumbs to the Par-6 CRIB-PDZ Module Is Regulated by Cdc42. *Biochemistry*, *55*(10), 1455–1461. https://doi.org/10.1021/acs.biochem.5b01342

Wu, J., & Izpisua Belmonte, J. C. (2015). Dynamic Pluripotent Stem Cell States and Their Applications. *Cell Stem Cell*, *17*(5), 509–525. https://doi.org/10.1016/j.stem.2015.10.009

Xia, S., Lim, Y. B., Zhang, Z., Wang, Y., Zhang, S., Lim, C. T., Yim, E. K. F., & Kanchanawong, P. (2019). Nanoscale Architecture of the Cortical Actin Cytoskeleton in Embryonic Stem Cells. *Cell Reports*, *28*(5), 1251-1267.e7. https://doi.org/10.1016/j.celrep.2019.06.089

Xia, S., Yim, E. K. F., & Kanchanawong, P. (2019). Molecular Organization of Integrin-Based Adhesion Complexes in Mouse Embryonic Stem Cells. *ACS Biomaterials Science & Engineering*, *5*(8), 3828–3842. https://doi.org/10.1021/acsbiomaterials.8b01124

Xiao, L., Yuan, X., & Sharkis, S. J. (2006). Activin A Maintains Self-Renewal and Regulates Fibroblast Growth Factor, Wnt, and Bone Morphogenic Protein Pathways in Human Embryonic Stem Cells. *Stem Cells*, *24*(6), 1476–1486. https://doi.org/10.1634/stemcells.2005-0299

Ying, Q.-L., Nichols, J., Chambers, I., & Smith, A. (2003). BMP Induction of Id Proteins Suppresses Differentiation and Sustains Embryonic Stem Cell Self-Renewal in Collaboration with STAT3. *Cell*, *115*(3), 281–292. https://doi.org/10.1016/S0092-8674(03)00847-X

Yu, L., Wei, Y., Sun, H.-X., Mahdi, A. K., Pinzon Arteaga, C. A., Sakurai, M., Schmitz, D. A., Zheng, C., Ballard, E. D., Li, J., Tanaka, N., Kohara, A., Okamura, D., Mutto, A. A., Gu, Y., Ross, P. J., & Wu, J. (2021). Derivation of Intermediate Pluripotent Stem Cells Amenable to Primordial Germ Cell Specification. *Cell Stem Cell*, *28*(3), 550-567.e12. https://doi.org/10.1016/j.stem.2020.11.003

Zhang, W., & Liu, H. T. (2002). MAPK signal pathways in the regulation of cell proliferation

in mammalian cells. *Cell Research*, *12*(1), 9–18. https://doi.org/10.1038/sj.cr.7290105

Zihni, C., Vlassaks, E., Terry, S., Carlton, J., Leung, T. K. C., Olson, M., Pichaud, F., Balda, M. S., & Matter, K. (2017). An apical MRCK-driven morphogenetic pathway controls epithelial polarity. *Nature Cell Biology*, *19*(9), 1049–1060. https://doi.org/10.1038/ncb3592

Zorzan, I., Pellegrini, M., Arboit, M., Incarnato, D., Maldotti, M., Forcato, M., Tagliazucchi, G. M., Carbognin, E., Montagner, M., Oliviero, S., & Martello, G. (2020). The transcriptional regulator ZNF398 mediates pluripotency and epithelial character downstream of TGF-beta in human PSCs. *Nature Communications*, *11*(1), 2364. https://doi.org/10.1038/s41467-020-16205-9

8 List of Figures

9 List of Tables

List of Tables

10 List of Abbreviations

(GSK3)β	Glycogen Synthase Kinase-3
aPKC	Atypical Protein Kinase C
BMP	Bone morphogenetic proteins
Co-IP	Co-Immunoprecipitation
CRB1-3	Crumbs
CRISPR/Cas9	Clustered regularly interspaced short palindromic repeats
DLW	Direct laser writing
ECM	extracellular matrix
ELC	Essential light chains
ERK	Extracellular signal-regulated Kinase
ERM	Ezrin, Radixin and Moesin
FACS	Fluorescence-Activated Cell Sorting
FGF	Fibroblast Growth factor
FGFR1	Fibroblast Growth factor receptor 1
FoxA2	Forkhead box A2
GFP	Green fluorescent protein
hESC	Human embryonic stem cells
hiPSCs	Human induced pluripotent stem cells
HPSC	Human pluripotent stem cells
ICM	Inner cell mass
KO	Knockout
LATS1/2	Large tumour suppressor Kinase 1/2
LCI	Live Cell imaging
LIF	Leukemia inhibitory factor
MAPK	Mitogen-activated protein Kinase
mEpiSC	Mouse epiblast-derived stem cells
mESC	Mouse embryonic stem cells
MOB1A/B	MOB kinase activators 1A and 1B
MRLC	myosin regulatory light chains
MST1/2	mammalian STE20-like Kinase 1/2
NHERF2	Na+/H+ exchanger regulatory cofactor 2
NMII	Non-muscle myosin II
OCT3/4	Octamer-binding transcription factor 3/4
PETA	Pentaerythritol triacrylate
PGRN	Pluripotency gene regulatory network
PI3	Phosphatidylinositol-4,5-bisphosphate 3-Kinase
PLCγ	Phospholipase C Gamma
PODXL	Podocalyxin-like protein 1
POI	Protein of interest
RLC	Regulatory light chain
ROCK	Rho-associated protein kinase
ROI	Regions of interest
RT-qPCR	Quantitative reverse transcription polymerase chain reaction
SAV1	Salvador homologue 1

SC	Single Cells
SOX1	SRY-box 1
SOX2	SRY-box 2
Std	Stardust
TAZ	WW-domain-containing transcription regulator 1
TE	Trophectoderm
TEAD	Transcriptional enhanced associated domain
TGF	Transforming Growth factor
YAP	Yes-associated protein 1

11 List of Publications and Manuscripts

C. Vazquez-Martel, L. Florido Martins, **E. Genthner**, C. Almeida, A. Martel Quintana, M. Bastmeyer, J. L. Gómez Pinchetti, E. Blasco, Printing Green: Microalgae-Based Materials for 3D Printing with Light. Adv. Mater. 2024, 36, 2402786. DOI: 10.1002/adma.202402786

Bertels S, Jaggy M, Richter B, Keppler S, Weber K, **Genthner E**, Fischer AC, Thiel M, Wegener M, Greiner AM, Autenrieth TJ, Bastmeyer M. 2021. Geometrically defined environments direct cell division rate and subcellular YAP localization in single mouse embryonic stem cells. Sci Rep 11, 9269.

Cunze S, Kochmann J, Koch LK, **Genthner E**, Klimpel S. 2019. Vector distribution and transmission risk of the Zika virus in South and Central America. PeerJ 7:e7920.

Acknowledgements

Firstly, I want to thank Prof. Dr. Martin Bastmeyer for giving me the opportunity to work on this topic and write my PhD thesis at his institute. I want to thank for the trust and support during my time as doctoral student, in particular, for supporting me in my pursuit of research exchanges abroad.

I also want to thank Prof. Dr. Sylvia Erhardt for readily agreeing to act as a co-referee for this work.

I want to thank all my colleagues, past and present, at the Zoological Institute that accompanied me through this work. I really enjoyed our time together every single day. In particular, I wholeheartedly thank Dr. Stephan Keppler, Dr. Annemarie Lange and Chiara Windsor for being good friends and helping me during my time as a doctoral student. I'm looking forward to the next get-together to eat some cake.

A special thanks goes to Dr. Kai Richler for proofreading and providing me with pictures of dogs. I really enjoyed your comments and they helped me find some amusement in this writing process.

My sincere thanks go to my family, my wonderful parents and the best sisters I could have hoped for.

Last but not least, I am forever grateful to Magdalena and my dear partner Max. You both are my rocks and I couldn't have done it without your support and help. We did it, Magdalena!